RICE UNIVERSITY

Multiple early Eocene hyperthermal events: Their lithologic expressions and environmental consequences

by

Micah John Nicolo

A THESIS SUBMITTED
IN PARTIAL FULFILLMENT OF THE
REQUIREMENTS FOR THE DEGREE

Doctor of Philosphy

Approved, Thesis Committee:

Gerald Dickens
Thesis Advisor, Associate Earth Science Professor

Cin-Ty Lee
Assistant Earth Science Professor

Adrian Lenardic
Associate Earth Science Professor

Jonathon Silberg
Assistant Biochemistry & Cell Biology Professor
Assistant Bioengineering Professor

Houston, Texas
April 2008

ABSTRACT

Multiple early Eocene hyperthermal events:

Their lithologic expressions and environmental consequences

by

Micah John Nicolo

ABSTRACT

A gradual rise in Earth's surface temperature marks a transition from the late Paleocene to the early Eocene ca. 58-51 Ma. Paleocene/Eocene boundary (~55.5 Ma) sediments deposited in the midst of this slow warming ubiquitously reveal evidence for a massive isotopically light carbon injection and an associated rapid but transient global warming event, or hyperthermal, that has been termed the Paleocene Eocene Thermal Maximum (PETM) and attributed to a carbon injection from multiple potential sources. The PETM has gained importance over the past two decades as a potential geologic analog to the modern anthropogenic carbon injection and climate change. However significant questions surrounding the nature of the carbon injection at the onset of the PETM remain.

The Clarence River valley, located in the Marlborough region, South Island, New Zealand, contains a series of outcrops of lithified late Paleocene to early Eocene sediments originally deposited on a paleo-slope margin. Within these sections, the Lower Limestone Member of the Amuri Limestone Formation records the interval of interest. A Lower Limestone prominent recessed unit consisting of multiple marl-rich beds and recording a pronounced negative carbon isotopic excursion (CIE) marks the PETM at

sections that have been bisected by tributaries to the Clarence River, including Mead Stream and Dee Stream.

Here I detail and discuss Clarence valley Lower Limestone sections and relate these records to global trends with an emphasis on adding constraints to the PETM carbon injection. Specifically, I document the lithologic and carbon isotopic expression of the PETM and two younger paired sets of early Eocene events that, similar to the Mead Stream and Dee Stream PETM sections, reveal negative CIEs and expanded marl-rich units coincident to identical CIEs and condensed carbonate dissolution horizons in deep-sea sections. I further quantify the abundance of bioturbating macrofauna trace fossils through the PETM at both Mead Stream and Dee Stream and argue that New Zealand margin intermediate waters became hypoxic precisely coincident to the PETM carbon injection. In concert, these findings suggest a PETM carbon addition mechanism capable of both diminishing intermediate water dissolved oxygen and of repeated early Eocene injections.

ACKNOWLEDGMENTS

I have had the considerable good fortune of working with and knowing many insightful and incredible people throughout this process. That situation started with my doctorate advisor, Jerry Dickens. I actually thought that I was unorganized until I met Jerry. But for all the less than smooth times that combination has brought me over the past years, I am more than confident that I have benefited greatly as a scientist in working with him. I thank Jerry for all he has done for me in every respect.

This work is intended to fit within much larger collaborative efforts both within a group that has been detailing outcrop sections in the Clarence River valley, South Island, New Zealand, for much longer than I have been thinking about these rocks, as well as an international group of researchers all interested in understanding the Paleocene Eocene Thermal Maximum (PETM). Over the course of my PhD I have enjoyed the distinct privilege of spending two field seasons in the Clarence, as well as two months aboard the *JOIDES Resolution* during Leg 208 of the Ocean Drilling Program. I have greatly appreciated knowing, working with, and discussing over probably a few too many drinks many of the ideas I present here, with a large number of researchers involved in those efforts, several (but certainly not all) of whom include: Chris Hollis, James Crampton, Percy Strong, Jim Zachos, Dave Hodell, Ed Hathorne, Clay Kelly, Lucas Lourens, Isabella Raffi, Christina Riesselman, Stephen Schellenberg, Appy Sluijs, Debbie Thomas, Ellen Thomas, and many others. In addition, quite a few individuals within the Rice Earth Science Department faculty, staff, and students have been important to me over the years.

Foremost, I would like to thank my family and close friends. Nothing I have ever done, or will ever do, will be accomplished alone because so many people have been an important part of who I am. My father, mother, and sister have always helped me to understand what is most important, and for that I can never be thankful enough. I have had a great number of close friends through the PhD portion of my life (and in rare instances for remarkably longer) that deserve thanks for having been immeasurably important in helping me navigate the non-work side of what grad school can sometimes become, some of whom include: Chris Carne, Jared Impson, Indrani Parker, Katie Cooper, David Heroy, Rich Fitton, Beatrice Magnani, Meghan Miller, Ashley Hubbard, Colin Wailling, Darrell Stanley, Becky Schultz, Cory Clechenko, Liz Clechenko, Christy Stewart, Vong Sokham, and Mike Tompkins. Finally, to Amanda Martin, I would like to say thank you for being the most incredible, beautiful, caring, intelligent, supportive, and easiest person to love I have ever known. Thank you all.

TABLE OF CONTENTS

LIST OF TABLES

LIST OF FIGURES

Appendix

CHAPTER 1.

A BRIEF INTRODUCTION

THE EARLY PALEOGENE

The early Paleogene, unofficially defined here as the beginning of the Paleocene to the inflection point that marks the transition between early Cenozoic warming and the global cooling trend that eventually allowed for the glaciation of Antarctica, represents approximately the first 15 Myrs of the Cenozoic. Within this interval, the general late Paleocene through early Eocene transition was characterized by extremely high atmospheric CO_2 (likely greater than 1,100 but less than ~4,000 ppmv) and a long term but relatively gradual warming trend that drove Earth's surface temperatures positive by ~5°C over a time interval spanning 58 – 51 Ma, ultimately culminating in the highest sustained global mean temperatures of the Cenozoic (Pearson et al., 2007; Zachos et al., 2008; Figure 1.1). Benthic foraminiferal stable carbon isotopic records (Zachos et al., 2001; Figure 1.1) show a general decrease across this time, suggesting some combination of increased carbon inputs and/or decreased carbon outputs to and from the ocean and atmosphere.

The early Paleogene has received increasing attention over the past decade, because it represents the most recent example from Earth's past when atmospheric CO_2 concentration was as high or higher than values predicted by the various estimates of the amount of fossil fuel burning the 'anthropocene' may

witness (Pearson et al., 2007; Zachos et al., 2008). Further, within this gradual quiescent climate shift there appears to have been at least one, and perhaps several additional major accelerations of this warming climate trend. These rapid (major environmental impacts appear to first affect records within <10 kyrs of onset) but transient (<200 kyrs) warming events have been termed hyperthermal events. The most extreme of these perturbations marks the boundary between the Paleocene and Eocone Epochs (ca. 55.5 Ma) at its onset.

THE PALEOCENE EOCENE THERMAL MAXIMUM

A pronounced negative shift in the stable carbon isotopic composition ($\delta^{13}C$) of marine and terrestrial sediments by ~3 ‰ deposited at the dawn of the Eocene Epoch stratigraphically defines the onset of a phenomenal global warming event known as the Paleocene Eocene Thermal Maximum (PETM) (Kennett and Stott, 1991; Koch et al., 1992). Approximately coincident to the sedimentary carbon $\delta^{13}C$ decrease, Earth surface temperatures increased by 5-10°C at all latitudes and remained near maximum values for ~100 kyrs (Sluijs et al., 2006; Zachos et al., 2001; Zachos et al., 2003). On land, the PETM resulted in the evolution and diversification of mammals (Bowen et al., 2002) and the expansion of tropical flora into higher latitudes (Wing et al., 2005). In the surface ocean, the PETM was related to the expansion of low-latitude planktonic foraminifera into sub-polar regions (Kelly, 2002), a trophic gradient enhancement between continental shelves and open ocean settings (Gibbs et al., 2006), and the proliferation of unique dinoflagellate species on continental margins (Crouch et al., 2003; Sluijs et al., 2007). In the deep oceans, the PETM was associated with a

~5°C increase in temperature (Zachos et al., 2001), the largest benthic foraminiferal extinction of the Cenozoic (Thomas, 2003), and massive but regionally variable dissolution of deep-sea carbonates related to a rise in dissolved CO_2 concentration and acidity (Zachos et al., 2005; Zeebe and Zachos, 2007). The last observation coupled with the large negative carbon isotopic excursion (CIE) found in both terrestrial and marine reservoirs indicates that the PETM almost certainly was the result of a tremendous injection of ^{13}C-depleted carbon from outside the traditional exogenic carbon reservoirs (Dickens et al., 1995).

QUESTIONS POSED AND PRINCIPAL FINDINGS

Significant questions regarding both the PETM and the general early Paleogene warming transition as a whole remain. This work has been aimed at constraining independent but ultimately related aspects of the PETM carbon injection. The carbon injection has previously been attributed to several mechanisms including the dissociation of marine slope methane clathrates (Dickens et al., 1997), the thermogenic release of methane as a result of igneous dike intrusions (Svensen et al., 2004), the oxidation of vast amounts of terrestrial organic carbon (Kurtz et al., 2003), and the impact of a tremendous carbonaceous meteorite (Kent et al., 2003).

HOW UNIQUE WAS THE PETM?

Available literature prior to the publication of *Chapter 2* had documented only one other potential hyperthermal event at a singular condensed deep-sea location (Lourens et al., 2005) that still had the distinct potential of being a local

phenomena. In *Chapter 2* I address how unique or prevalent hyperthermal events such as the PETM were in the early Eocene. This is a necessary and important constraint to understanding the driving mechanism of the PETM. If the PETM was a singular or unique occurrence a uniquely singular carbon injection mechanism may be suitable. However, if the PETM was merely the largest of a series of similar events, any plausible explanation for the carbon injection by necessity must rely on a fundamental early Paleogene Earth system process. My coauthors and I presented the first work to illustrate that a series of PETM-like early Eocene environmental perturbations were associated with a series of similar carbon isotopic excursions in all available locations.

DO ENVIRONMENTAL IMPACTS CORRELATE WITH THE CARBON INPUT?

No environmental characteristics of the PETM have previously been shown to stratigraphically relate to the structure of the carbon injection in terms of both its onset and end. The phase of the carbon injection here is discussed as the negative limb of the CIE. While many of the above noted consequences of the PETM began roughly approximate to the negative shift in carbon isotopes (e.g. the benthic extinction horizon) most PETM related phenomena stratigraphically relate much closer to the phase of the *thermal maximum* itself, which lasts ~30 kyrs longer than the carbon injection. In *Chapter 3* I present a novel quantitative image analysis approach to a classic sedimentary tool, the presence or absence of bioturbating trace fossils, in order to describe a relationship between intermediate water dissolved oxygen and the carbon injection. These results illustrate that precisely and only during the carbon injection, intermediate waters on the New

Zealand upper-slope became hypoxic; an observation that strongly supports a methane injection model for the PETM CIE.

HOW CONSISTENT ARE CIE RECORDS BETWEEN BASINS AND SETTINGS?

Fundamental aspects of the PETM including the mass of the carbon injection and the rate of input are constrained partly by the nature and amplitude of the CIE. In *Chapter 4* I discuss the variability of a suite of compiled bulk carbonate PETM CIE records as well as data I have generated on a series of sites originally deposited on the proto-New Zealand margin. I discuss these records in regard to modern ocean dissolved inorganic carbon $\delta^{13}C$ variability and carbonate fractionation. This work suggests that ocean circulation was reversed during the PETM relative to today, but that similar shelf and periplatform $\delta^{13}C$ gradients existed during the PETM as they do in the modern.

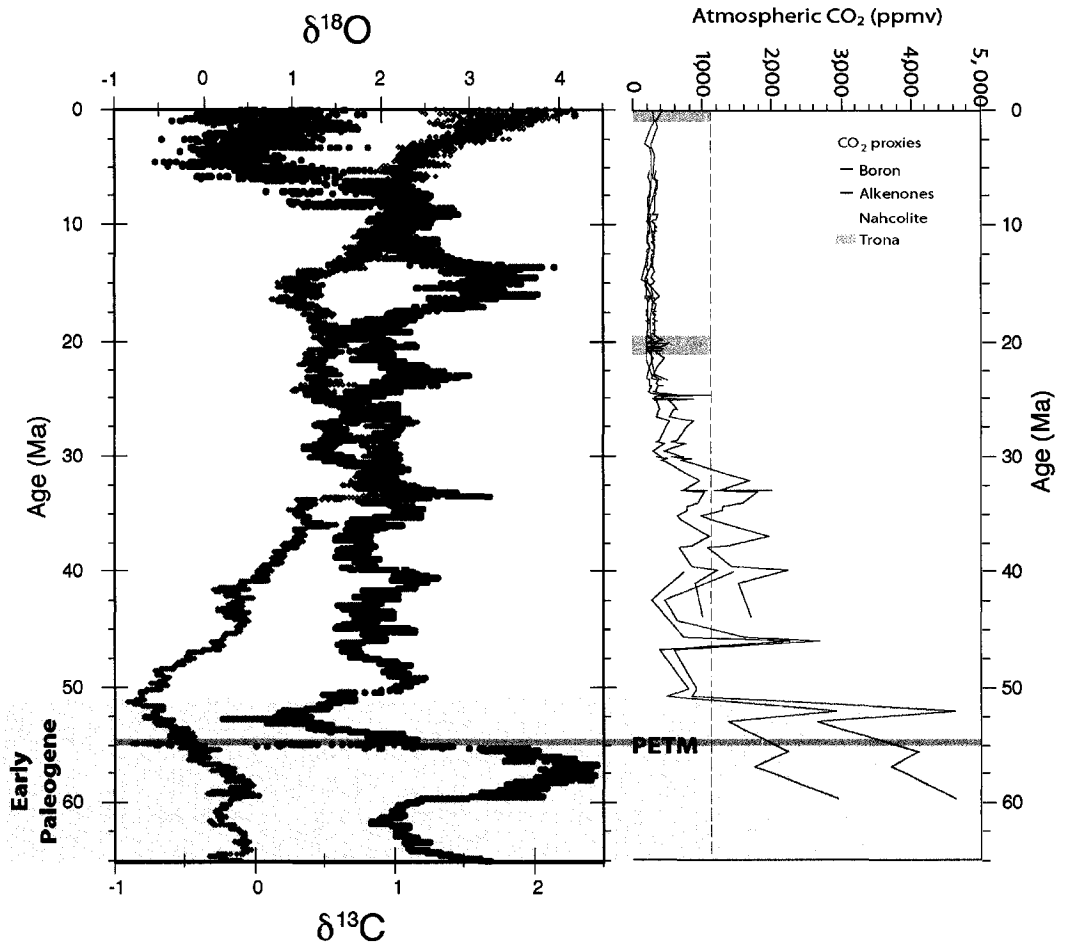

Figure 1.1. Cenozoic benthic foraminfera stable isotopes and CO_2 proxies. After Zachos et al., (2001) and Zachos et al., (2008). Red diamonds represent oxygen isotopes, while blue circles illustrate carbon isotopes. See Zachos et al., (2008) for dicsussion of CO_2 proxies. Light gray box represents the early Paleogene. Dark gray box represnts the PETM. Note that the PETM model is slightly different than discussed in text.

CHAPTER 2.

Multiple early Eocene hyperthermals: Their sedimentary expression on the New Zealand continental margin and in the deep-sea

Micah J. Nicolo[1], Gerald R. Dickens[1], Christopher J. Hollis[2], James C. Zachos[3]

[1]*Department of Earth Sciences, Rice University, Houston, TX 77005, USA*

[2]*Institute of Geological and Nuclear Sciences, PO Box 30-368, Lower Hutt, New Zealand*

[3]*Earth and Planetary Sciences Department, University of California, Santa Cruz, CA 95064, USA*

Published August 2007:

Geology, v. 35, no. 8, p. 699-702

ABSTRACT

The Paleocene-Eocene Thermal Maximum (PETM) ca. 55.5 Ma was a geologically brief interval characterized by massive influx of isotopically light carbon, extreme changes in global climate, and profound variations in Earth system processes. An outstanding issue is whether it was an isolated event, or the most prominent example of a recurring phenomenon. Recent studies of condensed deep-sea sections support the latter, but this finding remains uncertain. Here we present and discuss lithologic and carbon isotope records across two lower Eocene outcrops on South Island, New Zealand. The PETM manifests as a marl-rich horizon with a significant negative carbon isotope excursion (CIE). Above, in sediment deposited between 54 and 53 Ma, are four horizons with similar though less pronounced expressions. Marl beds of all five horizons represent increased terrigenous sedimentation, presumably linked to an accelerated hydrological cycle. Five corresponding clay-rich horizons and CIEs are found in deep-sea records, although the lithologic variations represent carbonate dissolution rather than siliciclastic dilution. The presence of five intervals with similar systemic responses in different environments suggests a mechanism(s) that repeatedly injected large masses of ^{13}C-depleted carbon during the early Eocene.

INTRODUCTION

Earth's surface warmed from the late Paleocene ca. 58 Ma through the early Eocene ca. 51 Ma (Zachos et al., 2001). Superimposed on this temperature rise was at least one transient "hyperthermal," the Paleocene-Eocene Thermal Maximum (PETM). During this event, which initiated between 55.3 and 55.7 Ma (Lourens et al., 2005), the carbon isotopic composition ($\delta^{13}C$) of marine and terrestrial carbon decreased by at least 2.5 ‰ over ~15–30 kyrs in association with warming of both the deep-sea by ~4-5°C and the surface ocean at all latitudes by ~5–9°C (see Bowen et al., 2006, and references therein). This global negative carbon isotope excursion (CIE) implicates massive addition of ^{13}C-depleted carbon to the ocean and atmosphere from an external carbon reservoir (Dickens et al., 1997). Such carbon input should have shoaled the ocean calcite compensation depth, increased atmospheric pCO_2 and temperature, accelerated the global hydrologic and weathering cycles (Dickens et al., 1997; Bowen et al., 2004), and ultimately enhanced continental erosion. Evidence for these expectations has been found in various records (Ravizza et al., 2001; Schmitz et al., 2001; Crouch et al., 2003; Bowen et al., 2004; Hollis et al., 2005a; Zachos et al., 2005; Sluijs et al., 2006, Giusberti et al., 2007).

One fundamental issue regarding the PETM is whether it was a unique event requiring an extraordinary cause, or an extreme example of a more common process. Posited sources of massive carbon input include reservoirs external to Earth (e.g., impact of a comet, Kent et al., 2003), from within Earth (e.g., exhalation of thermogenic methane, Svensen et al., 2004), or on Earth's surface (e.g., dissociation of marine clathrates, Dickens et al., 1997; oxidation of

terrestrial organic carbon, Kurtz et al., 2003). While each may explain a singular event (to a varying degree of plausibility), the identification of multiple perturbations with similar causes and consequences would necessitate a source capable of repeated carbon injections.

Benthic foraminiferal assemblages display an extinction event (BFEE) at the PETM, likely in response to variations in deep-water temperature, dissolved O_2, and/or pH (Thomas, 2003). Similar though less severe turnovers punctuate the long-term warming, suggesting additional PETM-like hyperthermals (Thomas and Zachos, 2000). Deep Sea Drilling Project (DSDP) and Ocean Drilling Program (ODP) sediment records may support this inference. At several sites (Figure 2.1), a series of significant (> 0.5 ‰) negative CIEs occurred over this interval (Cramer et al., 2003). The most pronounced of the post-PETM CIEs, termed "H1" (Cramer et al., 2003), occurred ~53.6 Ma (Lourens et al., 2005). On Walvis Ridge, South Atlantic, this CIE coincides with evidence for surface and deep-water warming, and a clay horizon referred to as "ELMO," which probably represents lysocline shoaling (Lourens et al., 2005), an oceanic response similar though less severe than that associated with the PETM (Zachos et al., 2005). Above H1/ELMO on Walvis Ridge are several distinct clay-rich horizons, which may represent additional lysocline shoaling events and correspond to other CIEs (specifically "H2", "I1", and "I2" defined by Cramer et al., 2003).

Presently, our understanding of post-PETM hyperthermals is unconstrained. This is largely because assessment has been limited to deep-sea records, where dissolution has condensed these events, and where complete recovery of lower Eocene sections has been rare. Here we present lithologic, $\delta^{13}C$,

and $CaCO_3$ content records across two upper Paleocene-lower Eocene shallow marine sequences exposed in New Zealand. Our results support a hypothesis that there were at least five significant and similar events between 56 and 53 Ma, of which the PETM is the most pronounced.

LOCATION AND PREVIOUS WORK

Clarence River valley, in northeast South Island, New Zealand, contains streams that cut an uplifted block of upper Cretaceous-upper Eocene marine sedimentary rocks (Reay, 1993). Sediments were deposited on the outer shelf and upper slope (~100–1000 m water depth) of a passive margin at 50–55°S latitude (Reay, 1993; Hollis et al., 2005a). Within the sequence, the Lower Limestone member of the Amuri Limestone formation accumulated during the late Paleocene and early Eocene, and primarily consists of pelagic carbonate, terrigenous aluminosilicates (mostly clay minerals), and biogenic silica (Figure 2.2) (Reay, 1993; Strong et al., 1995).

Two excellent Lower Limestone exposures are found along Mead and Dee streams. Previous work (Strong et al., 1995; Hancock et al., 2003; Hollis et al., 2005a) provides a good stratigraphy based on microfossil assemblages and bulk rock $\delta^{13}C$ (Figure 2.2). Both sections contain continuous upper slope sediment records from 56 to 53 Ma, although the thicker Mead section represents a deeper environment (Reay, 1993). They also display similar expressions of the PETM. A prominent marl-rich unit (2.4 m thick at Mead; 1.0 m thick at Dee) marks the base of the Eocene (Hancock et al., 2003; Hollis et al., 2005a). Consistent with expressions of the PETM at other sites, this unit has a significant (~2.5 ‰)

negative CIE, a BFEE, and brief warm-water plankton occurrences (Hancock et al., 2003; Hollis et al., 2005a). Like PETM horizons at other continental margin settings (Schmitz et al., 2001; Giusberti et al., 2007), marl-rich units across the PETM in Clarence Valley represent increased terrigenous accumulation and sedimentation rate (Hancock et al., 2003; Hollis et al., 2005a).

APPROACH AND METHODS

Marine carbon isotope records show five negative CIEs between 56 and 53 Ma. The oldest and most pronounced is the PETM; the other four occurred between 54 and 53 Ma (Figure 2.3; Figure 2.4). Walvis Ridge sediment sections have five seemingly contemporaneous magnetic susceptibility (MS) spikes (Figure 2.3; Figure 2.4), which mark clay-rich horizons.

Upper Paleocene-lower Eocene rocks at Mead and Dee streams have been logged perpendicular to dip above markers set at 0.0 m. The PETM onset is 157.6 m up-section of the Cretaceous/Tertiary Boundary at Mead (Hollis et al., 2005a), and 26.0 m up-section of a green bed at Dee (Hancock et al., 2003). Given available stratigraphy, sediment deposited from 54 to 53 Ma should lie from ~175-200 m at Mead, and from ~60-70 m at Dee. We re-logged these intervals, and exhumed fresh rock samples for laboratory analyses. Beds were delineated as limestone, siliceous limestone, marl, or marly-limestone.

Mead Stream sample splits were analyzed for $CaCO_3$ content using the "carbonate bomb" technique (Table 2.1), which has an analytical precision of ~0.5%. Crushed and dried splits of all samples from both sections were analyzed for carbon isotope composition in the Stable Isotope Laboratory at University of

California, Santa Cruz. Powdered samples (~100 μg) were analyzed using an Autocarb device coupled to either a Prism or Optima Mass Spectrometer. Carbon isotope values were calibrated to the vPDB standard using NBS-19 and an in house standard Carrara Marble (Table 2.1). Analytical precision for individual analyses is better than ±0.05 ‰. Oxygen isotope values were measured with a precision of ±0.1‰ (Table 2.1) but are not discussed because fluids have altered original $\delta^{18}O$.

RESULTS AND DISCUSSION

Studied intervals are principally limestone (Figure 2.2). However, both have two shorter intervals (181.6 – 188.1 m and 193.4 – 198.6 m at Mead; 62.2 – 64.8 m and 67.8 – 71.2 m at Dee) with two horizons of intermittent marl-rich beds. Marl-rich beds are 1–27 cm thick, and have lower $CaCO_3$ contents but higher amounts of fine silt to clay-sized siliciclastic material (~30%–45%) than "background" limestone beds (~15%) (Table 2.1; Figure 2.2). The only other Lower Limestone marl-rich horizon marks the PETM. Significant amounts of biogenic chert complicate some intervals (e.g. 160.0 – 182.5 m at Mead), which predictably record relatively low $CaCO_3$ content (Figure 2.2).

Bulk carbonate $\delta^{13}C$ records at Mead and Dee streams exhibit similar trends (Table 2.1; Figure 2.2; Figure 2.3; Figure 2.4). Across the studied interval, both records display background $\delta^{13}C$ values of 1.2–1.5 ‰ and four short, distinct decreases in $\delta^{13}C$ (n.b. lack of accessible outcrop precluded complete sampling at Mead). The lowest and upper middle anomalies are the largest (~0.9‰ and 0.6‰, respectively), whereas the lower middle and highest are the smallest (~0.2‰).

Although the four $\delta^{13}C$ anomalies span the four marl-rich horizons, adjacent limestone and marl beds have similar $\delta^{13}C$ values, suggesting these are primary signals in carbonate rather than manifestations of different lithology.

Rocks deposited in the Clarence River valley between 56 and 53 Ma contain five horizons characterized by marl-rich beds and significant decreases in $\delta^{13}C$. The lowermost horizon, with a ~2.5 ‰ drop in bulk carbonate $\delta^{13}C$, represents the PETM (Hancock et al., 2003; Hollis et al., 2005a). Based on shape, amplitude, and approximate timing of the other $\delta^{13}C$ anomalies, we correlate the overlying four horizons to the H1/ELMO, H2, I1, and I2 CIEs (Figure 2.2). The second horizon is found near the boundary of planktonic foraminiferal zones P6a and P6b, and just above the base of nannofossil zone NP11 (Figure 2.2). This is, with available data, the expected onset age (~53.6 Ma) of the H1 CIE and ELMO (Lourens et al., 2005). It has a CIE about one-third to one-half the amplitude of that across the PETM, similar to observations at other locations (Figure 2.1). The third horizon, positioned immediately above the H1 CIE and having a small $\delta^{13}C$ anomaly (Figure 2.2), is most likely the H2 CIE. The fourth horizon is found near the top of radiolarian zone RP8, within planktonic foraminiferal zone P6b and nannofossil zone NP11 (Figure 2.2). This correlates with the I1 CIE, and we note that the drop in $\delta^{13}C$ is less than that of H1, as found elsewhere (Figure 2.1). The fifth horizon, which lies just above I1, has a stratigraphic position and small $\delta^{13}C$ anomaly (Figure 2.2) similar to the I2 CIE. In summary, the same succession of CIEs – the PETM followed by two pairs, H1/H2 and I1/I2 - is recorded in lower Eocene sediments from widely separated deep-sea locations (Cramer et al., 2003)

and a high southern latitude upper slope environment. Clearly, all five CIEs represent global carbon cycle perturbations.

A remarkably complete lower Eocene section was recovered at ODP Site 1262 beneath 4755 m of water on Walvis Ridge. The lower two of five clay-rich horizons in this section correlate with the PETM and H1 CIEs, and mark $CaCO_3$ dissolution (Zachos et al., 2005; Lourens et al., 2005). We propose that the upper three clay-rich horizons correlate with the H2, I1, and I2 CIEs on the basis of their character (MS intensity) and stratigraphic position (Figure 2.4), and that they also represent periods of deep-sea $CaCO_3$ dissolution. Because absolute ages for all five events remain uncertain, we have derived an age model that is consistent with available age datums, but that accounts for decreasing sedimentation across the dissolution horizons. In this model, the average sedimentation rate between the end of the PETM, set at 55.4(7) Ma, and the onset of the H1 CIE, set at 53.6(2) Ma, is related to the average $CaCO_3$ content (extrapolated from MS, Lourens et al., 2005) over the same depth range (Table 2.2). Based on this relationship, variations in $CaCO_3$ content were linearly related to sedimentation rate between the onset of the H1 CIE and the conclusion of the I2 CIE. This gives onset ages for the H2, I1, and I2 CIEs of 53.5(2), 53.2(6), and 53.1(8) Ma, respectively. While these ages differ from those presented by Cramer et al. (2003), their ages also imply differential sedimentation rates at Site 1262 (Table 2.2), consistent with $CaCO_3$ dissolution and diminished deposition during the events.

Clay-rich horizons also mark the PETM in continental margin sections (e.g., Schmitz et al., 2001; Giusberti et al., 2007). In these cases, the PETM horizon is expanded, presumably because greater warmth and an accelerated

hydrological cycle enhanced continental erosion and terrigenous siliciclastic flux to continental margins (above references). Any simple sedimentation rate model for the Mead and Dee sections shows that clay-rich horizons representing the PETM, H1, H2, I1, and I2 are similarly expanded due to siliciclastic dilution. For example, our ages for the five events (Table 2.2) necessitate major increases in sedimentation rates across the PETM, H1, H2, I1, and I2 (Figure 2.3). Although evidence for warming has only been documented across the PETM and H1 CIEs, all five events are associated with enhanced terrestrial discharge to continental margins, and therefore, probably a rise in temperature. Interestingly, with our age model, sedimentation rate variations across the five horizons at Mead Stream do not scale to the magnitude of their associated CIEs. This may reflect differences in sea level or background temperature. In particular, the PETM occurred when background temperatures were relatively cool while the younger Eocene events occurred when temperatures were significantly warmer (Zachos et al., 2001).

CONCLUSIONS AND IMPLICATIONS

We document the lithology and bulk carbonate $\delta^{13}C$ of two outcrop sections originally emplaced on the upper continental slope of New Zealand during the early Paleogene. Five marl-rich horizons with low $\delta^{13}C$ and elevated sedimentation rates characterize both sections over the interval between 56 and 53 Ma. The lowest horizon marks the PETM (Hancock et al., 2003; Hollis et al., 2005a). Based on stratigraphic relationships and $\delta^{13}C$ signatures, the other four correlate to the H1, H2, I1, and I2 CIEs documented in deep-sea sections (Cramer et al., 2003; Lourens et al., 2005). However, in the deep-sea these events are marked by lowered sedimentation rates due to $CaCO_3$ dissolution. This suggests that there were five globally significant events between 56 and 53 Ma with similar characteristics at the same location but different responses between environments. Magnitude appears to be the primary distinguishing feature characterizing these events; the PETM was the most pronounced.

Because the five events have similar systemic responses in different environments, they probably have a similar generic cause. All five CIEs appear to represent massive inputs of isotopically light carbon during a long-term warming trend. As evidenced by condensed clay-layers at Walvis Ridge, the carbon inputs involved CO_2 increases that led to dissolution of carbonate on the sea floor. As evidenced by expanded marl-rich horizons in Clarence Valley, these carbon injections were associated with warming and an accelerated hydrologic cycle that increased continental erosion. If these inferences can be further substantiated, they constrain explanations for the PETM as well as early Paleogene climate and carbon cycling as a whole: a dynamic source must have *repeatedly* injected large

quantities of ^{13}C-depleted carbon into the ocean or atmosphere. Further, the nominal 100-kyr between carbon injection events (according to our age model) may indicate orbital pacing, as has been suggested for the PETM and HI CIEs (Lourens et al., 2005).

Marine gas hydrates have been the most widely cited source of the carbon injected during the PETM. This hypothesis argues that a precursor deep-sea warming dissociated gas hydrates in marine sediment to free gas bubbles, which escaped via seeps or sediment failure and subsequently oxidized to CO_2 (Dickens et al., 1997; Dickens, 2003). Our results may constrain this idea significantly. Modeling efforts suggest that marine gas hydrates, serving as a dynamic CH_4 "capacitor," could release a series of carbon injections across the early Eocene, but that due to estimates of the reservoir size and input flux to the capacitor itself, these injections would have to become successively smaller in mass (Dickens, 2003). The merits and demerits of other potential carbon sources have yet to be assessed within the context of multiple carbon injections.

ACKNOWLEDGMENTS

This work was funded by the U.S. National Science Foundation Biocomplexity Grant (EAR 0120727) and the N.Z. Foundation for Research, Science and Technology through the GNS Global Change Through Time programme. We thank Richard and Sue Murray for field access, and P. Strong, J. Crampton, J. Simes, V. Villasante-Marcos, and L. Lozano for field assistance.

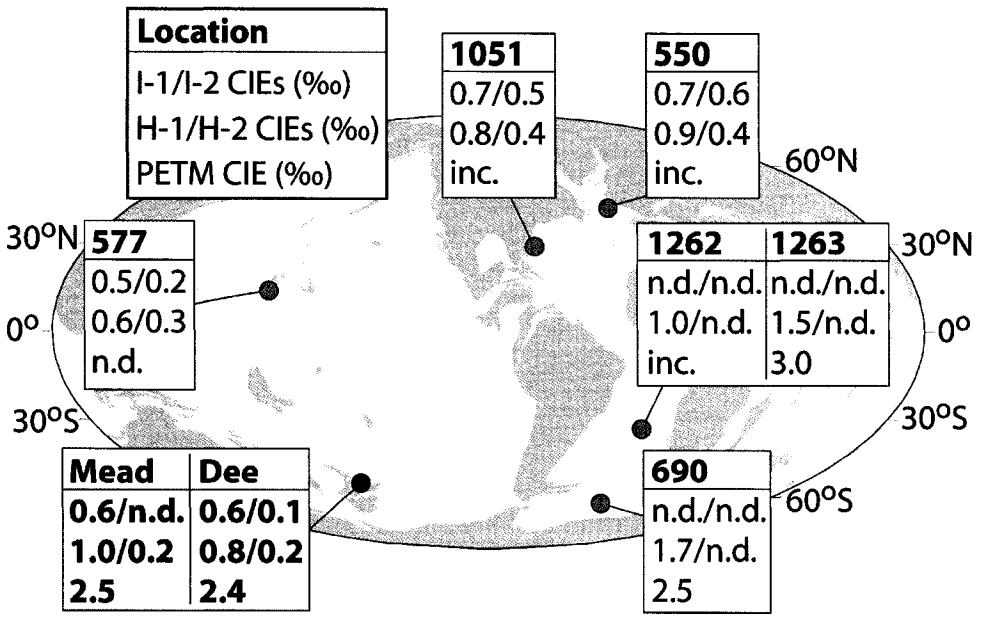

Figure 2.1: Earth at 53 Ma showing locations where early Eocene carbon isotope excursions (CIEs) have been documented in bulk carbonate (http://www.odsn.de/services/paleomap.html). These include DSDP Sites 550 and 577, ODP Sites 690 and 1051 (Cramer et al., 2003), ODP Sites 1262 and 1263 (Zachos et al., 2005; Lourens et al., 2005), and Mead Stream and Dee Stream (Hancock et al., 2003; Hollis et al., 2005; Table DR2). Numbers denote CIE magnitude; abbreviation "inc." denotes incomplete CIE recovery; abbreviation "n.d." denotes no data.

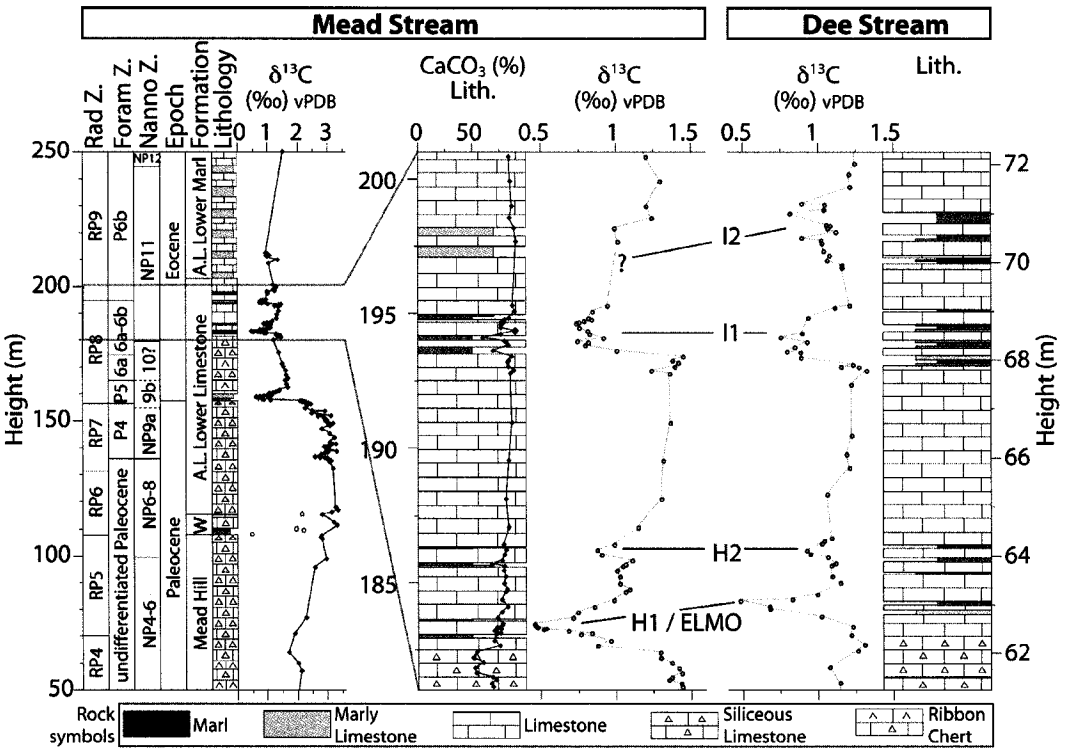

Figure 2.2. The early Paleogene sequence at Mead Stream and the detailed interval of interest (54 – 53 Ma) at Mead Stream and Dee Stream. Formation names, lithology, biostratigraphy, and bulk carbonate $\delta^{13}C$ for Mead Stream (excepting those across the interval of interest) are from Hollis et al. (2005) with minor biostratigraphic refinements. Mead Stream $\delta^{13}C$ open circles denote values depleted by organic carbon enrichment (Hollis et al., 2005). Formation abbreviations "W" and "A.L." refer to the Waipawa and Amuri Limestone, respectively. Mead Stream "Lower Marl" lithologic symbols, while emblematic of the section, do not represent actual heights. Four negative CIEs in the highlighted interval have been correlated to the H1, H2, I1, and I2 CIEs documented by Cramer et al. (2003).

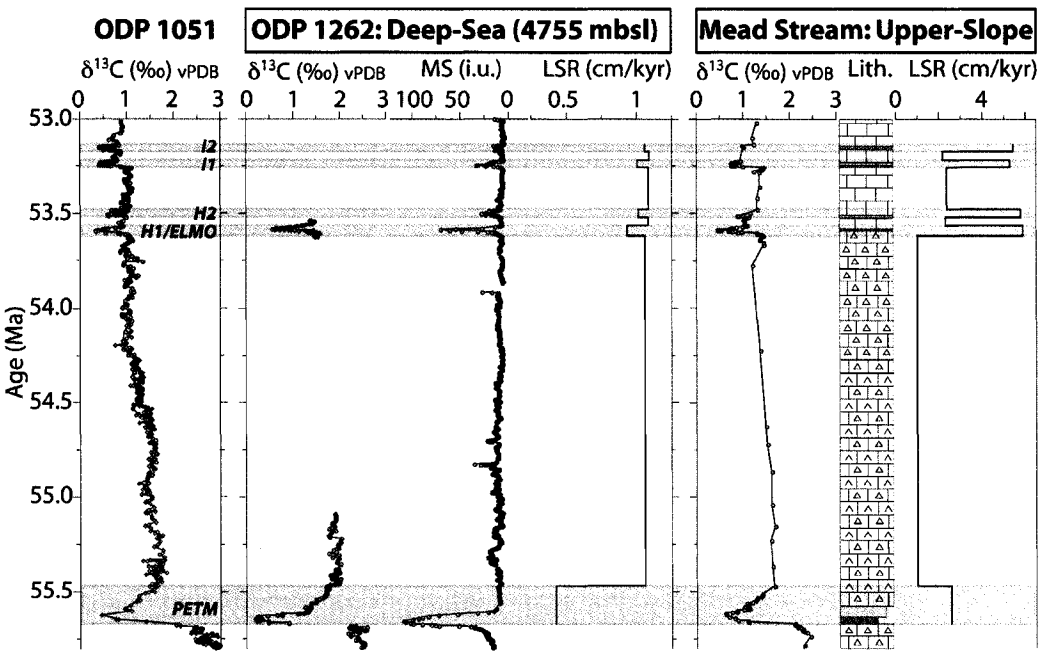

Figure 2.3. Linear sedimentation rates, deep-sea dissolution and marine margin dilution. The ODP Site 1051 early Eocene sequence contains a representative marine carbonate $\delta^{13}C$ record that highlights the PETM, H1, H2, I1, and I2 CIEs (Cramer et al., 2003). ODP Site 1262 bulk $\delta^{13}C$ records across the PETM (Zachos et al., 2005) and H1 (Lourens et al., 2005) CIEs, Site 1262 magnetic susceptibility (MS) (Zachos et al., 2004), and Mead Stream bulk carbonate $\delta^{13}C$ allow for correlation of these CIEs between locations. Increases in MS between the PETM and H1 correlate to a core break and an anomalous diagenetic bleb (Zachos et al., 2004). An age model generated for Site 1262 allows for calculation of linear sedimentation rate (LSR).

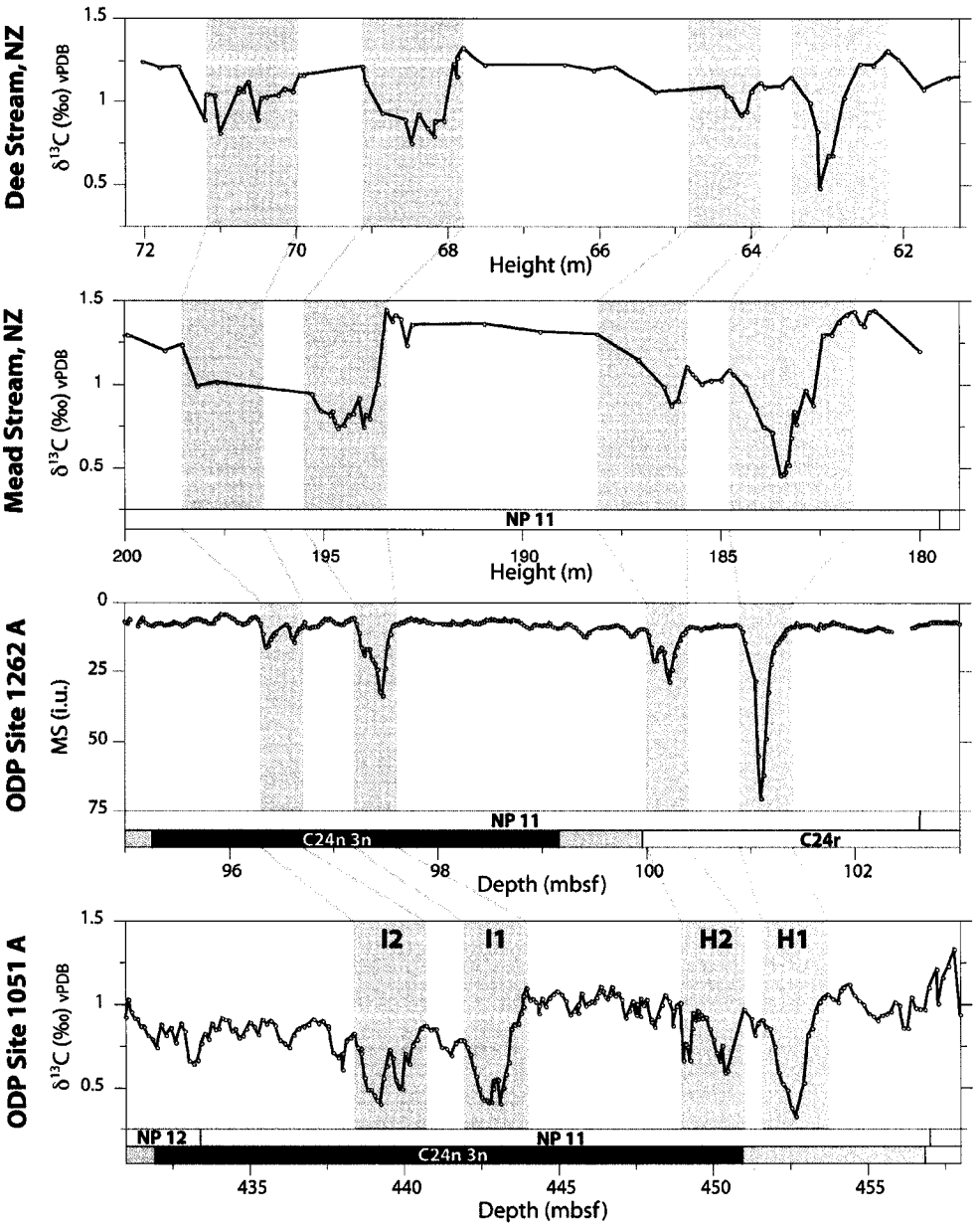

Figure 2.4. H1, H2, I1, and I2 correlations between sites of interest. Correlations based on a globally representative early Eocene marine $\delta^{13}C$ record from ODP Site 1051A (Cramer et al., 2003) across the H1, H2, I1, and I2 CIE intervals are illustrated for ODP Site 1262A, Mead Stream, and Dee Stream. Published magnetochron records from Sites 1051A (Mita, 2001; Cramer et al., 2003) and 1262A (Bowles, 2006) and nannofossil zonations from Sites 1051A (Cramer et al., 2003) and 1262A (Zachos et al., 2004) aid in establishing a link between shipboard measured magnetic susceptibility (MS) variations at Site 1262A (Zachos et al., 2004) and global CIEs. Mead Stream nannofossil zonations are reported in Hollis et al., (2005) and Figure 2.2.

TABLE 2.1. LITHOLOGIC AND ISOTOPIC RESULTS

Location	Field No.	NZFR (P30/)	Rock Type*	Height (m)	$CaCO_3$ (%)	$\delta^{13}C$ (‰)	$\delta^{18}O$ (‰)
Dee Stream	DS2-F12	f1237	M	93.95	N.D.	0.80	N.D.
Dee Stream	DS2-G20	f1238	L	92.45	N.D.	0.88	N.D.
Dee Stream	DS2-G18	f1241	L	90.25	N.D.	0.80	N.D.
Dee Stream	DS2-F10	f1242	M	89.75	N.D.	0.63	N.D.
Dee Stream	DS-F21	f1243	M	88.21	N.D.	0.40	N.D.
Dee Stream	DS2-G16	f1246	L	83.65	N.D.	0.89	N.D.
Dee Stream	DS-F20	f1247	M	83.45	N.D.	0.88	N.D.
Dee Stream	DS-F19	f1248	M	80.09	N.D.	0.83	N.D.
Dee Stream	DS-F18	f1249	M	77.20	N.D.	1.20	N.D.
Dee Stream	DS2-G13	f1250	L	77.10	N.D.	1.15	N.D.
Dee Stream	DEE ES-2 B119	N.A.	L	72.02	N.D.	1.24	-3.27
Dee Stream	DEE ES-2 B116	N.A.	L	71.80	N.D.	1.20	-3.35
Dee Stream	DEE ES-2 B114	N.A.	L	71.55	N.D.	1.21	-3.36
Dee Stream	DS2-G10	f1255	L	71.20	N.D.	0.89	N.D.
Dee Stream	DEE ES-2 B109 12-20	N.A.	L	71.18	N.D.	1.04	-3.25
Dee Stream	DEE ES-2 B109 0-10	N.A.	L	71.07	N.D.	1.04	-3.20
Dee Stream	DS-F17	f1256	M	71.00	N.D.	0.81	N.D.
Dee Stream	DEE ES-2 B107 16-21	N.A.	L	70.77	N.D.	1.05	-3.18

Dee Stream	DS2-G9	f1257	L	70.75	N.D.	1.08	N.D.
Dee Stream	DEE ES-2 B107 8-15	N.A.	L	70.70	N.D.	1.06	-3.41
Dee Stream	DEE ES-2 B107 0-9	N.A.	L	70.63	N.D.	1.12	-3.31
Dee Stream	DS2-F22	f1258	M	70.50	N.D.	0.89	N.D.
Dee Stream	DEE ES-2 B105	N.A.	ML	70.46	N.D.	1.02	-3.26
Dee Stream	DEE ES-2 B104 15-23	N.A.	L	70.39	N.D.	1.02	-3.08
Dee Stream	DEE ES-2 B104 0-7	N.A.	L	70.24	N.D.	1.04	-3.15
Dee Stream	DEE ES-2 B103	N.A.	L	70.15	N.D.	1.07	-3.09
Dee Stream	DEE ES-2 B101	N.A.	ML	70.04	N.D.	1.06	-3.29
Dee Stream	DEE ES-2 B99	N.A.	L	69.95	N.D.	1.16	-3.13
Dee Stream	DS2-G8	f1262	L	69.90	N.D.	1.16	N.D.
Dee Stream	DEE ES-2 B92	N.A.	L	69.12	N.D.	1.21	-3.08
Dee Stream	DS2-G7	f1263	L	69.07	N.D.	1.11	N.D.
Dee Stream	DEE ES-2 B90	N.A.	L	68.86	N.D.	0.93	-3.16
Dee Stream	DEE ES-2 B86 12-18	N.A.	L	68.55	N.D.	0.89	-3.15
Dee Stream	DS2-G6	f1266	L	68.47	N.D.	0.75	N.D.
Dee Stream	DEE ES-2 B85	N.A.	ML	68.38	N.D.	0.92	-3.24
Dee Stream	DEE ES-2 B82 15-20	N.A.	L	68.27	N.D.	0.84	-3.28
Dee Stream	DS-G26	f1268	L	68.17	N.D.	0.79	N.D.
Dee Stream	DEE ES-2 B82 3-11	N.A.	L	68.16	N.D.	0.88	-3.16
Dee Stream	DEE ES-2 B81	N.A.	ML	68.05	N.D.	0.89	-3.16

Dee Stream	DEE ES-2 B79	N.A.	ML	67.91	N.D.	1.23	-3.36
Dee Stream	DS-G25	f1271	L	67.87	N.D.	1.15	N.D.
Dee Stream	DEE ES-2 B78	N.A.	L	67.87	N.D.	1.27	-3.25
Dee Stream	DEE ES-2 B77	N.A.	L	67.79	N.D.	1.32	-3.21
Dee Stream	DEE ES-2 B74	N.A.	L	67.51	N.D.	1.22	-3.19
Dee Stream	DEE ES-2 B66	N.A.	L	66.46	N.D.	1.22	-3.24
Dee Stream	DEE ES-2 B62	N.A.	L	66.08	N.D.	1.19	-3.04
Dee Stream	DEE ES-2 B58	N.A.	L	65.80	N.D.	1.21	-2.99
Dee Stream	DEE ES-2 B55	N.A.	L	65.26	N.D.	1.06	-3.07
Dee Stream	DEE ES-1 B44	N.A.	L	64.38	N.D.	1.09	-2.89
Dee Stream	DEE ES-1 B43	N.A.	L	64.32	N.D.	1.04	-3.23
Dee Stream	DEE ES-1 B42	N.A.	L	64.26	N.D.	1.02	-2.93
Dee Stream	DEE ES-1 B40	N.A.	L	64.13	N.D.	0.92	-3.02
Dee Stream	DEE ES-1 B39	N.A.	L	64.05	N.D.	0.94	-3.10
Dee Stream	DEE ES-1 B38	N.A.	L	63.99	N.D.	1.06	-3.10
Dee Stream	DEE ES-1 B36 5-10	N.A.	L	63.87	N.D.	1.11	-2.92
Dee Stream	DEE ES-1 B36 0-5	N.A.	L	63.82	N.D.	1.09	-3.09
Dee Stream	DEE ES-1 B33	N.A.	L	63.59	N.D.	1.09	-2.93
Dee Stream	DEE ES-1 B32	N.A.	L	63.46	N.D.	1.15	-3.30
Dee Stream	DEE ES-1 B30 Top	N.A.	L	63.22	N.D.	0.99	-3.26
Dee Stream	DEE ES-1 B30 Bottom	N.A.	L	63.12	N.D.	0.83	-3.39

Dee Stream	DS2-F7	f1275	M	63.09	N.D.	0.48	
Dee Stream	DEE ES-1 B28 Top	N.A.	L	62.98	N.D.	0.67	-3.28
Dee Stream	DEE ES-1 B28 Bottom	N.A.	L	62.93	N.D.	0.68	-3.29
Dee Stream	DEE ES-1 B26	N.A.	L	62.77	N.D.	1.02	-3.14
Dee Stream	DEE ES-1 B21	N.A.	L	62.56	N.D.	1.23	-3.10
Dee Stream	DEE ES-1 B18	N.A.	L	62.39	N.D.	1.22	-3.19
Dee Stream	DEE ES-1 B14	N.A.	L	62.19	N.D.	1.30	-3.19
Dee Stream	DEE ES-1 B11	N.A.	L	62.06	N.D.	1.26	-3.22
Dee Stream	DEE ES-1 B5	N.A.	L	61.73	N.D.	1.07	-3.16
Dee Stream	DEE ES-1 B1	N.A.	L	61.41	N.D.	1.14	-3.12
Dee Stream	DS-G23	f1278	L	60.86	N.D.	1.17	N.D.
Dee Stream	DS2-F8	f1279	M	59.53	N.D.	1.28	N.D.
Dee Stream	DS-G22	f1282	L	55.66	N.D.	1.34	N.D.
Dee Stream	DS-F15	f1284	M	52.25	N.D.	1.55	N.D.
Dee Stream	DS-G21	f1285	L	50.32	N.D.	1.67	N.D.
Dee Stream	DS-G20	f1287	L	46.10	N.D.	1.65	N.D.
Dee Stream	DS-G19	f1289	L	41.59	N.D.	1.52	N.D.
Dee Stream	DS-G18	f1290	L	36.83	N.D.	1.49	N.D.
Dee Stream	DS-G17	f1291	L	31.89	N.D.	1.63	N.D.
Dee Stream	DSPE-36C	N.A.	L	29.93	N.D.	1.58	N.D.
Dee Stream	DSPE-36B	N.A.	L	29.89	N.D.	1.62	N.D.

Dee Stream	DSPE-36A	N.A.	L	29.85	N.D.	1.56	N.D.
Dee Stream	DSPE-33B	N.A.	L	29.32	N.D.	1.51	N.D.
Dee Stream	DSPE-33A	N.A.	L	29.27	N.D.	1.49	N.D.
Dee Stream	DSPE-27B	N.A.	L	28.56	N.D.	1.48	N.D.
Dee Stream	DSPE-27A	N.A.	L	28.53	N.D.	1.51	N.D.
Dee Stream	DSPE-26B	N.A.	L	27.99	N.D.	1.34	N.D.
Dee Stream	DSPE-26A	N.A.	L	27.95	N.D.	1.35	N.D.
Dee Stream	DSPE-25C	N.A.	L	27.68	N.D.	1.24	N.D.
Dee Stream	DSPE-25B	N.A.	L	27.65	N.D.	1.18	N.D.
Dee Stream	DSPE-25A	N.A.	L	27.61	N.D.	1.20	N.D.
Dee Stream	DSPE-24B	N.A.	L	27.43	N.D.	1.16	N.D.
Dee Stream	DSPE-24A	N.A.	L	27.38	N.D.	1.16	N.D.
Dee Stream	DSPE-23	N.A.	L	27.10	N.D.	1.09	N.D.
Dee Stream	DSPE-22B	N.A.	L	27.01	N.D.	1.16	N.D.
Dee Stream	DSPE-22A	N.A.	ML	26.92	N.D.	0.98	N.D.
Dee Stream	DSPE-21	N.A.	ML	26.81	N.D.	0.94	N.D.
Dee Stream	DSPE-20C	N.A.	ML	26.75	N.D.	0.86	N.D.
Dee Stream	DSPE-20B	N.A.	ML	26.71	N.D.	0.64	N.D.
Dee Stream	DSPE-20A	N.A.	ML	26.67	N.D.	0.76	N.D.
Dee Stream	DSPE-19C	N.A.	ML	26.53	N.D.	0.66	N.D.
Dee Stream	DSPE-19B	N.A.	ML	26.50	N.D.	0.79	N.D.

Dee Stream	DSPE-19A	N.A.	ML	26.44	N.D.	0.76	N.D.
Dee Stream	DSPE-18B	N.A.	ML	26.33	N.D.	0.94	N.D.
Dee Stream	DSPE-18A(C)	N.A.	ML	26.29	N.D.	1.03	N.D.
Dee Stream	DSPE-18A(B)	N.A.	ML	26.26	N.D.	1.14	N.D.
Dee Stream	DSPE-18A(A)	N.A.	ML	26.22	N.D.	1.33	N.D.
Dee Stream	DSPE-17A	N.A.	ML	25.97	N.D.	2.05	N.D.
Dee Stream	DSPE-15D	N.A.	L	25.82	N.D.	2.13	N.D.
Dee Stream	DSPE-15C	N.A.	L	25.78	N.D.	2.04	N.D.
Dee Stream	DSPE-15B	N.A.	L	25.74	N.D.	2.04	N.D.
Dee Stream	DSPE-15A	N.A.	L	25.69	N.D.	1.97	N.D.
Dee Stream	DSPE-14B	N.A.	L	25.63	N.D.	2.07	N.D.
Dee Stream	DSPE-14A	N.A.	L	25.59	N.D.	2.00	N.D.
Dee Stream	DSPE-13B	N.A.	L	25.37	N.D.	2.09	N.D.
Dee Stream	DSPE-13A2-(b)	N.A.	L	25.32	N.D.	2.05	N.D.
Dee Stream	DSPE-13A2-(a)	N.A.	L	25.27	N.D.	2.12	N.D.
Dee Stream	DS-F9	f1305	M	23.50	N.D.	2.57	N.D.
Dee Stream	DS-G12	f1306	L	23.35	N.D.	2.65	N.D.
Dee Stream	DS-F10	f1307	M	23.29	N.D.	2.58	N.D.
Dee Stream	DS-G10	f1308	L	22.70	N.D.	3.00	N.D.
Dee Stream	DS-F8	f1309	M	21.82	N.D.	2.93	N.D.
Dee Stream	DS-G9	f1310	L	18.05	N.D.	3.35	N.D.

Dee Stream	DS-F7	f1311	M	17.40	N.D.	3.14	N.D.
Dee Stream	DS-F6	f1313	M	14.26	N.D.	3.11	N.D.
Dee Stream	DS-G8	f1314	L	13.85	N.D.	3.26	N.D.
Dee Stream	DS-F5	f1315	M	11.04	N.D.	3.30	N.D.
Dee Stream	DS-G7	f1316	L	10.06	N.D.	3.48	N.D.
Dee Stream	DS-F4	f1322	M	5.93	N.D.	3.12	N.D.
Dee Stream	DS-G6	f1327	L	5.18	N.D.	3.64	N.D.
Dee Stream	DS-G5	f1331	L	1.14	N.D.	3.58	N.D.
Dee Stream	DS-G4	f1333	L	0.41	N.D.	3.55	N.D.
Dee Stream	DS-G3	f1334	L	0.10	N.D.	3.45	N.D.
Dee Stream	DS-G2	f1336	L	-0.10	N.D.	3.21	N.D.
Dee Stream	DS-F3	f1337	M	-0.30	N.D.	3.46	N.D.
Dee Stream	DS-G1C	f1338	L	-0.74	N.D.	2.38	N.D.
Dee Stream	DS-F2	f1339	M	-1.17	N.D.	1.98	N.D.
Dee Stream	DS-F1	f1342	M	-4.08	N.D.	1.86	N.D.
Dee Stream	DS-G1	f1343	L	-4.68	N.D.	2.12	N.D.
Mead Stream	MD77	f538		250.00	N.D.	1.51	N.D.
Mead Stream	MD LM 10.4	N.A.	L	211.87	N.D.	0.94	-3.02
Mead Stream	MD LM 10.3	N.A.	L	211.72	N.D.	0.99	-3.17
Mead Stream	MD LM 10.2 B	N.A.	L	211.62	N.D.	1.01	-3.27
Mead Stream	MD LM 10.2 A	N.A.	L	211.52	N.D.	1.01	-3.32

Mead Stream	MD LM 10.1	N.A.	L	211.45	N.D.	1.06	-3.33
Mead Stream	MD LM 9.5	N.A.	L	211.07	N.D.	0.96	-3.36
Mead Stream	MD LM 9.3	N.A.	L	210.95	N.D.	0.98	-3.26
Mead Stream	MD LM 9.2	N.A.	L	210.79	N.D.	0.98	-3.19
Mead Stream	MD79	N.A.		210.00	N.D.	1.34	N.D.
Mead Stream	MS3-G41	f1236		208.65	N.D.	1.04	N.D.
Mead Stream	MD EX-J	N.A.	L	200.83	83.7	1.20	-3.12
Mead Stream	MD EX-I	N.A.	L	199.93	84.9	1.29	-3.03
Mead Stream	MD EX-H	N.A.	L	198.99	86.7	1.20	-3.21
Mead Stream	MD EX-G	N.A.	L	198.56	84.5	1.24	-3.14
Mead Stream	MD EX-F	N.A.	L	198.18	88.5	0.99	-3.55
Mead Stream	MD EX-E	N.A.	L	197.68	90.4	1.01	-3.53
Mead Stream	MD ES-2 B23	N.A.	L	195.30	87.2	0.94	-3.25
Mead Stream	MD ES-2 B22	N.A.	L	195.07	88.7	0.84	-3.49
Mead Stream	MD ES-2 B20	N.A.	M	194.83	83.6	0.82	-3.47
Mead Stream	MD ES-2 B19	N.A.	L	194.76	79.7	0.84	-3.11
Mead Stream	MD ES-2 B18	N.A.	L	194.72	79.2	0.79	-3.14
Mead Stream	MD ES-2 B17	N.A.	L	194.68	76.9	0.75	-3.09
Mead Stream	MD ES-2 B16	N.A.	L	194.63	78.4	0.74	-3.30
Mead Stream	MD ES-2 B15	N.A.	L	194.58	76.7	N.D.	N.D.
Mead Stream	MD ES-2 B14	N.A.	L	194.48	76.6	0.76	-3.47

Mead Stream	MD ES-2 B13	N.A.	L	194.36	89.6	0.81	-3.79
Mead Stream	MD ES-2 B12	N.A.	L	194.24	76.5	0.82	-3.35
Mead Stream	MD ES-2 B11	N.A.	M	194.09	59.6	0.92	-2.65
Mead Stream	MD ES-2 B10	N.A.	L	193.98	79.7	0.74	-3.45
Mead Stream	MD ES-2 B9	N.A.	L	193.93	81.3	0.82	-3.45
Mead Stream	MD ES-2 B8	N.A.	L	193.83	83.5	0.80	-3.71
Mead Stream	MD ES-2 B7	N.A.	M	193.63	69.0	1.00	-2.88
Mead Stream	MD ES-2 B6	N.A.	L	193.40	86.3	1.44	-3.33
Mead Stream	MD ES-2 B5	N.A.	L	193.26	83.7	1.38	-3.17
Mead Stream	MD ES-2 B4	N.A.	L	193.18	82.7	1.41	-3.21
Mead Stream	MD ES-2 B3	N.A.	L	193.04	83.3	1.39	-3.20
Mead Stream	MD ES-2 B2	N.A.	L	192.89	88.5	1.23	-3.97
Mead Stream	MD ES-2 B1	N.A.	L	192.76	85.2	1.36	-3.34
Mead Stream	MD EX-D	N.A.	L	190.95	86.8	1.36	-3.22
Mead Stream	MD EX-C	N.A.	L	189.55	83.8	1.31	-3.06
Mead Stream	MD EX-B	N.A.	L	188.12	81.3	1.30	-3.18
Mead Stream	MD EX-A	N.A.	L	187.08	83.7	1.15	-3.44
Mead Stream	MD EX-AA	N.A.	L	186.43	79.2	0.99	-3.53
Mead Stream	MD ES-1 B32	N.A.	L	186.24	81.2	0.88	-3.45
Mead Stream	MD ES-1 B30 9-19	N.A.	L	186.07	79.9	0.90	-3.24
Mead Stream	MD ES-1 B29	N.A.	L	185.84	77.5	1.11	-3.00

Mead Stream	MD ES-1 B28	N.A.	M	185.71	68.0	1.06	-2.74
Mead Stream	MD ES-1 B27	N.A.	ML	185.63	79.7	1.04	-2.88
Mead Stream	MD ES-1 B26 B	N.A.	L	185.48	79.1	1.00	-3.39
Mead Stream	MD ES-1 B26 A	N.A.	L	185.25	81.0	1.02	-3.47
Mead Stream	MD ES-1 B25	N.A.	L	184.98	79.6	1.02	-3.25
Mead Stream	MD ES-1 B24	N.A.	L	184.78	82.2	1.09	-3.34
Mead Stream	MD ES-1 B23	N.A.	L	184.68	80.7	1.06	-3.19
Mead Stream	MD ES-1 B22 7-20	N.A.	L	184.38	77.2	0.99	-3.13
Mead Stream	MD ES-1 B21	N.A.	L	184.12	82.6	0.86	-3.34
Mead Stream	MD ES-1 B20	N.A.	L	183.92	77.2	0.75	-3.29
Mead Stream	MD ES-1 B18	N.A.	L	183.70	73.2	0.71	-3.09
Mead Stream	MD ES-1 B16 10-19	N.A.	L	183.49	77.9	0.46	-3.65
Mead Stream	MD ES-1 B16 5-10	N.A.	L	183.42	77.1	0.47	-3.64
Mead Stream	MD ES-1 B16 0-5	N.A.	L	183.37	72.6	0.48	-3.69
Mead Stream	MD ES-1 B15 B	N.A.	L	183.32	75.5	0.53	-3.55
Mead Stream	MD ES-1 B15 A	N.A.	L	183.28	76.7	0.52	-3.84
Mead Stream	MD ES-1 B14	N.A.	L	183.22	70.3	0.68	-3.37
Mead Stream	MD ES-1 B13 2-10	N.A.	L	183.14	76.0	0.84	-3.60
Mead Stream	MD ES-1 B13 0-2	N.A.	L	183.09	72.1	0.76	-3.46
Mead Stream	MD ES-1 B11	N.A.	L	182.86	70.3	0.96	-3.83
Mead Stream	MD ES-1 B10	N.A.	L	182.67	75.2	0.88	-3.74

Mead Stream	MD ES-1 B9	N.A.	L	182.42	54.2	1.29	-3.03
Mead Stream	MD ES-1 B8	N.A.	L	182.21	50.9	1.30	-3.11
Mead Stream	MD ES-1 B7	N.A.	L	182.03	60.1	1.37	-2.91
Mead Stream	MD ES-1 B6	N.A.	L	181.83	52.6	1.42	-3.41
Mead Stream	MD ES-1 B5	N.A.	L	181.63	54.0	1.44	-2.86
Mead Stream	MD ES-1 B4	N.A.	L	181.50	68.9	1.37	-3.21
Mead Stream	MD ES-1 B3	N.A.	L	181.39	72.0	1.35	-3.26
Mead Stream	MD ES-1 B2	N.A.	L	181.26	67.9	1.43	-3.05
Mead Stream	MD ES-1 B1	N.A.	L	181.12	69.3	1.44	-3.07
Mead Stream	MD83	f535	L	180.00	N.D.	1.20	N.D.
Mead Stream	MS3-G31	f1223	L	175.47	N.D.	1.37	N.D.
Mead Stream	MD-G25	f1150	RC	171.35	N.D.	1.49	N.D.
Mead Stream	MD-G24	f1149	RC	170.36	N.D.	1.52	N.D.
Mead Stream	MD-G23	f1148	RC	168.88	N.D.	1.61	N.D.
Mead Stream	MD-G22	f1146	RC	167.09	N.D.	1.62	N.D.
Mead Stream	MD-G21	f1145	RC	165.94	N.D.	1.68	N.D.
Mead Stream	MD-G20	f1144	RC	165.16	N.D.	1.60	N.D.
Mead Stream	MD-G19	f1143	RC	163.79	N.D.	1.63	N.D.
Mead Stream	MD-G18	f1141	RC	162.72	N.D.	1.67	N.D.
Mead Stream	MSPE135	f1222	RC	161.56	N.D.	1.40	-3.64
Mead Stream	MSPE134	f1221	RC	161.43	N.D.	1.40	-3.76

Mead Stream	MSPE133	f1220	RC	161.28	N.D.	1.38	-3.60
Mead Stream	MSPE132	f1219	RC	161.10	N.D.	1.30	-3.34
Mead Stream	MSPE131	f1218	RC	160.92	N.D.	1.28	-3.34
Mead Stream	MSPE130	f1217	RC	160.73	N.D.	1.26	-3.59
Mead Stream	MSPE129	f1216	RC	160.50	N.D.	1.19	-3.09
Mead Stream	MSPE128	f1215	RC	160.33	N.D.	1.07	-3.36
Mead Stream	MSPE127	f1214	RC	160.17	N.D.	1.10	-3.22
Mead Stream	MSPE126	f1213	ML	159.94	N.D.	1.02	-3.41
Mead Stream	MSPE123	f1212	ML	159.65	N.D.	1.13	-3.31
Mead Stream	MSPE122	f1211	ML	159.59	N.D.	1.09	-3.60
Mead Stream	MSPE121	f1210	ML	159.50	N.D.	1.00	-3.32
Mead Stream	MSPE120	f1209	ML	159.39	N.D.	0.87	-3.73
Mead Stream	MSPE118	f1208	ML	159.18	N.D.	0.85	-3.62
Mead Stream	MSPE117	f1207	ML	159.10	N.D.	0.75	-4.09
Mead Stream	MSPE116	f1206	ML	159.00	N.D.	0.62	-4.10
Mead Stream	MSPE114	f1205	ML	158.81	N.D.	0.62	-3.65
Mead Stream	MSPE111B	f1204	ML	158.49	N.D.	0.69	-3.95
Mead Stream	MSPE111A	f1203	ML	158.29	N.D.	0.81	-3.77
Mead Stream	MSPE110C	f1202	ML	158.04	N.D.	0.88	-3.91
Mead Stream	MSPE110B	f1201	ML	157.94	N.D.	1.09	-3.85
Mead Stream	MSPE110A	f1200	M	157.84	N.D.	1.10	-3.79

Mead Stream	MSPE107	f1399	M	157.60	N.D.	2.11	-3.59
Mead Stream	MSPE106	f1398	L	157.50	N.D.	2.10	-3.57
Mead Stream	MSPE104	f1397	L	157.38	N.D.	2.17	-3.25
Mead Stream	MSPE103	f1396	L	157.33	N.D.	2.16	-3.16
Mead Stream	MSPE102	f1395	L	157.29	N.D.	2.15	-3.24
Mead Stream	MSPE101	f1394	L	157.25	N.D.	2.22	-3.43
Mead Stream	MSPE99	f1393	L	157.10	N.D.	2.28	-3.39
Mead Stream	MSPE98	f1392	L	157.04	N.D.	2.28	-3.20
Mead Stream	MSPE97	f1391	L	156.98	N.D.	2.25	-3.87
Mead Stream	MSPE96	f1390	L	156.90	N.D.	2.28	-3.53
Mead Stream	MSPE94	f1389	L	156.76	N.D.	2.36	-3.08
Mead Stream	MD-G10	f1124	L	156.40	N.D.	2.44	N.D.
Mead Stream	MD-G9	f1123	L	155.59	N.D.	2.31	N.D.
Mead Stream	MD-G8	f1121	L	154.71	N.D.	2.25	N.D.
Mead Stream	MD-G7	f1119	L	153.90	N.D.	2.48	N.D.
Mead Stream	MS/J1	f1107	L	153.69	N.D.	2.91	N.D.
Mead Stream	MD-G6	f1117	L	152.89	N.D.	2.47	N.D.
Mead Stream	MS/J2	f1106	L	151.96	N.D.	3.12	N.D.
Mead Stream	MD-G5	f1115	L	151.80	N.D.	2.69	N.D.
Mead Stream	MD-G4	f1113	L	151.01	N.D.	2.89	N.D.
Mead Stream	MS/J3	f1105	L	150.34	N.D.	2.98	N.D.

Mead Stream	MD-G3	f1112	L	150.09	N.D.	2.94	N.D.
Mead Stream	MD-G2	f1110	L	149.14	N.D.	3.18	N.D.
Mead Stream	MS/J4	f1104	L	148.73	N.D.	3.03	N.D.
Mead Stream	MD-G1	f1109	L	148.31	N.D.	3.09	N.D.
Mead Stream	MS/J5	f1103	L	147.11	N.D.	2.81	N.D.
Mead Stream	MS/J6	f1101	L	145.41	N.D.	3.07	N.D.
Mead Stream	MS/J6B	f1102	L	143.79	N.D.	3.23	N.D.
Mead Stream	MS/J7	f1100	L	142.18	N.D.	3.09	N.D.
Mead Stream	MS/J39	f1098	L	141.47	N.D.	3.28	N.D.
Mead Stream	MS/J38	f1097	L	141.33	N.D.	3.14	N.D.
Mead Stream	MS/J8	f1096	L	140.40	N.D.	2.89	N.D.
Mead Stream	MS/J37	f1095	L	140.01	N.D.	3.05	N.D.
Mead Stream	MS/J36	f1093	L	139.42	N.D.	2.97	N.D.
Mead Stream	MS/J9	f1092	L	138.78	N.D.	3.31	N.D.
Mead Stream	MS/J35	f1091	L	138.45	N.D.	3.01	N.D.
Mead Stream	MS/J33	f1088	L	138.04	N.D.	2.92	N.D.
Mead Stream	MS/J28	f1086	L	137.60	N.D.	2.79	N.D.
Mead Stream	MS/J24	f1080	L	137.09	N.D.	2.77	N.D.
Mead Stream	MS/J12	f1075	L	136.79	N.D.	2.59	N.D.
Mead Stream	MS/J13	f1074	L	136.63	N.D.	2.76	N.D.
Mead Stream	MS/J15B	f1072	L	136.55	N.D.	2.76	N.D.

Mead Stream	MS/J16	f1070	L	136.47	N.D.	2.91	N.D.
Mead Stream	MS/J22	f1069	L	136.24	N.D.	3.00	N.D.
Mead Stream	MS/J17	f1066	L	135.76	N.D.	3.02	N.D.
Mead Stream	MS/J20	f1065	L	135.44	N.D.	3.12	N.D.
Mead Stream	MS/J18	f1064	L	135.13	N.D.	3.11	N.D.
Mead Stream	MS/J19B	f1063	L	134.75	N.D.	3.09	N.D.
Mead Stream	MS/J19	f1062	L	132.38	N.D.	3.20	N.D.
Mead Stream	MS/J31	f1059	L	118.03	N.D.	3.27	N.D.
Mead Stream	MS/J30	f1058	L	117.08	N.D.	3.35	N.D.
Mead Stream	MS/J29	f1057	L	116.35	N.D.	3.14	N.D.
Mead Stream	MS23	f1054	L	115.63	N.D.	2.15	N.D.
Mead Stream	MS26	f1050	M	115.44	N.D.	2.82	N.D.
Mead Stream	MS14	f1048	L	112.53	N.D.	3.22	N.D.
Mead Stream	MS15	f1047	L	111.53	N.D.	3.32	N.D.
Mead Stream	MS12	f1042	M	110.24	N.D.	1.95	N.D.
Mead Stream	MS11	f1041	M	109.70	N.D.	2.20	N.D.
Mead Stream	MS1A	f1033	M	108.30	N.D.	0.48	N.D.
Mead Stream	MS18	f1028	L	107.80	N.D.	2.81	N.D.
Mead Stream	MD/F12	f1027	L	107.08	N.D.	2.78	N.D.
Mead Stream	MD/F13	f1026	L	106.57	N.D.	2.82	N.D.
Mead Stream	MD93	N.A.	L	99.00	N.D.	2.96	N.D.

Mead Stream	MD94	N.A.	L	96.00	N.D.	2.58	N.D.
Mead Stream	MD95	N.A.	L	77.00	N.D.	2.29	N.D.
Mead Stream	MD96	N.A.	L	71.00	N.D.	1.91	N.D.
Mead Stream	MD97	N.A.	L	64.00	N.D.	1.71	N.D.
Mead Stream	MD98	f525	RC	60.00	N.D.	2.03	N.D.
Mead Stream	MD99	f524	RC	57.00	N.D.	2.14	N.D.
Mead Stream	MD100	N.A.	RC	47.00	N.D.	2.02	N.D.

*Rock type abbreviations are as follows: "M" = marl, "L" = limestone, "ML" = marly limestone, "RC" = ribbon chert.

TABLE 2.2. EARLY EOCENE CIE AGES

Event	Age used in this study (Ma)*	Source	Alternative age (Ma)†	Source	Mead Stream height (m)	Dee Stream height (m)	1051A/B depth (mbsf)§	1051 depth (mcd)	1262A depth (mbsf)	1262 depth (mcd)
PETM onset	55.67	L	55.67	L	157.60	26.00	§512.90	539.44	121.89	140.00
PETM conclusion	55.47	R	55.60	C	162.72	29.85	§510.60	537.14	121.04	139.15
H1 onset	53.62	L	54.36	C	181.63	62.19	453.73	474.05	101.40	117.45
H1 conclusion	53.57	this study	54.28	C	184.78	63.46	451.61	471.93	100.90	116.95
H2 onset	53.52	this study	54.25	C	185.84	63.87	451.03	471.35	100.40	116.45
H2 conclusion	53.48	this study	54.18	C	188.12	64.82	448.97	469.29	100.00	116.05
I1 onset	53.26	this study	53.98	C	193.40	67.79	443.99	464.31	97.60	113.65
I1 conclusion	53.22	this study	53.92	C	195.50	69.12	441.95	462.27	97.20	113.25
I2 onset	53.18	this study	53.87	C	196.50	70.04	440.73	461.05	96.70	112.75
I2 conclusion	53.14	this study	53.79	C	198.56	71.18	438.40	458.72	96.30	112.35

*One of two ages proposed by Lourens et al. (2005) for the onset of the PETM serves as the base age in our model. The PETM conclusion age was set by subtracting a proposed PETM duration (Röhl et al., 2000) from the noted PETM onset.

†Alternative event ages are proscribed from a floating age model (Cramer et al., 2003) constrained by a proposed PETM onset age (Lourens et al., 2005).

§Denotes 1051 B depths.

#Röhl, U., Bralower, T. J., Norris, R. D., and Wefer, G., 2000, New chronology for the late Paleocene thermal maximum and its environmental implications: Geology, v. 28, no. 10, p. 927-930.

Source abbreviatins "L", "R", and "C" refer to Lourens et al., (2005), Rohl et al., (2000), and Cramer et al., (2003) respectively

CHAPTER 3.

Bioturbation cessation at the Paleocene/Eocene Boundary: Intermediate water dissolved oxygen depletion during massive carbon injection

Micah J. Nicolo[1], Gerald R. Dickens[1], Christopher J. Hollis[2]

[1]*Department of Earth Science, Rice University, Houston, TX 77005, USA*

[2]*Institute of Geological and Nuclear Sciences, PO Box 30-368, Lower Hutt, New Zealand*

In preparation for submission to:

Paleoceonography

ABSTRACT

The Paleocene-Eocene Thermal Maximum (PETM) ca. 55.5 Ma was the most pronounced of a series of transient early Paleogene hyperthermal events. The PETM initiated at the Paleocene/Eocene boundary (P/E) and was associated with a massive isotopically depleted carbon injection as well as severe changes in deep-sea ecosystems and habitat. Because the PETM represents one potential analog to the modern anthropogenic carbon injection, understanding its cause and environmental consequences is imperative. One method posited to explain the PETM calls for the addition and oxidation of methane following the dissociation of a significant portion of the global marine methane hydrate reservoir, however supporting evidence has remained elusive. We present lithologic, carbon isotopic, and bioturbating macrofauna trace fossil abundance results from outcrop sections now exposed by Mead Stream and Dee Stream in the Clarence Valley, South Island, New Zealand. Our results suggest that the intermediate waters that bathed these paleo-upper-slope sites were hypoxic coincident to the phase of the PETM carbon injection. In addition to increased surface ocean temperatures, these records support two independent hypotheses that may have contributed to dissolved oxygen depletion at the P/E. These include a decrease in global ocean circulation driven by high-latitude runoff and oceanic freshening, and/or a phase of intermediate water methane oxidation.

INTRODUCTION

Earth's surface temperature gradually rose by ~5°C from the late Paleocene ca. 58 Ma through the early Eocene ca. 51 Ma (Pearson et al., 2007; Zachos et al., 2001). Punctuating this transition was a series of rapid, transient and global negative carbon isotope excursions (CIEs) that each occurred coincident to a succession of similar environmental perturbations that have been termed 'hyperthermal' events (Lourens et al., 2005; Nicolo et al., 2007). The Paleocene Eocene Thermal Maximum (PETM) was the most extreme example of these events. Within <65 kyr of the onset of the PETM, the carbon isotopic composition ($\delta^{13}C$) of carbonate and organic matter deposited in the ocean and on land decreased by 2.5 - 4.0 ‰ (Kennett and Stott, 1991; Koch et al., 1992). This drop coincided with widespread but variable dissolution of carbonate in deep-sea records (Zeebe and Zachos, 2007), demonstrating that the CIE resulted from a tremendous injection of ^{13}C-depleted carbon into the ocean or atmosphere, somewhat analogous to current and future anthropogenic inputs (Dickens et al., 1997).

Understanding the PETM carbon injection is however complicated by carbon isotopic records of various types (e.g. bulk marine carbonate, Bains et al., 1999; Kaiho et al., 2006, and single specimen planktonic foraminifera, Thomas et al., 2002; Zachos et al., 2003) from the same sites and reservoirs that imply different specific carbon injection rates (Figure 3.1). However $\delta^{13}C$ and $CaCO_3$ dissolution records from all oceanic reservoirs are broadly consistent with an initial large injection and a secondary smaller prolonged carbon influx (Zeebe and Zachos, 2007) that age constraints suggest were in sum input over ~50-65 kyrs

(Rohl et al., 2000; Farley and Eltgroth, 2003). While the specific timing and magnitude of the carbon injection are not yet entirely clear, the relative temporal relationship between the phase of carbon input (regarded here as the negative limb of PETM $\delta^{13}C$ bulk records) and the elevated warmth of the PETM is better understood. Expanded continental margin sites indicate that an initial warming preceded the carbon injection by <10 kyrs (Sluijs et al., 2007) while various temperature proxies from multiple sites suggest that the thermal maximum persisted as much as 20-30 kyrs past the minimum $\delta^{13}C$ value that marks the end of the carbon injection phase (Figure 3.1) (Sluijs et al., 2006; Zachos et al., 2003).

Several lines of evidence suggest that dissolved oxygen (DO) concentrations in the ocean dropped during the PETM (e.g. faintly laminated sediments; Bralower et al., 1997, low-oxygen characteristic benthic foraminifera; Kaiho et al., 1996, 2006, and magnetic minerals possibly indicative of anoxic environments; Lippert and Zachos, 2007). Lowered dissolved O_2 may, in fact, be a crucial component of environmental change during the PETM. The dissolved O_2 concentration of a given parcel of intermediate to deep water is governed by O_2 solubility at the location of deep-water formation, and the amount of organic carbon oxidized as the water advects through ocean basins. Warmer sea surface temperatures during the PETM should have decreased O_2 solubility and the amount of O_2 in sinking water. The oceans also may have been more stratified, which could have increased the amount of organic carbon respiration per unit of water over time. Additionally, and importantly, dissolved O_2 may constrain the mode of carbon injection during the PETM. Release of methane from the seafloor, either through thermal dissociation of gas hydrates (Dickens et al., 1995) or the

heating of sedimentary organic carbon (Svensen et al., 2004), has been implicated as the primary source. Such an influx might be expected to remove dissolved O_2 from intermediate waters because methane injected to an oxic oceanic reservoir should have removed two mols of O_2 for every one mol of injected methane during oxidation to CO_2 (Dickens, 2003).

In the marine realm, much of the previous work on the PETM has focused on condensed sections from open ocean environments or expanded sections on the shelf. Ideally, however, to understand DO evolution through the PETM, sites located at water depths typical of high O_2 variability (500-2000 m water depth, (Levin, 2003) are required. In this study, we examine the PETM interval in two sections that now outcrop in South Island, New Zealand (Figure 3.2). These sections were originally deposited in an upper slope setting, and our work focuses on changes in the type and abundance of trace fossils made by bioturbating macrofauna. Our results indicate that intermediate waters bathing this high-latitude margin became hypoxic during and only during the massive carbon injection.

SITE LOCATION AND BACKGROUND

OUTCROP LOCATIONS

Clarence River valley, located in the Marlborough region of South Island, New Zealand, hosts an uplifted and rotated block of upper Cretaceous - upper Eocene marine sedimentary rocks (Reay, 1993; Strong et al., 1995). The rocks were originally emplaced as sediments on the outer shelf and upper slope (~100-1000 m water depth) of a passive continental margin adjacent to a neritic

carbonate platform at 50-55°S latitude (Hollis et al., 2005a; Reay, 1993). The limestone, marl and chert that now comprise the sequence were probably deposited as pelagic carbonate, terrigenous detrital clay minerals, and biogenic silica (Reay, 1993).

Within the overall sequence, the Lower Limestone Member of the Amuri Limestone Formation was deposited during the late Paleocene and early Eocene. Excellent examples of this lithologic unit member, with greater than 90% exposure, have been cut approximately perpendicular to strike by a series of streams, including Mead Stream and Dee Stream. The overall Lower Limestone member thickens to the northeast end of Clarence Valley, such that sections at Mead Stream and Dee Stream represent apparently continuous deposition in a mid-bathyal environment, although the section at Mead Stream is thicker and likely was deposited deeper than contemporaneous Dee Stream sediments (Reay, 1993; Strong et al., 1995). Prior work on these two sections has examined foraminiferal, nannofossil, and radiolarian assemblages, and analyzed bulk carbonate rocks for stable isotopes (Hancock et al., 2003; Hollis et al., 2005a; Strong et al., 1995). This work provides good stratigraphic control for the Lower Limestone interval of interest (Figure 3.3).

PETM LITHOLOGIC EXPRESSION

The PETM outcrops similarly at both Mead Stream and Dee Stream. It begins abruptly as a recessed interval containing multiple marl-rich beds that are collectively referred to as Dee Marl (Hancock et al., 2003), and grades progressively up-section into limestone and siliceous limestone beds. Like PETM intervals at other locations (e.g. (Kelly et al., 1996; Kennett and Stott, 1991; Thomas, 2003), Dee Marl records an extinction in benthic foraminifera, short-lived occurrences of warm-water planktic foraminifera, and a prominent negative CIE in bulk carbonate (Hancock et al., 2003; Hollis et al., 2005a). Moreover, similar to PETM intervals on several other continental margins (Crouch et al., 2003; Giusberti et al., 2007; Schmitz et al., 2001), the clay-rich unit represents an interval of increased sedimentation rates and detrital siliciclastic accumulation (Hancock et al., 2003; Hollis et al., 2005a; Nicolo et al., 2007). The PETM is recorded by ~3.7 m at Mead Stream and ~1.5 m at Dee Stream (Hancock et al., 2003; Hollis et al., 2005a).

Obvious expressions of bioturbation (e.g., simple dark burrows and spirals indicative of *zoophycos* ichnofacies) mark most Lower Limestone rocks in Clarence Valley. Such trace fossils likely appear dark in color relative to the background light colored limestone due to slight increases in organic carbon concentration. Low-resolution samples from our previous fieldwork on these sites qualitatively suggested that the Dee Marl was at least partially devoid of such trace fossil markings.

METHODS AND APPROACH

SAMPLE COLLECTION

Lower Limestone outcrop sections at Mead Stream and Dee Stream have been logged perpendicular to dip relative to marker horizons set at 0.0 m (Hancock et al., 2003; Hollis et al., 2005a). The onset of the PETM, as defined by both biostratigraphy and the onset of the CIE, is located 157.6 m up-section of the Cretaceous/Tertiary (K/T) Boundary at Mead Stream (Hancock et al., 2003; Hollis et al., 2005a), and 26.0 m up-section of a distinctive greenish Paleocene bed at Dee Stream (Hancock et al., 2003; Hollis et al., 2005a).

We made detailed lithostratigraphic logs across the PETM at each outcrop section (Figure 3.3), measuring from the base of Dee Marl. Beds were qualitatively delineated in the field as limestone, siliceous limestone, marl, or marly-limestone. We then chiseled out large (500–1000 cm^3) fresh rock samples for laboratory analyses, orienting each relative to dip. In total, we collected 54 samples at Mead Stream, and analyzed 33 Dee Stream samples previously collected by (Hancock et al., 2003; Hollis et al., 2005a). Samples were cut with a rock saw along their longest axis perpendicular to bedding. One half was used for geochemical analyses, the other for imaging.

GEOCHEMICAL ANALYSES

Sample splits for geochemical analysis were taken from the interior of each sample, powdered, and dried. Splits of the Mead Stream samples were analyzed for $CaCO_3$ content on a UIC Coulometer (precision of $\pm$ 0.1%), and for stable carbon isotope composition on a Micromass Prism Mass Spectrometer,

both housed in the Stable Isotope Laboratory at the University of Florida (Table 3.1). Carbon isotope values were calibrated to vPDB using the NBS-19 standard. Analytical precision for individual analyses is better than ±0.05 ‰. Oxygen isotope values were also measured (Table 3.1), but they are not discussed because meteoric water has significantly altered the $\delta^{18}O$ of carbonate in Lower Limestone sections. Mead Stream carbon isotopic results are as presented in Nicolo et al. (chapter 4). Splits of Dee Stream samples were measured for bulk carbonate stable isotopic compositions (Table 3.1) in the Stable Isotope Laboratory at University of California, Santa Cruz, and are as reported in Hancock et al., 2003.

BIOTURBATION IMAGE ANALYSIS

One sawed bed face of every sample was cleaned, polished and digitally imaged at high-resolution (~16,900 pixels / cm^2). Images were taken under consistent diffuse light and at a fixed distance adjacent to a 5 cm scale bar. The percentage of a rock face marked by dark-gray macrofauna trace fossils (B%) was measured using ImageJ (freely available at http://rsb.info.nih.gov/ij), a USA National Institute of Health digital image processing and statistical analysis software package. This software was designed to find and measure color heterogeneities in images, and its predecessor, NIH Image, has been used previously to quantify the imprint of bioturbation on sedimentary microfabrics (Francus, 2001). The method is effective on polished Paleogene rocks from Clarence Valley because the dark-gray trace fossils can be distinguished easily from the light-gray background limestone following several image processing steps.

Original high-resolution color images were first converted to a 0-255 8-bit grayscale and scaled using the reference bar. A 50-pixel rolling ball background filter was applied to remove slight but consistent lighting effect resulting from a fixed position light source. A consistent contrast enhancement was then performed to convert every grayscale pixel value lower than 210 to 0 (black); the remaining grayscale histogram (211-255) was then "stretched" to cover a full range of values (0-255). An image filter was applied to augment every pixel's grayscale value to the median of all values within a 2-pixel radius, so as to smooth the image without loosing significant features. Lastly, all pixel grayscale values <210 were converted to black (0) and all values >210 were changed to white (255). These processing steps result in binary images for rock samples where the background rock surface appears white and the macrofauna trace fossils appear black (Figure 3.4). An ImageJ algorithm was then applied. This algorithm finds a perimeter around all shapes created by adjacent black pixels, measures several characteristics of the shapes including area, and disregards shapes with an area smaller than a consistent threshold (here set at 3 mm^2 which is significantly smaller than the trace fossils we describe). The areas of black shapes are then summed and divided by the total area within the measured sample perimeter to arrive at B% (Table 3.1).

The accuracy and precision of B% depend on three factors. The first is the total area of the rock face being examined. In general, larger samples should be more representative and should give more reproducible results. Second, the amount (percent) and heterogeneity of bioturbation will impact results. The absolute error should be minimal for homogenous non-bioturbated samples but

increase with bioturbation until trace fossils dominate the rock face (>50 B%). The third error is the extent to which our image processing accurately delineates bioturbation. To address the first and second potential errors, we systematically re-examined three of our largest samples (areas = 52.54 cm^2, 75.43 cm^2, and 54.28 cm^2) that have a wide range of B% (27.5 B%, 13.7 B%, and 2.5 B%, respectively) at sets of progressively smaller sample areas (e.g. sets of 2 samples of 40 cm^2, 4 samples of 20 cm^2, 8 samples of 10 cm^2, and 16 samples of 5 cm^2). The first standard deviation of each sample set (Table 3.2), to which we have applied power law curve fits (Figure 3.5a), represents B% error as a function of sample area. Error also clearly increases as the measured B% of the whole sample increases (Figure 3.5a), a relationship we fit with 2nd order polynomials (Figure 3.5b). B% error for each sample was determined through application of both sets of functions (Figure 3.5b; Table 1). The third factor is inherently difficult to calculate because it necessitates the comparison of our results to accurate visual bioturbation determinations, a measurement that is highly subjective (Francus, 2001).

RESULTS

LITHOLOGIC LOG

The studied intervals at both Mead Stream and Dee Stream are principally limestone with a prominent recessed unit containing multiple recessed marl-rich beds (Hancock et al., 2003; Hollis et al., 2005a). Biogenic carbonate and detrital clay to fine-silt sized siliciclastic grains represent the primary lithologic components, however siliceous microfossils, which are a minor component throughout the interval of interest but a major factor in the overlying ribbon cherts (Hancock et al., 2003; Hollis et al., 2005a), also are preserved. At base these sections are bioturbated limestone composed of 60-72% $CaCO_3$ (Figure 3.3; Table 3.1). Above, and separated by a sharp contact, is the base of the Dee Marl (Hancock et al., 2003; Hollis et al., 2005a). The Dee Marl is ~1.8 m thick at Mead Stream, ~0.8 m thick at Dee Stream, and is qualitatively nearly devoid of trace fossils at base, but heavily bioturbated at top. Measured individual marl beds within the Dee Marl record less than 60% $CaCO_3$. $CaCO_3$ content is lowest at the base of the Dee Marl (37%) and increases consistently up section through the Dee Marl and the overlying limestone to a peak value of 80%.

BULK CARBON ISOTOPES

At both Mead Stream and Dee Stream, $\delta^{13}C$ records of bulk carbonate show a prominent negative CIE (Hancock et al., 2003; Hollis et al., 2005a). With the new data (Table 1), the initial drop begins at the base of Dee Marl. The decreasing $\delta^{13}C$ limb occurs over 1.45 m at Mead Stream and 0.42 m at Dee Stream. The more detailed Mead Stream record (Figure 3.3) shows an overall

1.51 ‰ amplitude CIE with three negative steps and two intervening slightly negative dipping plateaus; a trend consistent with other bulk carbonate records not exposed to severe dissolution at the onset of the PETM (Bains et al., 1999; Zachos et al., 2005). While the Mead Stream PETM CIE amplitude is significantly dampened relative to most records, its character and biostratigraphic position confirm its identity.

PETM bulk carbonate carbon isotopic records from sites not subjected to severe dissolution show consistent trends (Zachos et al., 2005). Based on distinct tie-points (Figure 3.1; Figure 3.3) we have correlated our Clarence Valley, NZ bulk carbonate $\delta^{13}C$ records to a similar record (ODP Site 690) that has been dated by two independent methods (Farley and Eltgroth, 2003; Rohl et al., 2000). Using these two age-models we fit both linear and interpolated functions in order to estimate high-end, low-end, and average bulk sedimentation rates for the Mead Stream PETM sequence. We further calculate component specific sedimentation rates by multiplying both the $CaCO_3$ and the terrigenous contents by each interpolated sedimentation rate. Terrigenous content is approximately equal to the non-$CaCO_3$ fraction in the majority of our section as siliceous material represents $< \sim 10$ % of the bulk rock.

COMPONENT SPECIFIC SEDIMENTATION RATES

Lithologic compositions are a function of the component specific sedimentation rates, which yield similar results independent of age-model (Figure 3.6). The Mead Stream detrital terrigenous sedimentation rate was ~0.5 cm/kyr at the base of the section, increased sharply at the onset of the Dee Marl to ~1

cm/kyr, reached a maximum of ~1.3 cm/kyr at the mid-point of the Dee Marl, and steadily fell to a sustained ~0.5 cm/kyr ~35 cm above the top of the Dee Marl. The Mead Stream $CaCO_3$ sedimentation rate was ~1 cm/kyr at the base of the section, dropped slightly over the first 20 cm of the Dee Marl to ~0.6 cm/kyr, returned to ~1 cm/kyr through the overlying 40 cm, increased to 1.5-2.0 cm/kyr through the upper portion of the Dee Marl, and maintained an enhanced rate of ~1.3 cm/kyr above the Dee Marl.

BIOTURBATION

Where present, macrofauna trace fossils consist of low angle (<10° although this may be decreased slightly by lithologic compaction) back filled burrows with no apparent sidewall and thin homogenous tube traces. These types of feeding structures (*Fodinichnia*) are most consistent with quiescent environments characterized by the *Zoophycos* ichnofacies (Frey and Pemberton, 1985). This interpretation is consistent with benthic foraminiferal assemblages, which place the Mead Stream and Dee Stream sections at low-energy upper-slope water depths during the late Paleocene and early Eocene (Strong et al., 1995).

The abundance of bioturbating macrofauna trace fossils (B%) varies significantly across the PETM at both Mead Stream and Dee Stream sections (Figure 3.3; Figure 3.6; Figure 3.7). At the base of the studied sections, in the latest Paleocene interval, B% ranges between 13-35. Values drop dramatically at the base of the Dee Marl coincident to the onset of the PETM CIE and stay anomalously low (average = 2.3 B%, n = 36) through an interval that precisely corresponds to the negative limb of the CIE (the first 1.45 m and 0.4 m of Dee

Marl at Mead Stream and Dee Stream, respectively). Just above this unit, through the top of the Dee Marl and the base of the overlying limestone, the most heavily bioturbated sediments of the studied interval (40-43 B%) are found. Trace fossil abundance ranges between 13-38 above this horizon, similar to that of the limestone below the PETM. Calculated errors in B% are higher for Dee Stream samples (Figure 3.5b; Table 3.1) because their measured surface areas (average = 11.0 cm^2) are considerably smaller than those for Mead Stream samples (average = 27.8 cm^2). Nonetheless, the trends are similar at both sections, indicating robust observations.

DISCUSSION

The onset of the negative CIE, which marks the P/E boundary, is recorded at Mead Stream and Dee Stream at the base of the Dee Marl. The Dee Marl is the result of increased detrital siliciclastic delivery to the New Zealand margin (Figure 3.6), and perhaps at base, a small degree of carbonate dissolution (although a more precise age-model is necessary to further substantiate this). The elevated terrigenous accumulation lasts longer than the phase of carbon injection, and likely is a product of enhanced runoff and erosion in response to warmer global temperatures and an accelerated hydrologic cycle.

Clarence Valley PETM paleo-upper-slope sections are also marked at the P/E contact by the onset of hypoxic conditions. This anomalously low-oxygen environment is expressed in the rock record by a near complete lack of bioturbating macrofauna trace fossils that only begin to reappear near the $\delta^{13}C$ minimum (Figure 3.6), or the end of the carbon injection phase.

In the modern oceans, bioturbating macrofauna are absent from sediments beneath oxygen minimum zone (OMZ) waters containing <~0.2 ml/L DO, but increase in abundance dramatically on the fringes of the OMZ (Levin, 2003). This observation suggests that coincident to the onset of the PETM carbon injection, intermediate water DO dropped to approximately 0.2 ml/L or lower, a range slightly lower than a DO estimate made from benthic foraminifera assemblages at a shallower NZ margin site (Kaiho et al., 1996).

A warmer surface ocean during the PETM would necessarily have decreased DO because of solubility gas laws, however likely not to the hypoxic levels we report given maximum warming estimate of ~10°C at high latitudes (Dickens, 2003). Also, the thermal maximum appears to have lasted longer than the phase of hypoxia, suggesting no direct link between the two. While any explanation for PETM intermediate water hypoxia must partly include elevated surface ocean temperatures, we find two additional and independent possible causal mechanisms consistent with our results.

An increase in high-latitude temperature and runoff should have created a more stratified ocean because of density relationships between temperature and salinity. A slower overturning thermohaline circulation system would increase the net amount of organic carbon oxidized at depth (assuming constant productivity), so that a link between increased detritus, runoff, and dissolved oxygen is possible. Indeed, the highest rate of detrital siliciclastic delivery, and presumably fresh-water runoff, our records describe occurred during the phase of PETM hypoxia (Figure 3.6). However relatively enhanced terrigenous accumulation persisted

beyond the end of the hypoxic phase and continued into the interval containing the most heavily bioturbated sediments, suggesting a non-causal relationship.

Stratigraphically, our records do suggest a close relationship between intermediate water hypoxia and the PETM carbon injection. A plausible explanation for this relationship is that at the P/E a prolonged injection of a large mass of methane oxidized to CO_2 at intermediate water depths at one or multiple locations en route to the New Zealand margin. Methane oxidation drove a DO depletion that expanded and intensified an OMZ above Mead Stream and Dee Stream locations at the onset of the carbon injection that eventually weakened and dissipated as the carbon injection ceased. Then during the beginning of the $\delta^{13}C$ recovery, as the limit of the OMZ approached and migrated past these locations, the abundance of bioturbating macrofauna increased to the highest recorded values.

CONCLUSION

Mead Stream and Dee Stream exposure early Paleogene rock sequences representing sediment deposition on the upper-slope of a passive continental margin. Increased detrital siliciclastic accumulation and a lack of bioturbating macrofauna trace fossils characterize the outcrop sequence beginning at the P/E carbon injection. While the bioturbation cessation ended coincident to the termination of the carbon injection, the accelerated terrigenous accumulation persisted for ~10-20 kyrs into an interval highlighted by the greatest abundance of macrofauna trace fossils. The accelerated rate of detrital siliciclastic delivery likely was a function of higher global temperatures and increased high-latitude

runoff and erosion. This finding agrees well with previous work that has suggested that the thermal maximum lasted longer than the carbon injection. The lack of bioturbation records a phase of hypoxia that was likely caused by an expansion and intensification of an OMZ on the New Zealand margin following the oxidation of a large mass of methane within intermediate water depths.

ACKNOWLEDGMENTS

This work was funded by the U.S. National Science Foundation Biocomplexity Grant (EAR 0120727) and the N.Z. Foundation for Research, Science and Technology through the GNS Global Change Through Time programme. We thank Richard and Sue Murray for access to both the Mead Stream and Dee Stream outcrops, located on their Marlborough, N. Z. ranch, Percy Strong, James Crampton, John Simes, and Victor Villasante, for assistance during fieldwork, Jason Curtis and David Hodell for geochemical analysis, and Maximiliano J. Bezada V. for photography.

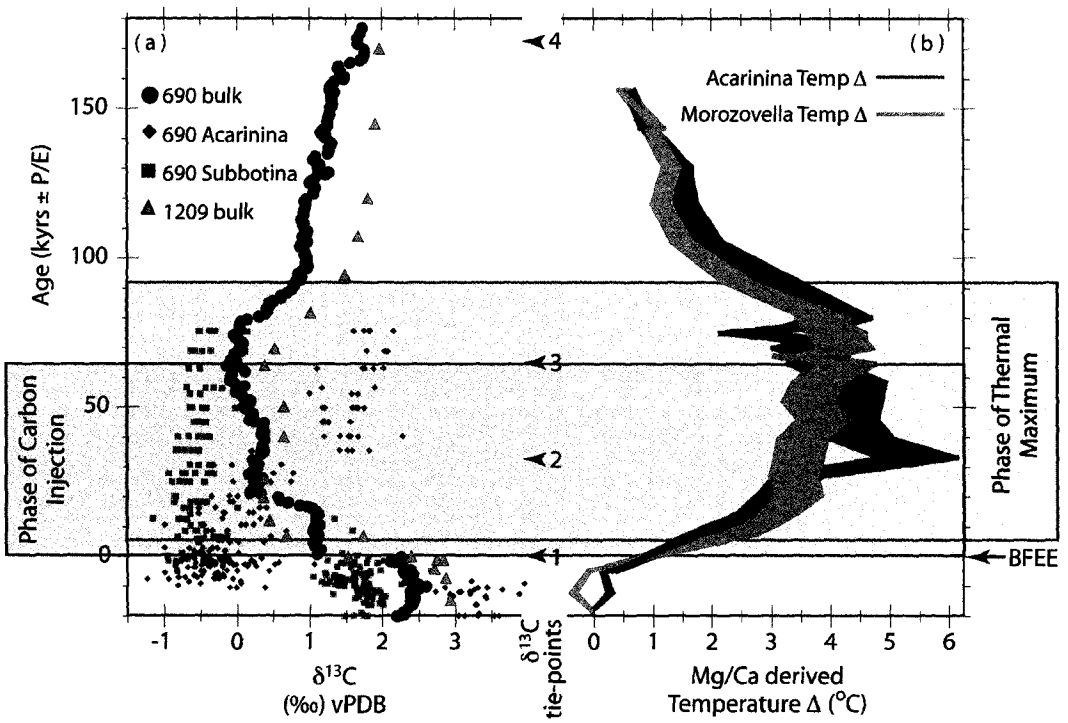

Figure 3.1. Phases of the PETM: ODP Sites 690 and 1209. (a) The PETM carbon injection phase (blue rectangle), as delineated by the negative limb of bulk carbonate $\delta^{13}C$ records from ODP Site 690 (Bains et al., 1999) and ODP Site 1209 (Kaiho et al., 2006). ODP Site 690 surface and intermediate water single specimen foraminifera $\delta^{13}C$ records (Thomas et al., 2002) imply a slightly different carbon injection rate. (b) The phase of the PETM thermal maximum as recorded by single species planktic foraminifera Mg/Ca variations persisted for > 20 kyrs after the $\delta^{13}C$ minima (Zachos et al., 2003). Common $\delta^{13}C$ tie-points (numbered 1-4) allow for correlation between ODP Site 690, which has been dated by two independent methods, and Mead Stream, and Dee Stream PETM records. Ages for both "a" and "b" were generated as a function of the "average" interpolated sedimentation rate (Figure 3.6).

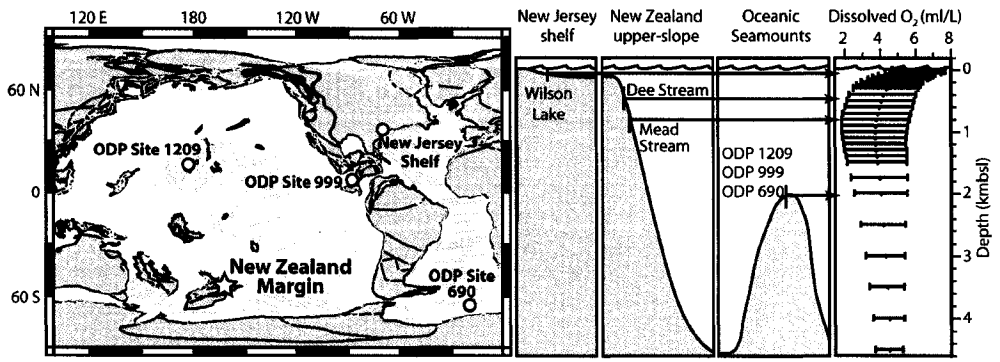

Figure 3.2. Site locations and environments during the PETM. Paleogeographic map (http://www.odsn.de/services/paleomap/paleomap.html) and idealized paleobathymetric illustration describing studied outcrop sequences' (white star) and other discussed sites' (white circles) locations and paleodepths (i.e. Wilson Lake: ~0.025-0.1 kmbsl, Zachos et al., 2006; Dee Stream and Mead Stream: ~0.3-0.8 kmbsl, Strong et al., 1995; ODP Sites 690, 999, and 1209: ~2 kmbsl, Thomas et al., 2003; Bralower et al., 1997; Kaiho et al., 2005 respectively) at ~55.5 Ma plotted next to modern global average dissolved oxygen concentrations and first standard deviations at various depths (Levitus and Boyer, 1994). Kmbsl refers to kilometers below sea level.

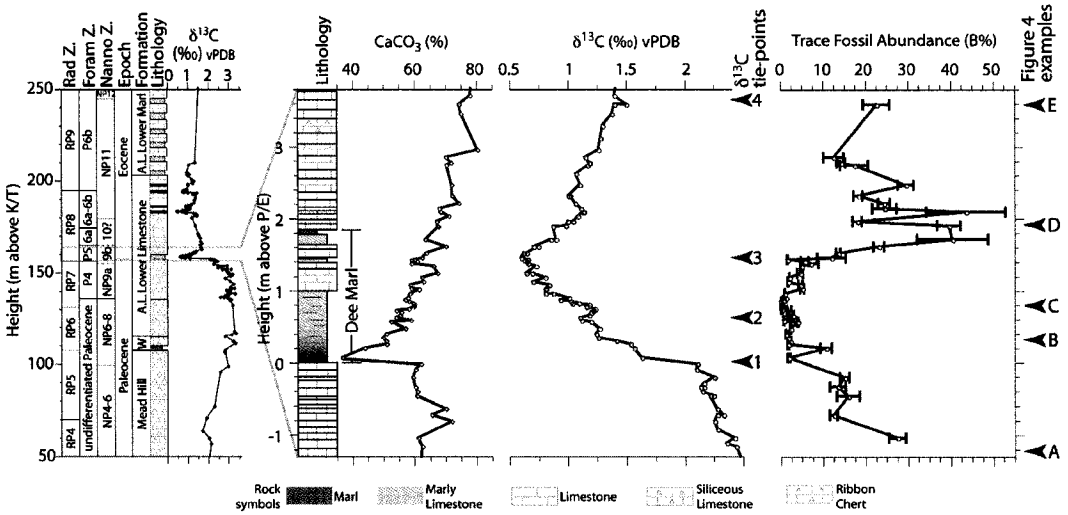

Figure 3.3. Mead Stream PETM sequence. The Early Paleogene succession at Mead Stream with a detailed record across the PETM including the lithologic log, calcium carbonate content, bulk carbonate $\delta^{13}C$ composition, $\delta^{13}C$ tie-points common to other PETM sites (Figure 3.1), and trace fossil abundance results with reference made to example samples illustrated in Figure 3.4. Formation names, lithology, biostratigraphy, and bulk carbonate carbon isotopes for Mead Stream (excepting those across the interval of interest) are from Hollis et al. (2005) and Nicolo et al. (2007).

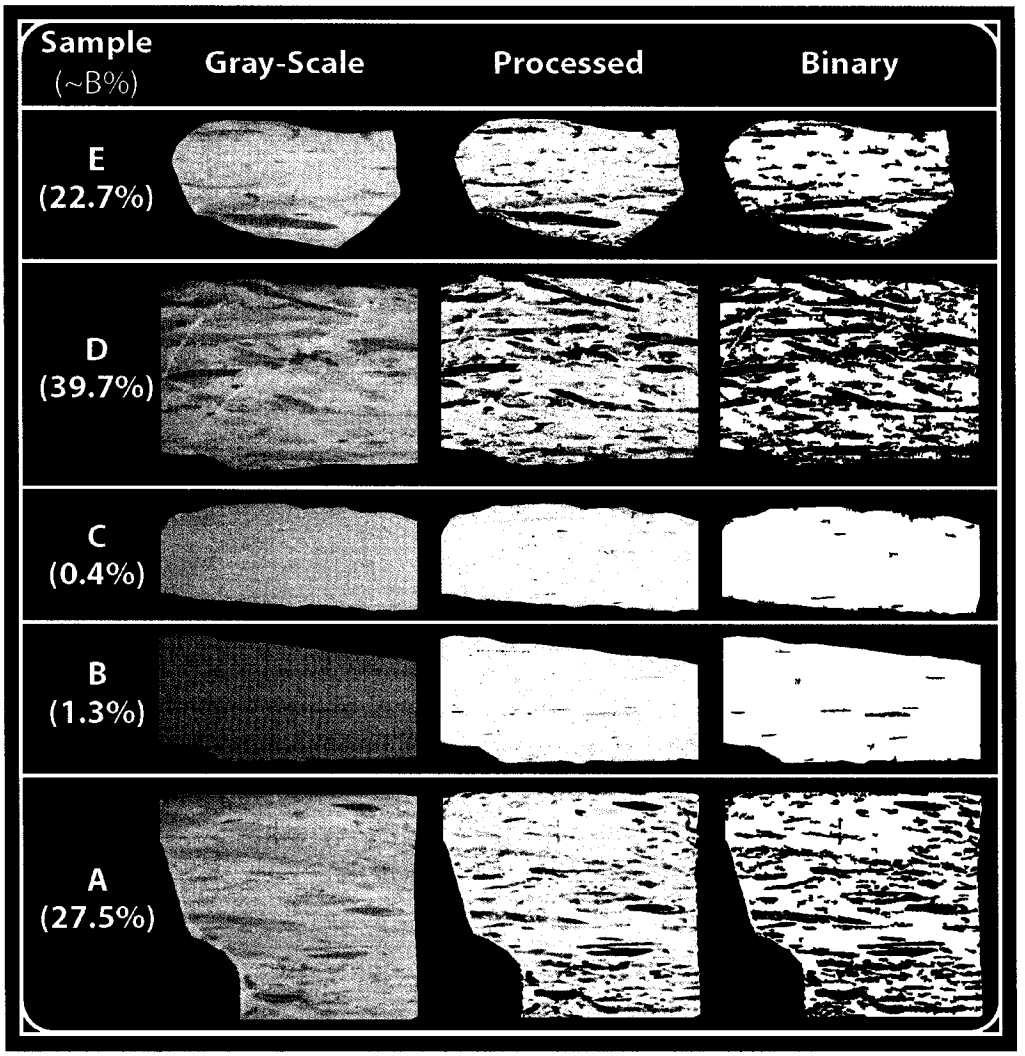

Figure 3.4. Bioturbation image processing and analysis. Example rock samples and their measured trace fossil abundance (B%) referred to in Figure 3.3. "Processed" images are the result of the application of a background removal, histogram enhancement, and a median filter to "gray-scale" images. "Binary" images are threshold limited "processed" images.

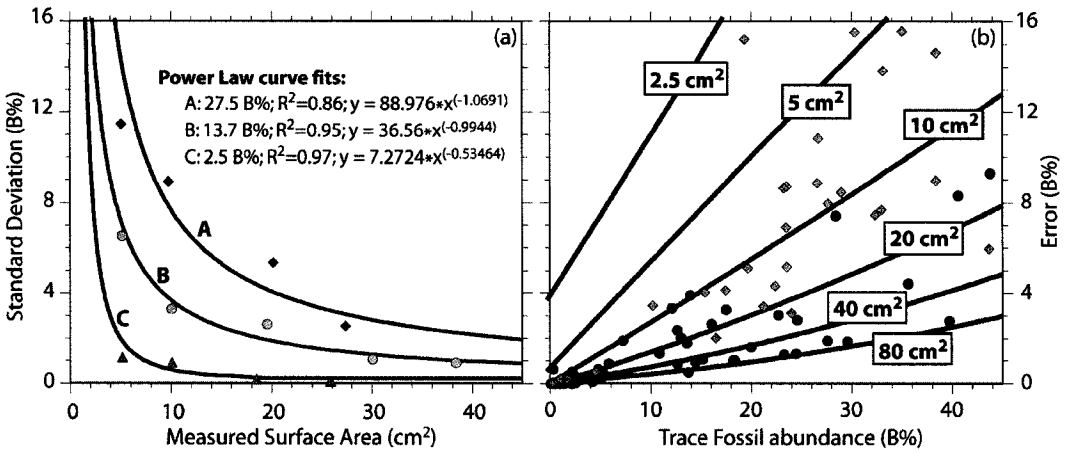

Figure 3.5. Bioturbation abundance (B%) error estimation.

(a) Sample set trace fossil abundance (B%) standard deviation versus measured surface area and power law curve fits for three samples recording a range of B% values. (b) Error estimates along lines of equal measurement area and Dee Stream (orange diamonds) and Mead Stream (blue circles) calculated B% error for all samples as a function of both measured sample area and bioturbation abundance.

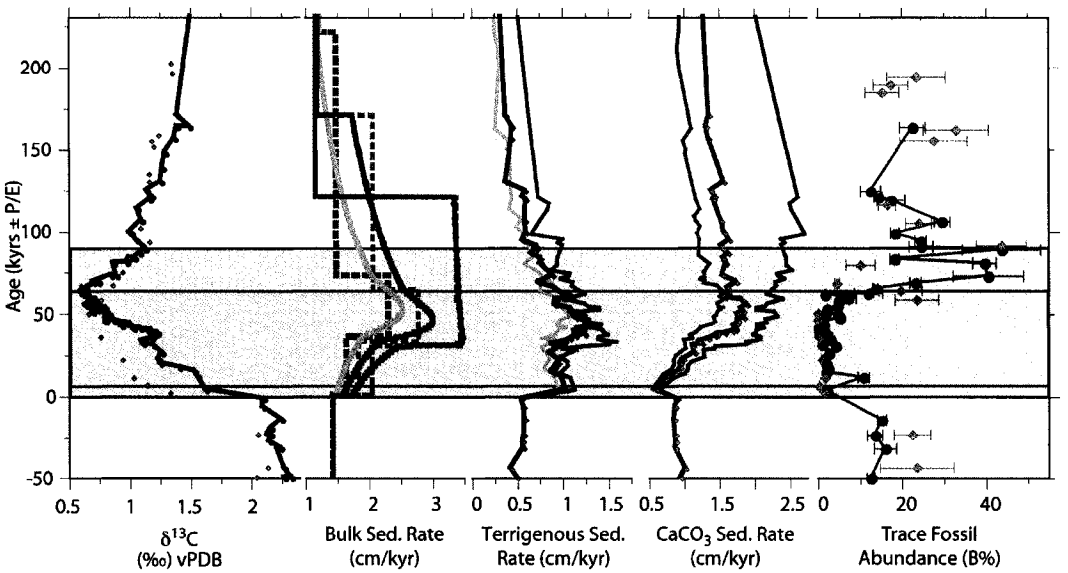

Figure 3.6. Mead Stream and Dee Stream P/E bioturbation and lithologic variation. Mead Stream (blue diamonds) and Dee Stream (orange diamonds) bulk carbonate $\delta^{13}C$ PETM records are plotted next to bulk linear sedimentation rates representing two independent age-models (Rohl et al. (2000) cyclostratigraphic = light blue dotted line; Farley and Eltgroth (2003) He accumulation = dark blue dotted line) and their average (medium blue dotted line), interpolated sedimentation rates (cyclostratigraphic = orange line; He based = dark red line; average = medium red line), terrigenous and carbonaceous specific sedimentation rates (cyclostratigraphic = orange and light blue lines; He based = dark red and dark blue lines; average = medium red and medium blue solid lines respectively) calculated using interpolated bulk sedimentation rates, and trace fossil abundance results for both sites (Mead Stream = red circles; Dee Stream = orange diamonds) versus age relative to the Paleocene/Eocene boundary. Ages were generated as a function of the "average" interpolated sedimentation rate. The phases of the carbon injection (blue rectangle) and the thermal maximum (red rectangle) are as illustrated in Figure 3.1.

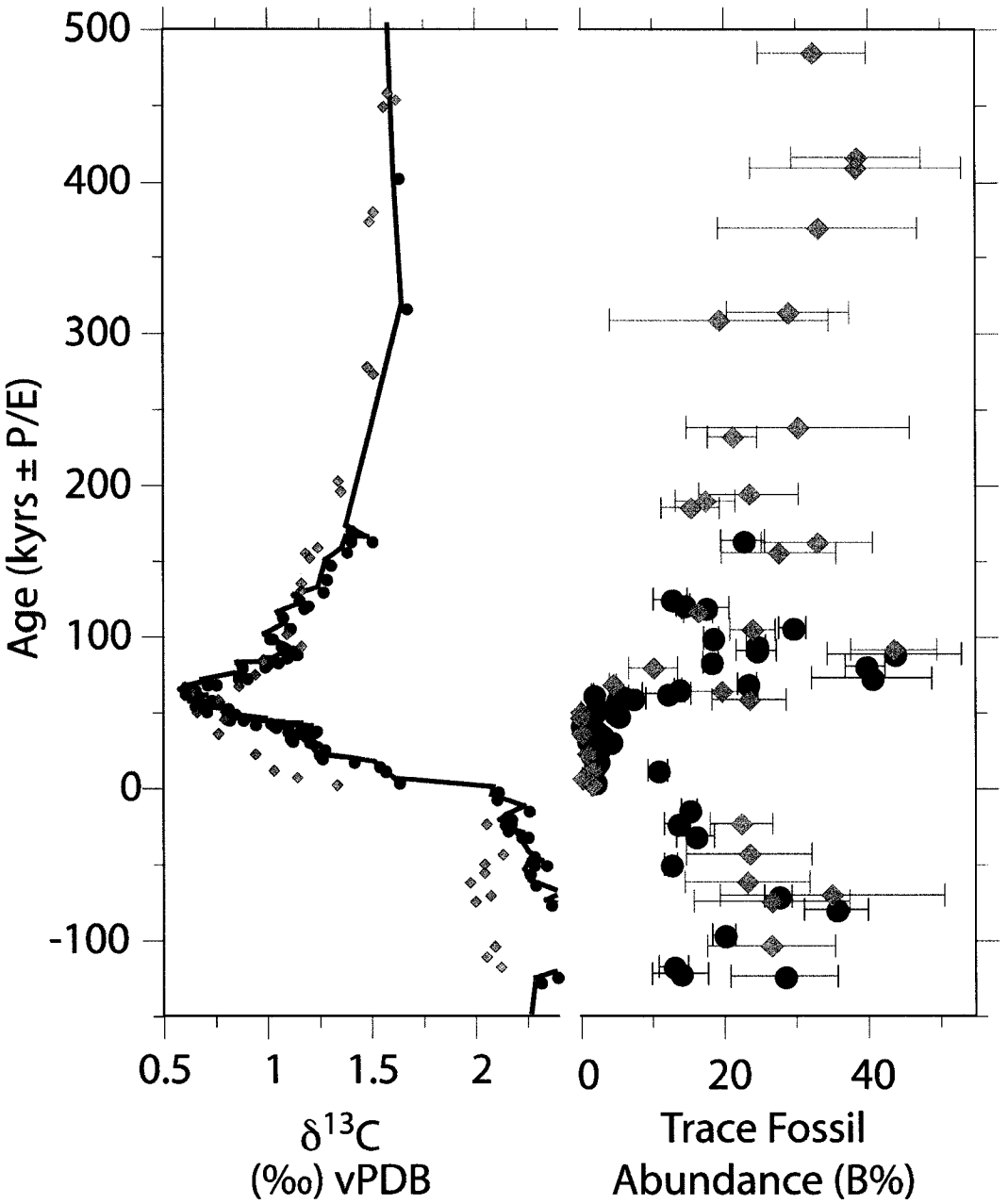

Figure 3.7. Long-term Mead Stream and Dee Stream bioturbation variation. Mead Stream and Dee Stream bulk carbonate $\delta^{13}C$ PETM records are plotted next to trace fossil abundance results for both sites versus age relative to the Paleocene/Eocene boundary. The applied age-model and all symbols are as reported in Figure 3.6.

Table 3.1 Mead Stream and Dee Stream geochemical and bioturbation results.

Location	Height (m above P/E)	d13C	d18O	B %	Area measured (cm^2)	B% error	CaCO3 %
Mead	3.59	1.50	-3.31	22.65	22.40	3.06	74.51
Mead	2.85	1.15	-3.24	12.57	13.91	2.39	70.26
Mead	2.78	1.18	-3.28	14.37	42.08	0.98	71.89
Mead	2.74	1.17	-3.07	17.42	14.56	3.30	70.40
Mead	2.47	1.11	-3.26	29.52	60.86	1.88	72.06
Mead	2.32	1.00	-3.35	18.31	55.30	1.05	72.28
Mead	2.21	1.06	-3.52	24.42	65.53	1.35	74.48
Mead	2.14	1.11	-3.11	24.52	27.41	2.84	68.21
Mead	2.09	1.14	-3.37	43.69	14.28	9.31	68.57
Mead	1.96	1.04	-3.35	18.17	53.75	1.07	67.35
Mead	1.90	0.98	-3.51	39.65	60.25	2.79	67.47
Mead	1.71	0.90	-3.50	40.53	14.82	8.34	63.61
Mead	1.61	0.71	-3.91	23.22	62.13	1.32	70.18
Mead	1.52	0.65	-3.38	13.66	75.43	0.53	63.90
Mead	1.45	0.60	-3.46	12.03	9.29	3.37	62.52
Mead	1.43	0.66	-3.48	1.69	14.82	0.13	59.99
Mead	1.41	0.65	-3.41	5.75	14.65	0.91	61.01
Mead	1.37	0.66	-3.64	7.16	9.41	1.93	59.12
Mead	1.34	0.72	-3.84	5.00	37.43	0.26	66.17
Mead	1.25	0.64	-4.10	4.69	15.51	0.66	67.44
Mead	1.19	0.80	-3.84	2.13	55.61	0.01	62.56
Mead	1.13	0.70	-3.91	1.88	22.54	0.06	62.93
Mead	1.08	0.84	-3.51	4.73	21.87	0.44	58.83

Mead	1.03	0.81	-3.62	5.19	23.64	0.46	59.01
Mead	0.96	0.81	-3.87	1.06	26.80	-0.05	58.69
Mead	0.90	1.01	-3.66	1.33	24.36	-0.01	58.00
Mead	0.87	0.94	-3.84	0.75	14.39	-0.04	57.04
Mead	0.85	1.02	-3.90	0.00	14.52	-0.19	58.26
Mead	0.82	1.03	-4.03	0.22	4.97	0.65	59.74
Mead	0.80	1.18	-3.79	0.19	12.35	-0.14	59.99
Mead	0.78	1.16	-3.73	0.08	15.48	-0.18	59.94
Mead	0.75	1.23	-3.68	0.40	24.03	-0.12	58.23
Mead	0.72	1.22	-3.64	2.11	8.87	0.54	54.27
Mead	0.70	1.20	-3.60	2.20	10.39	0.43	55.83
Mead	0.66	1.18	-3.55	2.91	22.57	0.19	55.51
Mead	0.59	1.11	-3.92	0.86	16.77	-0.05	58.96
Mead	0.57	1.20	-3.60	4.10	62.43	0.10	52.60
Mead	0.47	1.27	-3.86	2.44	43.15	0.04	57.13
Mead	0.40	1.24	-3.61	1.32	33.90	-0.03	51.07
Mead	0.35	1.26	-3.78	1.84	27.57	0.03	50.01
Mead	0.30	1.41	-3.63	2.30	15.84	0.22	50.97
Mead	0.26	1.53	-3.66	1.87	13.28	0.20	51.21
Mead	0.20	1.56	-3.47	10.77	20.47	1.37	44.09
Mead	0.06	1.63	-3.72	1.97	10.79	0.34	36.81
Mead	-0.21	2.25	-3.05	15.13	39.91	1.10	59.64
Mead	-0.35	2.14	-3.18	13.51	20.12	1.82	60.35
Mead	-0.47	2.24	-3.04	15.99	16.56	2.66	60.85
Mead	-0.73	2.33	-3.16	12.56	38.48	0.89	65.69
Mead	-1.05	2.43	-2.82	27.54	52.54	1.93	61.24
Mead	-1.17	2.44	-3.05	35.56	27.75	4.44	62.59
Mead	-1.41	2.51	-2.86	19.95	37.87	1.65	62.07

Mead	-1.71	2.44	-2.56	12.93	16.88	2.05	62.67
Mead	-1.78	2.43	-2.66	13.84	9.18	3.94	63.96
Mead	-1.80	2.39	-2.79	28.37	10.50	7.45	65.23
Dee	-0.78	-0.78	2.09	26.56	7.80	8.88	
Dee	-0.56	-0.56	2.00	26.64	6.14	10.85	
Dee	-0.53	-0.53	2.07	35.00	5.43	15.58	
Dee	-0.46	-0.46	1.97	23.21	6.84	8.66	
Dee	-0.33	-0.33	2.13	23.49	6.87	8.74	
Dee	-0.18	-0.18	2.05	22.38	14.72	4.33	
Dee	0.02	0.02	1.33	1.65	12.87	0.17	
Dee	0.05	0.05	1.14	0.27	8.07	0.05	
Dee	0.08	0.08	1.03	1.63	11.75	0.21	
Dee	0.15	0.15	0.94	0.98	8.91	0.20	
Dee	0.24	0.24	0.76	0.21	9.61	-0.06	
Dee	0.30	0.30	0.79	0.00	7.50	0.01	
Dee	0.33	0.33	0.66	0.00	10.96	-0.16	
Dee	0.38	0.38	0.76	23.54	12.77	5.17	
Dee	0.42	0.42	0.64	19.65	10.32	5.12	
Dee	0.45	0.45	0.86	4.51	18.03	0.52	
Dee	0.53	0.53	0.94	10.14	7.58	3.46	
Dee	0.62	0.62	0.98	43.63	25.79	5.97	
Dee	0.72	0.72	1.16	23.99	23.69	3.13	
Dee	0.81	0.81	1.09	16.47	23.27	2.01	
Dee	1.10	1.10	1.16	27.63	9.32	7.98	
Dee	1.15	1.15	1.16	32.95	12.29	7.70	
Dee	1.32	1.32	1.20	15.38	10.06	4.04	
Dee	1.35	1.35	1.18	17.44	11.35	4.14	
Dee	1.39	1.39	1.24	23.46	9.02	6.92	

Dee	1.67	1.67	1.35	21.20	17.95	3.43	
Dee	1.72	1.72	1.34	30.32	4.59	15.54	
Dee	2.24	2.24	1.51	19.34	2.93	15.23	
Dee	2.28	2.28	1.48	28.93	9.18	8.48	
Dee	2.69			33.08	5.88	13.85	
Dee	2.99	2.99	1.49	38.33	6.58	14.65	
Dee	3.04	3.04	1.51	38.36	12.46	8.98	
Dee	3.55	3.55	1.56	32.32	12.42	7.49	

Table 3.2. B% Error estimation

Sample	Number of Analyses	Area Measured (cm2)	B% Average	B% 1 Standard Deviation
MD-95	2	27.34	27.60	2.55
	3	20.15	27.58	5.36
	4	9.74	27.88	8.94
	8	5.05	29.25	11.48
MD-116	2	38.30	14.02	0.94
	3	29.99	14.26	1.09
	4	19.50	14.71	2.65
	8	10.00	14.20	3.33
	16	5.05	12.57	6.57
MD-111_1-4	2	25.85	2.28	0.09
	3	18.52	2.51	0.17
	4	10.10	2.00	0.93
	8	5.17	2.09	1.16

CHAPTER 4.

Paleocene Eocene Thermal Maximum surface ocean $\delta^{13}C$ heterogeneity: Interbasinal and depositional setting bulk carbonate variability

Micah J. Nicolo[1] and Gerald R. Dickens[1]

[1]*Department of Earth Science, Rice University, Houston, TX 77005, USA*

In preparation for submission to:

Nature

ABSTRACT

A series of similar carbon cycle and global warming events mark the transition from the late Paleocene to the early Eocene. The Paleocene-Eocene Thermal Maximum (PETM) ca. 55.5 Ma describes the most pronounced of these intervals. The PETM was a geologically brief interval marked at onset by a tremendous influx of isotopically light carbon, extreme changes in global environments, and pronounced variations in many Earth system processes. One principal constraint on the mass of carbon injected at the PETM relates to the nature of stable carbon isotopic records. However as modern surface ocean dissolved inorganic carbon (DIC) $\delta^{13}C$ is not homogenous, one might expect PETM surface ocean records to document similar variability. We explore the heterogeneity of PETM bulk carbonate $\delta^{13}C$ records at a suite of open ocean and marine margin locations and find trends consistent with ocean circulation driven variability and the influence of continental sourced isotopically light DIC. Additionally, we report results across the PETM as well as several younger global warming or 'hyperthermal' events that suggest a repeated influence of neritic carbonate production at high latitude margin sites now exposed as outcrop on South Island, New Zealand.

INTRODUCTION

At the onset of the Eocene Epoch (ca. 55.5 Ma) in the midst of a gradual global warming trend that took place from ~58-51 Ma Earth surface temperatures at all latitudes rose dramatically by ~5-10°C over ~20 kyrs and remained high for ~100 kyrs before returning to latest Paleocene values (Pearson et al., 2007; Sluijs et al., 2006; Zachos et al., 2003). This rapid but transient global event is known as the Paleocene Eocene Thermal Maximum (PETM). Approximately coincident to the PETM rise in global temperature, a pronounced negative shift in the stable carbon isotopic composition ($\delta^{13}C$) of marine and terrestrial sediments of >2.5 ‰ (in most records) occurred over ~65 kyrs (Farley and Eltgroth, 2003; Kennett and Stott, 1991; Koch et al., 1992; Rohl et al., 2000). This carbon isotope excursion (CIE) coincided with the dissolution of deep-sea carbonates, implying an increase in dissolved CO_2 and acidity (Zeebe and Zachos, 2007), and supporting the general hypothesis that a large mass of ^{13}C-depleted carbon was injected into the Earth's ocean-atmosphere system at this time (Dickens et al., 1997).

Constraints on the mass and rate of carbon injected at the onset of the PETM are derived from an estimate of the $\delta^{13}C$ of the input carbon and the nature of the PETM CIE in terms of its amplitude, structure, and the absolute $\delta^{13}C$ value of key time slices (Dickens et al., 1995). Therefore, heterogeneities in CIE records have the potential to affect key interpretations of the PETM. However modern surface ocean dissolved inorganic carbon (DIC) is not homogenous with respect to $\delta^{13}C$ (Bauch et al., 2004; Östlund, 1987) so that it may be expected that PETM surface ocean derived carbonate sediments would have recorded similar variability.

The PETM also had significant but non-uniform impacts on Earth system processes and biota. In the surface ocean, the PETM was related to the expansion of low-latitude planktonic foraminifera into sub-polar regions (Kelly, 2002), a trophic gradient enhancement between continental shelves and open ocean settings (Gibbs et al., 2006), and the proliferation of unique dinoflagellate species on continental margins (Crouch et al., 2003; Sluijs et al., 2007). On land, the PETM resulted in the diversification of mammals (Bowen et al., 2002) and the expansion of tropical flora into higher latitudes (Wing et al., 2005). While the characteristics of the PETM are phenomenal, they were not unique. The PETM was in fact merely the most extreme example of a series of similar early Eocene events including the successively younger H1 (a.k.a. ETM2/ELMO, Lourens et al., 2005), H2, I1, and I2 events (Lourens et al., 2005; Nicolo et al., 2007), such that one might expect each event to have similar types of responses.

Over the past two decades considerable effort has been put forth by many workers to expand the number of locations where PETM sections have been identified and bulk carbonate $\delta^{13}C$ measured (Figure 4.1). We examine fourteen previously published globally distributed open-ocean and marine margin PETM bulk carbonate $\delta^{13}C$ records and present new comparable records from two periplatform high-latitude South Pacific PETM sites now exposed as outcrop by Mead Stream and Muzzle Stream on South Island, New Zealand. Further, we measure the trace element concentration of carbonate sediments through the PETM, H1, H2, I1, and I2 at Mead Stream. We interpret these findings with respect to modern surface ocean $\delta^{13}C$ heterogeneity and find results consistent with $\delta^{13}C$ variability driven by ocean circulation dynamics, riverine influenced

continental margin DIC, and the nature of carbon fractionation during neritic platform carbonate production.

LOCATIONS, APPROACH, AND METHODS

COMPILATION OF PUBLISHED PETM BULK CARBONATE $\delta^{13}C$ RECORDS

We have selected a suite of available bulk carbonate $\delta^{13}C$ data from locations that represent a diverse collection of marine margin and open ocean depositional settings (Figure 4.1). We refer the reader to the original published works for more detailed lithostratigraphic frameworks and site-specific discourse. Marine margin locations include Gebel Duwi, Egypt (Speijer and Morsi, 2002), Ermua, Spain (Schmitz et al., 2001), Wilson Lake, New Jersey, U.S. (Sluijs et al., 2007), Bass River, New Jersey, U.S. (Sluijs et al., 2007), and Forada, Italy (Giusberti et al., 2007). Marine open ocean sites include ODP Site 1209, Shatsky Rise, North Pacific (Kaiho et al., 2006), ODP Site 690, Maud Rise, Southern Ocean (Bains et al., 1999), ODP Site 1263, Walvis Ridge, South Atlantic (Zachos et al., 2005), ODP Site 1001, Nicaraguan Rise, Caribbean Sea (Bralower et al., 1997), DSDP Site 213, Ninety-East Ridge, Indian Ocean (Ravizza et al., 2001), and DSDP Site 549, Goban Spur (Ravizza et al., 2001), and Zumaia, Spain, North Atlantic (Schmitz et al., 1997). In this schematic, selection of a location to represent the North Atlantic is problematic, as no relatively complete true open ocean records have been recovered there. We therefore principally discuss the Zumaia section as the North Atlantic open ocean value as it represents the most oceanic member of the well documented Spanish shelf-basin transect (Schmitz et al., 2001), and because of the similar nature of the isotopic values documented

there relative to the DSDP Site 549 record, another outer margin North Atlantic site.

In an effort to evaluate open ocean sections relative to each other in the time domain, we have placed the selected records on a common age scale relative to the onset of the CIE. The stratigraphy of the PETM is typically defined by relating inflection points in the bulk carbonate $\delta^{13}C$ record of a given location to that of the ODP Site 690 record (Kaiho et al., 2006; Zachos et al., 2005), which has been dated by two independent methods (i.e. cyclostratigraphy (Rohl et al., 2000); and extraterrestrial He^3 accumulation, (Farley and Eltgroth, 2003)). The age model we employ is based on a linear sedimentation rate (LSR) at Site 690 fit to average age points taken from the two available age models at key $\delta^{13}C$ inflection points (i.e. the $\delta^{13}C$ CIE onset at 0 kyrs, the $\delta^{13}C$ CIE minimum at 65 kyrs, and the $\delta^{13}C$ CIE conclusion at 170 kyrs; Table 4.1). We then ascribe the generated LSR age of additional $\delta^{13}C$ inflection points from Site 690 to $\delta^{13}C$ points of similar nature in the other open ocean bulk carbonate records (Table 4.1) and generate reported ages for each site as a linear function between those points. Interpolated curve fits (Stineman, 1980) of the bulk carbonate $\delta^{13}C$ of each record as a function of time then allow for comparison between sites at consistent time slices. One significant limitation to this chemostratigraphic method across the PETM is that sites that experienced severe dissolution are missing some fraction of their latest Paleocene to earliest Eocene $\delta^{13}C$ record (Zachos et al., 2005). We address this issue by utilizing sites with minimal dissolution where possible, and when not, by proscribing an appropriate gap in the $\delta^{13}C$ record through the clay

horizon. Ages of sediments before and after the CIE are based on published biostratigraphic datums placed in a cyclostratigraphic framework also relative to the onset of the PETM CIE (Westerhold et al., 2007; Table 4.1).

NEW ZEALAND LOCATIONS AND ANALYSES

The mountains adjacent to the Clarence River, located in Marlborough region, South Island, New Zealand, yield a block of sedimentary rock that has been uplifted and rotated to its present position during Neogene deformation (Crampton et al., 2003). The sedimentary rocks that comprise this block represent deposition during the late Cretaceous through middle Eocene at an outer shelf to slope (~100-1000 m water depth) passive margin setting that was proximal to both proto-New Zealand and a neritic carbonate platform at ~50-55°S latitude (Figure 4.1) during this interval (Gordon and Taylor, 1999; Strong et al., 1995).

The Lower Limestone Member of the Amuri Limestone Formation records sediments emplaced during the late Paleocene to early Eocene (Hollis et al., 2005a; Strong et al., 1995). A series of tributary streams to the Clarence River including Muzzle Stream, Dee Stream, and Mead Stream have nicely cut through these limestone mountains roughly perpendicular to strike (Hancock et al., 2003; Hollis et al., 2005a; Hollis et al., 2005b; Nicolo et al., 2007; Strong et al., 1995). These sites record a progressively thicker Lower Limestone unit from the thinnest section at the upper-bathyal Muzzle Stream, through the intermediary Dee Stream, to the thickest interval at the mid-bathyal Mead Stream (Hollis et al., 2005a; Hollis et al., 2005b; Strong et al., 1995). The major sedimentary constituents of the Lower Limestone consist of pelagic carbonates (foraminiferal

bearing nannofossil ooze), detrital clay grains, and biogenic silica (Hancock et al., 2003; Hollis et al., 2005b; Strong et al., 1995), although the proximity to a neritic carbonate platform allows for the possibility that some fraction of neritic carbonate may have been transported to these sites.

Previous radiolarian, foraminiferal, nannofossil and bulk carbonate $\delta^{13}C$ stratigraphies on all three sections have well constrained the Paleocene – Eocene transition including the PETM interval at Muzzle, Dee and Mead, (Hollis et al., 2005a; Hollis et al., 2005b; Strong et al., 1995) and the younger H (including both H1 and H2) and I (including both I1 and I2) paired CIE events at Mead and Dee (Nicolo et al., 2007). A pronounced recessed marl horizon referred to as Dee Marl (Hancock et al., 2003) marks the onset of the PETM CIE at all three locations. Lower Limestone sequences at each site have been measured in stratigraphic heights relative the base of this unit. The PETM is recorded at Muzzle Stream from 0.0 – 1.70 m (Hollis et al., 2005b), at Dee Stream from 0.0 – 2.56 m (Hancock et al., 2003), and at Mead Stream from 0.0 – 3.71 m (Nicolo et al., chapter 3). Multiple pronounced marl-rich beds also mark each younger CIE event horizon and suggest an increase in continental erosion and siliciclastic detritus accumulation on the New Zealand margin similarly accompanied the PETM and each younger CIE interval (Nicolo et al., 2007). The H and I CIEs are located from 36.22 – 38.85 m and 41.82 – 45.21 m respectively at Dee Stream, and from 24.45 – 30.94 m and 36.22 – 41.38 m respectively at Mead Stream.

To gain a better understanding of the relationship between the bulk $\delta^{13}C$ records of New Zealand sites relative to both each other and those generated at other locations we collected 54 fresh rock samples from Mead Stream through the

PETM interval in order to increase the resolution of the available $\delta^{13}C$ record (Nicolo et al., 2007), and analyzed 25 splits of Muzzle Stream samples (Hollis et al., 2005b). We then applied the same chemostratigraphic age model as discussed above for the open ocean locations for the PETM. The age model of Nicolo et al., (2007) augmented to correlate with the long term cyclostratigraphic age model of Westerhold et al., (2007) was then applied to intervals containing the H and I CIE events at Mead Stream, Dee Stream, and DSDP Site 577, Shatsky Rise, North Pacific (Cramer et al., 2003).

Geochemical sample splits were taken from the interior of each rock sample, crushed, and dried. Mead Stream and Muzzle Stream samples were analyzed for bulk carbonate stable carbon isotope composition in the Stable Isotope Laboratory at the University of Florida and the Stable Isotope Laboratory at University of California, Santa Cruz respectively (Table 4.2). Carbon isotope values were calibrated to vPDB using the NBS-19 standard. Analytical precision for individual analyses is better than ±0.05 ‰. We do not discuss measured oxygen isotope values (Table 4.2) as Lower Limestone rocks clearly record a meteoric influence.

To address the possibility of a neritic carbonate fraction in Lower Limestone sediments, we selected 35 geochemical sample splits from Mead Stream through the PETM, H, and I CIEs for carbonate fraction elemental analysis. For this procedure 100 - 110 mg of each powdered, dry, sample was first reacted with 10 mL of $NaC_2H_3O_2$ (adjusted to pH = 5 with acetic acid) for 5 hours on a wrist-action shaker at room temperature (Li et al., 1995). The supernatant leachate was then collected from centrifuged samples and diluted to 1:10. Sample

dilutions and known standards also diluted to 1:10 1-N $NaC_2H_3O_2$ were then spiked with 1% vol/vol concentrated HNO_3 and 1 ppm of an in house Yttrium standard in order to correct for instrument drift. Dissolved Ca and Mg concentrations of samples (Table 4.2) and standards were measured on a Varian Vista-Pro Inductively Coupled Plasma Atomic Emission Spectrometer (ICP-AES) housed in the Rice University Geochemistry Laboratory and compared.

RESULTS

PETM MARGIN AND OPEN OCEAN BULK CARBONATE $\delta^{13}C$ RECORDS

Available bulk carbonate $\delta^{13}C$ records through the PETM CIE generated at marine margin locations reveal trends inconsistent with either other margin sites or open ocean sites in terms of both magnitude and structure (Figure 4.2A). Because of this, any attempt to correlate such records via $\delta^{13}C$ stratigraphy is a useless exercise. Hence we plot all such records in the depth/height domain provided by their primary author. All studied margin sites record latest Paleocene $\delta^{13}C$ values between -1.0 – 1.0 ‰, a wide range of CIE minimum $\delta^{13}C$ values between –2.6 - -5.7 ‰, and (where available) conclusion CIE values approximately between –1.0 – 1.0 ‰. Sites on the same margin illustrate a much more negative and heterogeneous CIE record the closer the site's proximity to land (i.e. Wilson Lake records a ~7.3 ‰ CIE amplitude while Bass River documents a ~3.5 ‰ CIE amplitude). All studied margins sites document $\delta^{13}C$ values prior to and after the CIE that are more negative than their open ocean counterparts.

Open ocean sites during the PETM CIE interval document generally consistent bulk carbonate $\delta^{13}C$ trends but significantly different absolute values. In comparison of all available open ocean bulk carbonate $\delta^{13}C$ PETM records, an interbasinal gradient through the entirety of the PETM CIE interval is apparent (Figure 4.2B; Figure 4.3). Before the CIE onset there is a $\delta^{13}C$ gradient between ocean basins of ~1.5 ‰. Site 1209 in the tropical North Pacific records the most positive values, followed on a negative trend by Site 690 in the Southern Ocean, Sites 1263 and 1001 in the South Atlantic and Caribbean respectively, and finally Zumaia in the North Atlantic. During the CIE $\delta^{13}C$ minimum, this gradient relationship between sites is not only maintained but amplified to ~3.2 ‰. Near an inflection point in the CIE $\delta^{13}C$ positive recovery, the interbasinal gradient drops to ~1.0 ‰ and remains low but consistent in terms of ocean-to-ocean relationships throughout the remainder of the interval of interest. The PETM CIE interval concludes with every open ocean site (except Site 213 which does not have Paleocene aged sediments) recording $\delta^{13}C$ values 0.1 – 1.0 ‰ lower than their pre-CIE levels.

NEW ZEALAND PETM BULK CARBONATE $\delta^{13}C$ AND Mg/Ca

Clarence Valley Lower Limestone records from Muzzle Stream, Dee Stream, and particularly Mead Stream record excellent examples of the PETM CIE in bulk carbonate (Figure 4.4). All three sites record pre-PETM CIE bulk carbonate $\delta^{13}C$ values significantly lower (0.6 – 1.1 ‰) than Site 1209, an open ocean Pacific location. Additionally there is a $\delta^{13}C$ gradient between our New

Zealand sites before the PETM, such that Mead Stream, the deepest depositional location, records the most positive values that are closest to Site 1209 levels, while Muzzle Stream, representing the shallowest setting records the most negative $\delta^{13}C$ values. Near the CIE onset, coincident to a positive shift in the Mg/Ca ratio of the Mead Stream bulk carbonate fraction from ~5.5 to ~8.8 mmol/mol, these relationships begin to change. While an initial 0.3 – 0.4 ‰ offset between Dee Stream and Mead Stream values is apparent ~100 kyrs before the CIE, at ~20 kyrs before the CIE onset this gradient is gone. An initial increase in the $\delta^{13}C$ gradient between Muzzle Stream and the Dee and Mead Stream records of ~1.0 ‰ at the CIE onset begins to diminish at approximately the same time Mead Stream sediments first record $\delta^{13}C$ values more positive than Site 1209. This trend was maintained until an inflection in the $\delta^{13}C$ record during the recovery interval at ~100 kyrs past the CIE onset. At the conclusion of the PETM CIE, while all of our New Zealand sites record $\delta^{13}C$ values lower than Site 1209, the pre-event $\delta^{13}C$ gradient between the site was not present, and the Mg/Ca ratio of bulk carbonate was still moderately high at ~7 mmol/mol.

Above the PETM we find similar trends (Figure 4.4) in both the Mead Stream bulk carbonate Mg/Ca ratio and the Dee Stream and Mead Stream bulk carbonate $\delta^{13}C$ records relative to an open ocean Pacific site drilled near Site 1209, DSDP Site 577 (Cramer et al., 2003). During each noted CIE interval the background $\delta^{13}C$ gradient of ~0.1 – 0.25 ‰ between Mead Stream and Dee Stream sites diminishes following a rise in the Mead Stream bulk carbonate Mg/Ca ratio.

DISCUSSION

The stable carbon isotopic composition of modern surface ocean DIC is not homogenous. Average values of the upper 100 m of the water column from a series of GEOSECS stations located in each major ocean basin reveal a positive gradient between the North Pacific Ocean, which averages ~1.21 ‰, and the South Atlantic Ocean, where average values reach ~1.87 ‰ (Östlund, 1987). Presumably this relationship is a product of the advection of ^{12}C enriched deep waters into the surface layers of the Pacific Ocean. The variability of surface ocean DIC $\delta^{13}C$ on continental margins is significantly more pronounced with values as negative as –5 - -8 ‰ associated with more proximal and riverine dominated settings (Bauch et al., 2004; Chanton, 1999).

Available bulk carbonate $\delta^{13}C$ records from open ocean locations across the PETM depict a consistent positive gradient between the Atlantic and Pacific oceans that becomes amplified through the interval of minimum bulk carbonate $\delta^{13}C$. Single specimen planktonic foraminiferal records of the same genera from Sites 1209 and 690 depict broadly similar relationships to each other (i.e. *Acarnina* from Site 1209 [Zachos et al., 2003] are consistently more positive than *Acarnina* from Site 690 [Thomas et al., 2002]). Further, nannofossil specific $\delta^{13}C$ records generated at Sites 690 and 1209 (Stoll, 2005; Stoll et al., 2007) illustrate consistent trends and absolute values to bulk $\delta^{13}C$ records from the same sites, suggesting that the bulk records we discuss represent primary surface ocean signals. These observations suggest that the global surface ocean $\delta^{13}C$ gradient during the PETM was reversed relative to the modern environment. This

corroborates well with early Paleogene neodymium isotopic analyses of fish teeth (Thomas et al., 2003) and a PETM carbonate ion concentration reconstruction (Zeebe and Zachos, 2007) that both are consistent with deep waters upwelling in the North Atlantic.

Marine shelf margin bulk carbonate $\delta^{13}C$ records of the PETM, with the exception of the New Zealand sites we describe, are uniformly more variable and isotopically negative than their open ocean counterparts. Further, where shallow depth transects are available (e.g. the New Jersey margin and the New Zealand margin intervals not deposited during CIEs), a mixing between more land proximal negative values and more positive values recorded at deeper depositional settings is evident. Continental shelf margins represent a mixing zone between isotopically light riverine derived DIC and relatively more positive open ocean DIC. One explanation for these trends would be that local or regional variations in the influence of riverine DIC on a particular location varied significantly through the PETM to the extent that an impact on the bulk carbonate $\delta^{13}C$ was realized at multiple locations. This may also explain the high $\delta^{13}C$ variability measured between sites, as the $\delta^{13}C$ of the continentally derived DIC may have been controlled by a variety of factors including the regional biosphere dynamics, the local and regional precipitation / evaporation patterns, the influence of seasonality, and further how these variables evolved through the PETM.

The New Zealand margin sites we document including Muzzle Stream, Dee Stream, and Mead Stream, illustrate consistent $\delta^{13}C$ gradient trends relative to each other as well as open ocean $\delta^{13}C$ records generated on sediments from Shatsky Rise in the tropical North Pacific through the PETM, H, and I CIEs.

During background early Paleogene sedimentation New Zealand margin records exhibit a bulk carbonate $\delta^{13}C$ gradient consistent with other margin locations such that the more distal deep location, Mead Stream, records the most positive values and the progressively shallower locations (Dee Stream and Muzzle Stream, respectively) document consistently more negative $\delta^{13}C$ trends. However, just prior to the onset of the CIEs that mark noted early Eocene hyperthermal events this gradient is weakened and eventually lost. Coincident to the decrease in the $\delta^{13}C$ gradient is an increase in the Mg/Ca ratio of the carbonate fraction of Mead Stream sediments.

We find two plausible mechanisms by which the margin $\delta^{13}C$ gradient may have been lost during the PETM and younger hyperthermal events. First, a local increase in productivity and photosynthesis may have preferentially removed ^{12}C from the surface waters and therefore increased the $\delta^{13}C$ of the DIC the carbonate we measure formed in. This is consistent with previous work on other margins that suggests that such locations become increasingly eutrophic through the PETM due to enhanced nutrient supply as a function of weathering and runoff increases (Gibbs et al., 2006). However 10 samples analyzed for total organic carbon content through the PETM at Mead Stream all yield less than the detection limit (<0.02 wt %), limiting this interpretation.

A second possible interpretation calls for an increase in the neritic carbonate production on the adjacent platform. Recent periplatform locations retain bulk carbonate $\delta^{13}C$ records that are enriched by as much as 3-5 ‰ relative to contemporaneous open ocean pelagic records, indicating that neritic carbonate, which is largely composed of aragonite and high-Mg calcite, fractionates carbon

isotopes significantly heavier than does low-Mg calcite (Malone, 2000; Swart and Eberli, 2005). However, while digenesis of such sediments makes it inherently difficult to quantify the amount or existence of an original neritic carbonate component by mineralogical characterization (Swart and Eberli, 2005) the $\delta^{13}C$ values and Mg/Ca increases we document are supportive of the concept that slight increases in high-Mg calcite deposition at Mead Stream did occur during noted hyperthermal events. Further, neritic carbonate production on the Chatham Rise (Figure 4.1) has been documented previously through the Paleocene – Eocene transition (Gordon and Taylor, 1999). This observation is interesting, as neritic carbonate production dominantly occurs at lower latitudes (Swart and Eberli, 2005). However such an occurrence would be consistent with other flora and fauana records that record high-latitude migrations of tropical organisms during the PETM (e.g. Bowen et al., 2002; Kelly, 2002; Wing et al., 2005).

CONCLUSIONS

Records of the carbon isotopic composition of bulk marine carbonate deposited through the PETM CIE interval at multiple global sites do not display homogenous trends, amplitudes, or absolute values. Nor should they be expected to, given the modern surface ocean DIC $\delta^{13}C$ variability. A surface ocean $\delta^{13}C$ gradient likely existed between the Pacific and Atlantic oceans throughout the PETM CIE interval, such that the Pacific was significantly more positive than the Atlantic. This gradient was accentuated during the PETM CIE minimum. This trend is opposite of what is measured in today's oceans, and suggests deepwater

upwelling occurred in the North Atlantic, rather than the North Pacific as it does today.

In contrast to open ocean locations, bulk carbonate $\delta^{13}C$ records generated on continental margins are difficult to chemostratigraphically tie to one another because of local and/or regional variations in the $\delta^{13}C$ composition and balance of continentally derived riverine DIC and open ocean DIC. A transect of the New Jersey margin supports this concept particularly well as two sites located there display a steep gradient between a more land proximal and negative $\delta^{13}C$ bulk carbonate record at Wilson Lake and a more distant and positive $\delta^{13}C$ bulk carbonate record at Bass River.

Marine margin sites that now outcrop on South Island, New Zealand including Mead Stream, Dee Stream, and Muzzle Stream reveal a similar bulk carbonate $\delta^{13}C$ gradient between more shallow and deep sites during some portions of the late Paleocene – early Eocene transition. However, this gradient is eliminated during the PETM, H, and I CIEs when bulk carbonate $\delta^{13}C$ records at all three sites decrease at a lesser rate than open ocean sites. This observation is consistent with a small increase in a neritic carbonate lithologic component that is further substantied by the Mg/Ca ratio of the bulk carbonate fraction of Mead Stream samples. Such an increase may relate to an intensification of neritic carbonate production at relatively high latitudes during global warming events.

ACKNOWLEDGMENTS

This work was funded by the U.S. National Science Foundation Biocomplexity Grant (EAR 0120727) and the N.Z. Foundation for Research, Science and

Technology through the GNS Global Change Through Time programme. We thank Richard and Sue Murray for access to both Mead Stream, Dee Stream, and Muzzle Streaam outcrops, located on their Marlborough, N. Z. ranch, Percy Strong, James Crampton, John Simes, and Victor Villasante, for assistance during fieldwork.

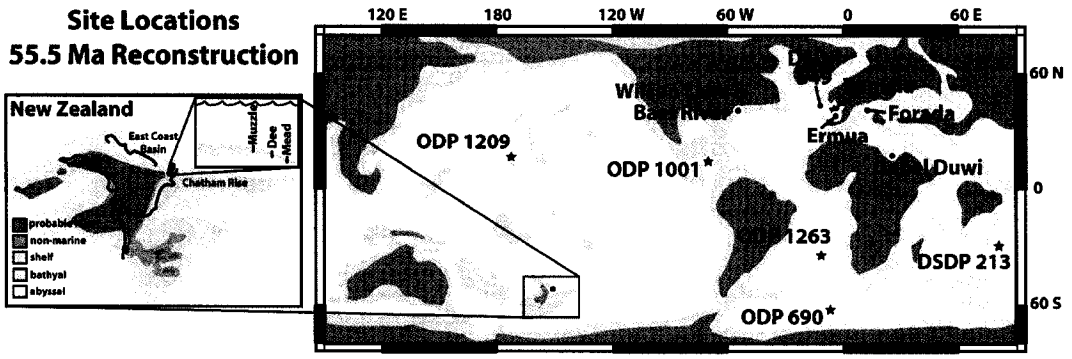

Figure 4.1. Site locations at 55.5 Ma. (A) Discussed sites on a paleoreconstruction (http://www.odsn.de/services/paleomap/paleomap.html) of the Earth at the Paleocene / Eocene boundary. Light grey shapes represent continental lithosphere and oceanic rises. Dark grey shapes represent approximation of land area. Stars denote sites used in open ocean compilation and animation. (B) The proto-New Zealand continent at the same time as (A) after Hollis et al., 2005.

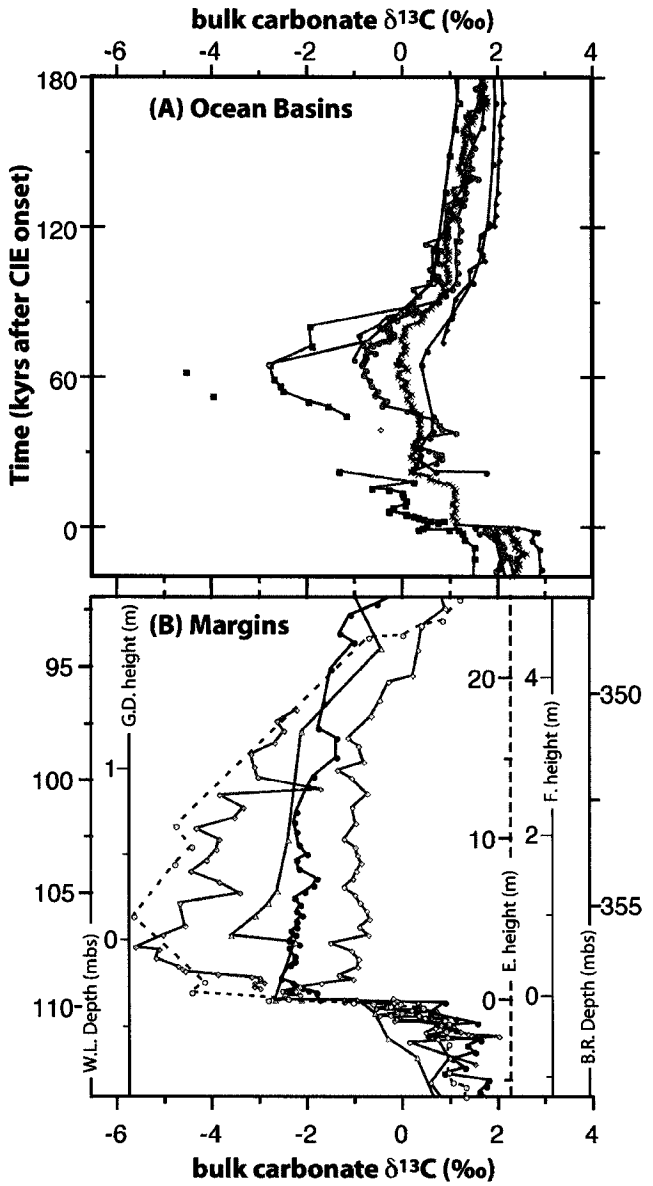

Figure 4.2. Compiled published PETM bulk carbonate d13C records. (A) Marine margin records from Wilson Lake, New Jersey, U.S. (orange diamonds), Bass River, New Jersey, U.S. (blue circles), Forada, Italy (grey diamonds), Gebel Duwi, Egypt (grey triangles), and Ermua, Spain (grey circles). (B) Open ocean records from ODP Site 1209 (dark grey circles), DSDP Site 213 (blue diamonds), ODP Site 690 (dark red X's), ODP Site 1263 (purple circles), ODP Site 1001 (pink circles), DSDP Site 549 (orange diamonds), and Zumaia, Spain (dark red squares). See text for record citation. Note that margin sections are plotted versus depth and are not meant to correspond to any time interval except for the onset of the CIE while open ocean sections are plotted versus time. W.L. = Wilson Lake, G.D. = Gebel Duwi, E. = Ermua, F. = Forada, and B.R. = Bass River.

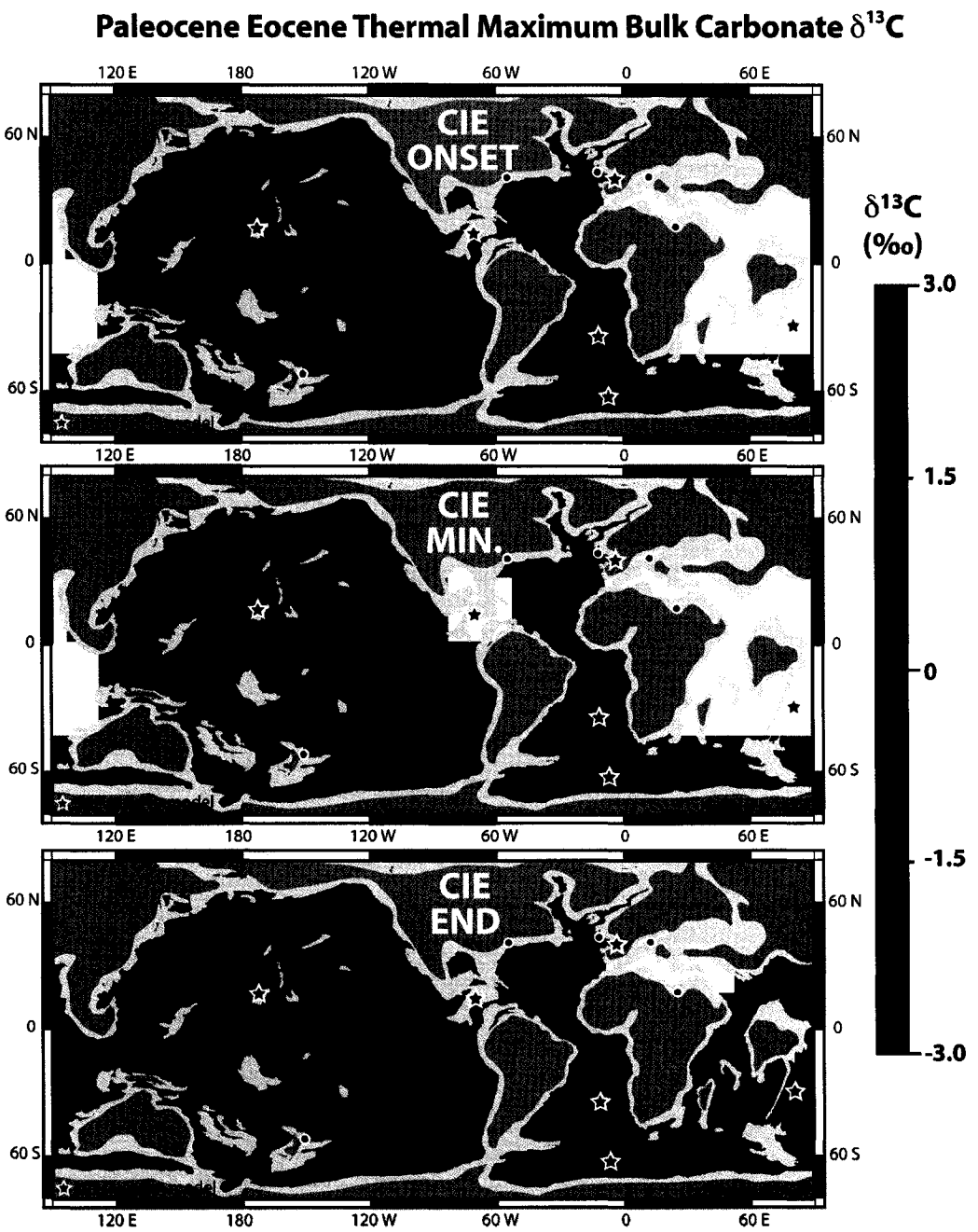

Figure 4.3. Open ocean bulk carbonate $\delta^{13}C$ animation time slices. Time slices at 0, 66, and 170 kyrs past the onset of the PETM CIE. Earth reconstruction, land area, and site locations are as described in Figure 4.1.

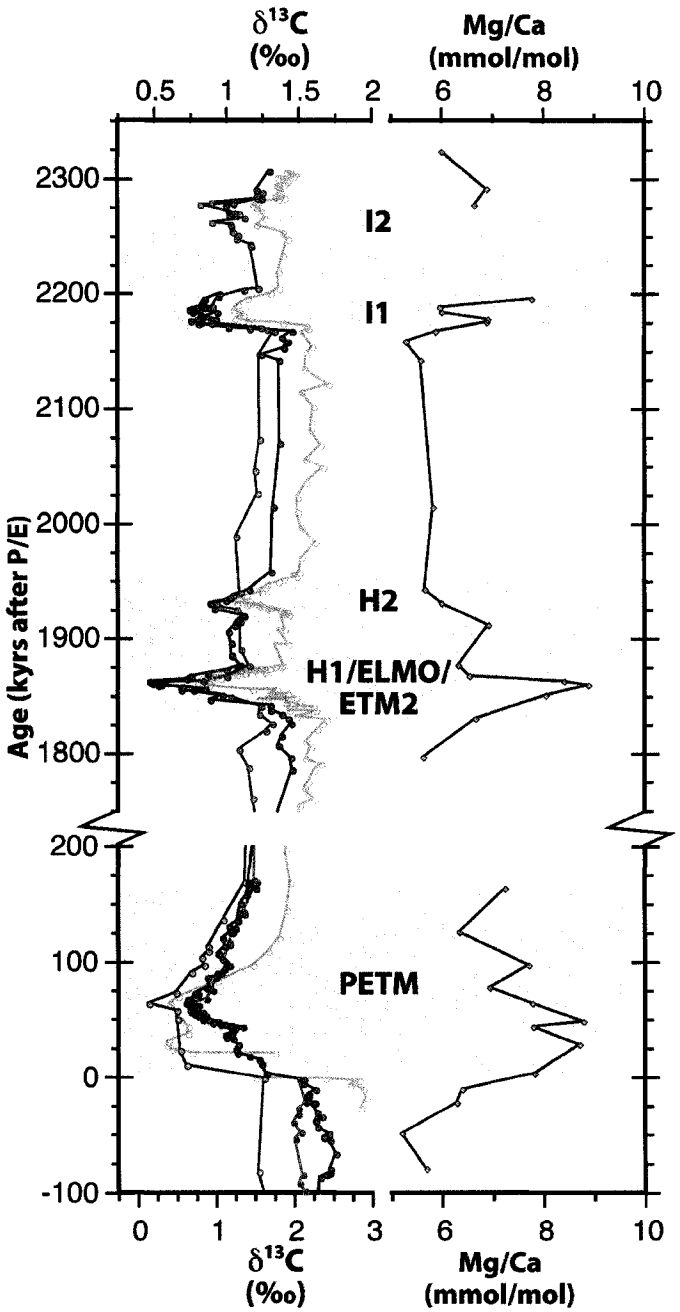

Figure 4.4. Pacific Ocean site carbonate geochemistry through 5 similar environmental perturbations. Bulk carbonate $\delta^{13}C$ records for Mead Stream (purple circles), Dee Stream (pink circles), Muzzle Stream (orange circles), and Shatsky Rise (open grey circles). The Shatsky Rise PETM record is from ODP Site 1209, while the H and I CIEs are documented at DSDP Site 577. Mead Stream carbonate fraction Mg/Ca ratio (green diamonds). Note changes in both the age scale between the PETM and H1, and the $\delta^{13}C$ scale between the PETM and the younger four events.

Table 4.1. Open ocean correlation points.

Location	Depth domain	Pre-PETM datum	Pre-PETM datum source	Pre-PETM datum depth/height	CIE onset depth/height	Plateau 2 base depth/height	Plateau 2 top depth/height
690	mbsf	base C24r	Spieß, V., 1990	185.48	170.65	170.41	170.17
1209	mbsf	FO D. nobilis	Shipboard Scientific Party, 2002. Site 1209	204.75	196.45	196.44	196.37
1263	mcd	FO D. multiradius	Shipboard Scientific Party, 2004. Site 1263	357.88	335.71	335.69	335.43
1001	mcd	FO D. multiradius	Shipboard Scientific Party, 1997. Site 1001	29.54	3.61		
213	mbsf						
Zumaia	m	LSR	Schmitz, 1997		0	0.491	1.513
549	mbsf	FO D. multiradius	Muller, 1985	353.095	339.35		

Table 4.1. Open ocean correlation points continued.

CIE min. depth/height	CIE recovery inflection depth/height	CIE recovery end depth/height	Post-PETM datum	Post-PETM datum source	Post-PETM datum depth/height
169.97	169.05	167.05	H1 onset	Cramer et al., 2003	135.58
196.35	196.23	195.93	FO D. diastypus	Shipboard Scientific Party, 2002. Site 1209	192.60
335.23	334.56	333.71	H1 onset	Lourenset al., 2005	295.45
	3.31	1.87	LO Fasculithus tympaniformis Average	Shipboard Scientific Party, 1997. Site 1001	-2.3
	147.38	145.77	HO Fasciculithus spp.	S. Gartner, 1974	142.895
3.611	5.292	7.001	LSR	Schmitz, 1997	
338.75	337.87	337.49	HO Fasciculithus spp.	Muller, 1985	335.06

Table 4.2. Mead Stream and Muzzle Stream geochemical analyses.

Location	sample height (m above P/E)	$\delta^{13}C$	Mg (mmol/kg)	Ca (mmol/kg)	Mg/Ca (mmol/mol)
Mead	43.65	€	2882.20	17.24	5.98
Mead	42.75	1.29			
Mead	41.81	1.20	3042.53	20.90	6.87
Mead	41.38	1.24			
Mead	41.00	0.99	2902.97	19.23	6.63
Mead	40.50	1.01			
Mead	38.12	0.94			
Mead	37.89	0.84	3269.60	25.34	7.75
Mead	37.65	0.82			
Mead	37.58	0.84			
Mead	37.54	0.79	3060.18	18.19	5.95
Mead	37.50	0.75			
Mead	37.45	0.74			
Mead	37.30	0.76	2872.81	17.17	5.98
Mead	37.18	0.81			
Mead	37.06	0.82			
Mead	36.91	0.92	3055.15	21.05	6.89
Mead	36.80	0.74			
Mead	36.75	0.82	2764.80	18.96	6.86
Mead	36.65	0.80			
Mead	36.45	1.00			
Mead	36.22	1.44	2971.16	17.40	5.86
Mead	36.08	1.38			
Mead	36.00	1.41	3080.63	16.26	5.28
Mead	35.86	1.39			
Mead	35.71	1.23			
Mead	35.58	1.36	3098.22	17.25	5.57

Mead	33.77	1.36			
Mead	32.37	1.31	3066.41	17.81	5.81
Mead	30.94	1.30			
Mead	29.90	1.15	3053.73	17.23	5.64
Mead	29.25	0.99			
Mead	29.06	0.88	2834.13	16.94	5.98
Mead	28.89	0.90			
Mead	28.66	1.11			
Mead	28.53	1.06			
Mead	28.45	1.04	2954.96	20.37	6.89
Mead	28.30	1.00			
Mead	28.07	1.02			
Mead	27.80	1.02			
Mead	27.60	1.09	3118.58	19.65	6.30
Mead	27.50	1.06			
Mead	27.20	0.99			
Mead	26.94	0.86			
Mead	26.74	0.75	3005.47	19.60	6.52
Mead	26.52	0.71			
Mead	26.31	0.46	3213.00	26.96	8.39
Mead	26.24	0.47			
Mead	26.19	0.48			
Mead	26.14	0.53			
Mead	26.10	0.52	2874.18	25.46	8.86
Mead	26.04	0.68			
Mead	25.96	0.84			
Mead	25.91	0.76			
Mead	25.68	0.96	2861.83	22.96	8.02
Mead	25.49	0.88			
Mead	25.24	1.29			
Mead	25.03	1.30			

Mead	24.85	1.37			
Mead	24.65	1.42	2839.89	18.85	6.64
Mead	24.45	1.44			
Mead	24.32	1.37			
Mead	24.21	1.35			
Mead	24.08	1.43	2767.35	15.53	5.61
Mead	23.94	1.44			
Mead	22.82	1.20			
Mead	18.29	1.37			
Mead	14.17	1.49			
Mead	13.18	1.52			
Mead	11.70	1.61			
Mead	9.91	1.62			
Mead	8.76	1.68			
Mead	7.98	1.60			
Mead	6.61	1.63			
Mead	5.54	1.67			
Mead	3.71	1.40			
Mead	3.59	1.50	2889.60	20.84	7.21
Mead	3.59	1.40			
Mead	3.46	1.38			
Mead	3.29	1.30			
Mead	3.12	1.28			
Mead	2.96	1.26			
Mead	2.85	1.15			
Mead	2.78	1.18			
Mead	2.78	1.19			
Mead	2.74	1.17	2933.80	18.52	6.31
Mead	2.62	1.07			
Mead	2.47	1.11			
Mead	2.47	1.10			

Mead	2.32	1.00			
Mead	2.32	1.02			
Mead	2.21	1.06			
Mead	2.14	1.11			
Mead	2.09	1.14	3073.64	23.59	7.68
Mead	2.09	1.13			
Mead	2.03	1.09			
Mead	1.96	1.04			
Mead	1.96	1.00			
Mead	1.90	0.98			
Mead	1.89	0.87			
Mead	1.71	0.90	2592.72	17.92	6.91
Mead	1.71	0.85			
Mead	1.61	0.71			
Mead	1.61	0.75			
Mead	1.52	0.65			
Mead	1.52	0.62			
Mead	1.45	0.60	2571.86	19.92	7.75
Mead	1.43	0.66			
Mead	1.42	0.62			
Mead	1.41	0.65			
Mead	1.37	0.66			
Mead	1.34	0.72			
Mead	1.25	0.64			
Mead	1.25	0.69			
Mead	1.19	0.80			
Mead	1.13	0.70			
Mead	1.08	0.84			
Mead	1.03	0.81			
Mead	1.02	0.81			
Mead	0.96	0.81			

Mead	0.96	0.88			
Mead	0.90	1.01	2600.90	22.78	8.76
Mead	0.87	0.94			
Mead	0.85	1.02			
Mead	0.83	1.09			
Mead	0.82	1.03			
Mead	0.80	1.18			
Mead	0.78	1.16			
Mead	0.75	1.23	2776.15	21.55	7.76
Mead	0.72	1.22			
Mead	0.70	1.20			
Mead	0.66	1.18			
Mead	0.62	1.10			
Mead	0.59	1.11			
Mead	0.57	1.20			
Mead	0.47	1.27	2896.28	25.15	8.68
Mead	0.40	1.24			
Mead	0.35	1.26			
Mead	0.30	1.41			
Mead	0.26	1.53			
Mead	0.20	1.56			
Mead	0.06	1.63	2092.42	16.32	7.80
Mead	-0.03	2.11			
Mead	-0.10	2.10			
Mead	-0.21	2.25	2934.08	18.69	6.37
Mead	-0.29	2.17			
Mead	-0.35	2.14			
Mead	-0.35	2.16			
Mead	-0.41	2.15			
Mead	-0.47	2.24	2500.15	15.66	6.26
Mead	-0.47	2.22			

Mead	-0.65	2.28			
Mead	-0.73	2.33			
Mead	-0.73	2.28			
Mead	-0.82	2.25			
Mead	-0.93	2.28			
Mead	-1.05	2.43	2361.41	12.24	5.18
Mead	-1.12	2.36			
Mead	-1.17	2.44			
Mead	-1.41	2.51			
Mead	-1.71	2.44	2635.54	14.93	5.66
Mead	-1.78	2.43			
Mead	-1.80	2.39			
Mead	-1.86	2.31			
Mead	-2.74	2.25			
Mead	-3.55	2.48			
Muzzle	2.715	1.31			
Muzzle	2.325	1.42			
Muzzle	1.695	1.36			
Muzzle	1.235	1.08			
Muzzle	0.905	0.88			
Muzzle	0.845	0.88			
Muzzle	0.765	0.80			
Muzzle	0.675	0.83			
Muzzle	0.635	0.67			
Muzzle	0.525	0.47			
Muzzle	0.465	0.12			
Muzzle	0.415	0.48			
Muzzle	0.355	0.49			
Muzzle	0.145	0.53			
Muzzle	0.045	0.61			
Muzzle	-0.045	1.60			

Muzzle	-0.395	1.53			
Muzzle	-0.635	1.76			
Muzzle	-0.745	1.66			
Muzzle	-0.805	1.91			
Muzzle	-1.205	2.42			
Muzzle	-1.615	2.46			
Muzzle	-2.465	2.38			
Muzzle	-3.225	2.32			
Muzzle	-3.245	2.45			

CHAPTER 5.

CONCLUSIONS AND FUTURE WORK

CLARENCE VALLEY, NEW ZEALAND

I document and discuss the late Paleocene to early Eocene sedimentary succession of a series of paleo-slope margin sites now exposed as outcrops in the Clarence River valley, and relate these records to the broad early Paleogene global trends outlined in *Chapter 1* with special attention paid to the noted questions posed in *Chapter 1* regarding the Paleocene Eocene Thermal Maximum (PETM) carbon injection. Clarence valley, situated in Marlborough Region, South Island, New Zealand, contains an uplifted and rotated block of Muzzle Group rocks that once were emplaced on the proto-New Zealand margin where they accumulated as sediments at upper to mid bathyal depths (Strong et al., 1995, Crampton et al., 2003). Within the Muzzle Group, the Lower Limestone member of the Amuri Limestone Formation represents rocks of late Paleocene to early Eocene age (Strong et al., 1995). Lower Limestone rocks are principally composed of pelagic carbonates, detrital siliciclastic clay grains, biogenic silica, secondary chert (Reay, 1993), and potentially a small fraction of neritic carbonates sourced from the nearby Chatham Rise. A series of tributary streams to the Clarence River bisect the Lower Limestone block approximately perpendicular to strike resulting in excellent outcrops with nearly complete exposure. These outcrops represent a paleo-depth transect from shallow relatively

thin sections in the south to deeper relatively thick sequences to the north. Two of the latter, Mead Stream and Dee Stream, have previously been shown to retain a relatively complete and expanded Lower Limestone sequence including a recessed marl-rich interval known as Dee Marl, which marks the PETM (Hancock et al., 2003; Hollis et al., 2005a).

QUESTIONS ADDRESSED

HOW UNIQUE WAS THE PETM?

The PETM is embodied at Mead Stream and Dee Stream outcrop sections by Dee Marl (Hancock et al., 2003); a prominent recessed unit comprised of multiple marl-rich beds that grades up section into limestone and records a prominent negative carbon isotope excursion (CIE) at base. I illustrate in *Chapter 3* that independent of age model, the elevated terrigenous concentration that created the Dee Marl was likely the result of increased terrigenous accumulation as a function of increased temperatures, a more vigorous hydrologic cycle, and ultimately enhanced erosion of the New Zealand continent. This increase in terrigenous sediment accumulation is accompanied by an increase in carbonate accumulation, resulting in an overall expanded PETM sequence at both Mead Stream and Dee Stream (~3.7 and ~2.6 m thick respectively) relative to condensed deep-sea sites, which were subjected to carbonate dissolution because of an increase in CO_2 and acidity (e.g. the 0.85 m thick Walvis Ridge Site 1262). I detail in *Chapter 2* that above the PETM at Mead Stream, Dee Stream, and several deep-sea sites, similar phenomena are apparent. I document two younger paired sets of early Eocene hyperthermal events that each reveal negative CIEs

and expanded marl-rich units at Mead Stream and Dee Stream that accumulated coincident to identical CIEs and condensed carbonate dissolution horizons in deep-sea sections. This work suggests that a mechanism was in place in the early Paleogene that was capable of repeated injections of istopically light carbon resulting in multiple hyperthermal events during a long term warming trend. Critically, this suggests that the PETM was not a unique event, but rather that it should be treated as an extreme example of a more fundamental Earth system process.

DO ENVIRONMENTAL IMPACTS CORRELATE WITH THE CARBON INPUT?

To date, no published environmental consequences of the PETM have been shown to have precisely coincided with the phase of the carbon injection at both onset and end. This has limited a direct understanding of the nature of the actual carbon injection. In *Chapter 3* I develop and employ an image analysis based method to quantify the abundance of bioturbating macrofauna trace fossils through the PETM sequence at both Mead Stream and Dee Stream. Both sites illustrate consistent trends through the entire PETM interval with background levels of trace fossils present before and after a zone nearly completely devoid of all bioturbation structures. This zone precisely coincides with the phase of the carbon injection. In the modern oceans, bioturbating macrofauna are not found beneath hypoxic water masses containing less than ~0.2 ml/L dissolved O_2 (Levin, 2003). This suggests that the water mass that bathed the New Zealand margin during the PETM became depleted with respect to dissolved O_2 precisely during the massive carbon injection. I present two plausible mechanisms for this

relationship including a decrease in ocean circulation rate as a function of enhanced high-latitude runoff that would have resulted in increased organic carbon oxidation for every parcel of intermediate-deep water, and the oxidation of a large mass of methane within intermediate waters that would have removed two mols of dissolved O_2 for every one mol of carbon added. The records I present are more stratigraphically consistent with the latter.

HOW CONSISTENT ARE CIE RECORDS BETWEEN BASINS AND SETTINGS?

The nature of the carbon isotopic excursion at the PETM in terms of its structure, amplitude, and the absolute value of key time-slices, offers important constraints on the mass and rate of the carbon input via simple mass balance arguments (Dickens et al., 1995). Therefore, if heterogeneities in the nature of the CIE between sites exist, they complicate these interpretations. In *Chapter 4* I have collected a suite of thirteen available PETM bulk carbonate CIE records and compared them to records I have collected and expanded on from Mead Stream, Dee Stream, and Muzzle Stream (the shallowest slope site available in the Clarence River valley). I document that before, during, and after the PETM there was a consistent gradient between open ocean settings such that the Pacific recorded heavier values while the Atlantic recorded lighter values, and argue that likely this was a function of where deep ^{12}C enriched waters were upwelling. Importantly, this relationship appears to have been reversed during the PETM relative to the modern oceans, such that waters appear to have been upwelling in the Atlantic. I further document in *Chapter 4* that margin sites with the notable exception of those now outcropping on New Zealand record significantly more

variable and negative PETM CIEs that likely are a product of their location relative to the confluence of istopically light continentally derived dissolved inorganic carbon (DIC) with the heavier open ocean (DIC). Clarence valley sites however reveal the opposite affect, as they record diminished CIE amplitudes relative to open ocean sites, a trend consistent during the PETM and each younger hyperthermal. Additionally, I present work that shows that the Mg/Ca ratio of the bulk carbonate component of Mead Stream sediments increases coincident to each CIE. These results suggest one explanation of the dampened CIE affect may be that an increase in the production of ^{13}C-enriched neritic carbonate consisting of high-Mg calcite on Chatham Rise occurred coincident to each hyperthermal.

FUTURE WORK

It has been hypothesized here that intervals of marl deposition on the New Zealand margin during the late Paleocene to early Eocene, represent periods of elevated temperatures and an associated acceleration of the hydrologic cycle and erosion. This work has focused on the Lower Limestone Member of the Amuri Limestone Formation. However, above the Lower Limestone, in a sequence known as the Lower Marl, the sedimentary sequence at every Clarence valley location becomes dominated by terrigenous detrital material. Preliminary resolution work suggests that the Lower Marl represents the Early Eocene Climatic Optimum (EECO) ca. 52-48 Ma, however further work is needed to constrain a more precise stratigraphy. This interval, particularly at Mead Stream, reveals an intricate series of bed packets, each containing multiple marl beds and binding thicker limestone beds. One might suppose that each bed packet

represents a discrete event that is difficult to distinguish in deep-sea sequences because of dissolution and low-sedimentation rates, so that the expanded Mead Stream section may reveal in fact more 'hyperthermal' events upon future work.

The notion of multiple events overall offers an interesting perspective on early Paleogene paleoclimatology as an analog to modern anthropogenic carbon cycle and climate perturbations, because the scale of each event may prove useful. In other words, multiple events of variable size carbon injections may yield different magnitudes of responses or a better understanding of environmental thresholds. In this respect, one might predict that a detailed record of the abundance of bioturbating macrofauna trace fossils through each younger event at Mead Stream for example may show no change through smaller events but similar variability as the PETM through larger events, as this is a measurement of a dissolved oxygen concentration threshold. Future work is necessary to constrain this, and other environmental responses to each younger hyperthermal event relative to the scale of the event in order to gain a better understanding of each event's utility for understanding modern climate dynamics.

BIBLIOGRAPHY

Bains, S., Corfield, R.M., and Norris, R.D., 1999, Mechanisms of Climate Warming at the End of the Paleocene: Science, v. 285, p. 724-727.

Bauch, H.A., Erlenkeuser, H., Bauch, D., Mueller-Lupp, T., and Taldenkova, E., 2004, Stable oxygen and carbon isotopes in modem benthic foraminifera from the Laptev Sea shelf: implications for reconstructing proglacial and profluvial environments in the Arctic: Marine Micropaleontology, v. 51, p. 285-300.

Boven, K.L., and Rea, D.K., 1998, Partitioning of eolian and hemipelagic sediment in eastern Equatorial Pacific core TR 163-31B and late Quaternary Paleoclimate of the Northern Andes: Journal of Sedimentary Research, v. 68, p. 850-855.

Bowen, G.J., Beerling, D.J., Koch, P.L., Zachos, J.C., and Quattlebaum, T., 2004, A humid climate state during the Palaeocene/Eocene thermal maximum: Nature, v. 432, p. 495-499.

Bowen, G.J., Bralower, T.J., Delaney, M.L., Dickens, G.R., Kelly, D.C., Koch, P.L., Kump, L.R., Meng, J., Sloan, L.C., Thomas, E., Wing, S.L., and Zachos, J.C., 2006, Eocene hyperthermal event offers insight into greenhouse warming: Eos (Transactions, American Geophysical Union), v. 87, p. 165-169.

Bowen, G.J., Clyde, W.C., Koch, P.L., Ting, S., Alroy, J., Tsubamoto, T., Wang, Y., and Wang, Y., 2002, Mammalian Dispersal at the Paleocene/Eocene Boundary: Science, v. 295, p. 2062-2065.

Bowles, J., 2006, DATA REPORT: Revised Magnetostratigraphy and magnetic Mineralogy of sediments from Walvis Ridge, Leg 208.

Bralower, T.J., Thomas, D.J., Zachos, J.C., Hirshmann, M.M., Rohl, U., Sigurdsson, H., Thomas, E., and Whitney, D.L., 1997, High-resolution records of the late Paleocene thermal maximum and circum-Caribbean volcanism: Is ther a causal link?: Geology, v. 25, p. 963-966.

Chanton, J.P., 1999, Plankton and dissolved inorganic carbon isotopic composition in a river-dominated estuary: Apalachicola Bay, Florida: Estuaries, v. 22, p. 575-583.

Cramer, B.S., Wright, J.D., Kent, D.V., and Aubry, M.P., 2003, Orbital climate forcing of delta C-13 excursions in the late Paleocene-early Eocene (chrons C24n-C25n): Paleoceanography, v. 18.

Crampton, J., Laird, M., Nicol, A., Townsend, D., and Van Dissen, R., 2003, Palinspastic reconstructions of southeastern Marlborough, New Zealand, for mid-Cretaceous-Eocene times: New Zealand Journal of Geology and Geophysics, v. 46, p. 143-175.

Crouch, E.M., Dickens, G.R., Brinkhuis, H., Aubry, M.P., Hollis, C.J., Rogers, K.M., and Visscher, H., 2003, The Apectodinium acme and terrestrial discharge during the Paleocene-Eocene thermal maximum: new palynological, geochemical and calcareous nannoplankton observations at Tawanui, New Zealand: Palaeogeography Palaeoclimatology Palaeoecology, v. 194, p. 387-403.

Dickens, G.R., 2003, Rethinking the global carbon cycle with a large, dynamic and microbially mediated gas hydrate capacitor: Earth and Planetary Science Letters, v. 213, p. 169-183.

Dickens, G.R., Castillo, M.M., and Walker, J.C.G., 1997, A blast of gas in the latest Paleocene: Simulating first-order effects of massive dissociation of oceanic methane hydrate: Geology, v. 25, p. 259-262.

Dickens, G.R., Oneil, J.R., Rea, D.K., and Owen, R.M., 1995, Dissociation of Oceanic Methane Hydrate as a Cause of the Carbon-Isotope Excursion at the End of the Paleocene: Paleoceanography, v. 10, p. 965-971.

Farley, K.A., and Eltgroth, S.F., 2003, An alternative age model for the Paleocene-Eocene thermal maximum using extraterrestrial He-3: Earth and Planetary Science Letters, v. 208, p. 135-148.

Francus, P., 2001, Quantification of bioturbation in hemipelagic sediments via thin-section image analysis: Journal of Sedimentary Research, v. 71, p. 501-507.

Frey, R.W., and Pemberton, S.G., 1985, Biogenic Structures in Outcrops and Cores .1. Approaches to Ichnology: Bulletin of Canadian Petroleum Geology, v. 33, p. 72-115.

Gartner, S., 1974, Nannofossil biostratigrpahy, Leg 22, *in* von der Borch, C.C., and Sclater, J.G., eds., Deep Sea Drilling Project Inifial Reports: Washington, p. 577-599.

Gibbs, S.J., Bralower, T.J., Bown, P.R., Zachos, J.C., and Bybell, L.M., 2006, Shelf and open-ocean calcareous phytoplankton assemblages across the Paleocene-Eocene Thermal Maximum: Implications for global productivity gradients: Geology, v. 34, p. 233-236.

Giusberti, L., Rio, D., Agnini, C., Backman, J., Fornaciari, E., Tateo, F., and Oddone, M., 2007, Mode and tempo of the Paleocene-Eocene thermal maximum in an expanded section from the Venetian pre-Alps: Geological Society of America Bulletin, v. 119, p. 391-412.

Gordon, D.P., and Taylor, P.D., 1999, Latest Paleocene to earliest Eocene bryozoans from Chatham Island, New Zealand: Bulletin of the Natural History Museum, London, Geology Series, v. 55, p. 1-45.

Hancock, H.J.L., Dickens, G.R., Strong, C.P., Hollis, C.J., and Field, B.D., 2003, Foraminiferal and carbon isotope stratigraphy through the Ppaleocene-Eocene transition at Dee Stream, Marlborough, New Zealand: New Zealand Journal of Geology and Geophysics, v. 46, p. 1-19.

Hollis, C.J., Dickens, G.R., Field, B.D., Jones, C.M., and Strong, C.P., 2005a, The Paleocene-Eocene transition at Mead Stream, New Zealand: a southern Pacific record of early Cenozoic global change: Palaeogeography Palaeoclimatology Palaeoecology, v. 215, p. 313-343.

Hollis, C.J., Field, B.D., Jones, C.M., Strong, C.P., Wilson, G.J., and Dickens, G.R., 2005b, Biostratigraphy and carbon isotope stratigraphy of uppermost Cretaceous-lower Cenozoie Muzzle Group in middle Clarence valley, New Zealand: Journal of the Royal Society of New Zealand, v. 35, p. 345-383.

Honjo, S., 1982, Seasonality and interaction of biogenic and lithogenic particulate flux at the Panama basin: Science, v. 218, p. 883-884.

Hovan, S.A., and Rea, D.K., 1992, Paleocene/Eocene boundary changes in atmospheric and oceanic circulation: A southern hemisphere record: Geology, v. 20.

Janecek, T.R., and Rea, D.K., 1983, Eolian deposition in the northeast Pacific Ocean: Cenozoic history of atmospheric circulation: Geological Society of America Bulletin, v. 94, p. 730-738.

Kaiho, K., Arinobu, T., Ishiwatari, R., Morgans, H.E.G., Okada, H., Takeda, N., Tazaki, K., Zhou, G., Yoshimichi, K., Matsumoto, R., Hirai, A., Niitsuma, N., and Wada, H., 1996, Latest Paleocene benthic foraminiferal extinctin and environmental changes at Tawanui, New Zealand: Paleoceanography, v. 11, p. 447-465.

Kaiho, K., Takeda, K., Petrizzo, M.R., and Zachos, J.C., 2006, Anomalous shifts in tropical Pacific planktonic and benthic foraminiferal test size during the Paleocene-Eocene thermal maximum: Palaeogeography Palaeoclimatology Palaeoecology, v. 237, p. 456-464.

Kelly, D.C., 2002, Response of Antarctic (ODP Site 690) planktonic foraminifera to the Paleocene-Eocene thermal maximum: Faunal evidence for ocean/climate change: Paleoceanography, v. 17.

Kelly, D.C., Bralower, T.J., Zachos, J.C., Silva, I.P., and Thomas, E., 1996, Rapid diversification of planktonic foraminifera in the tropical Pacific (ODP Site 865) during the late Paleoecene thermal maximum: Geology, v. 24, p. 423-426.

Kennett, J.P., and Stott, L.D., 1991, Abrupt Deep-Sea Warming, Palaeoceanographic Changes and Benthic Extinctions at the End of the Paleocene: Nature, v. 353, p. 225-229.

Kent, D.V., Cramer, B.S., Lanci, L., Wang, D., Wright, J.D., and Van der Voo, R., 2003, A case for a comet impact trigger for the Paleocene/Eocene thermal maximum and carbon isotope excursion: Earth and Planetary Science Letters, v. 211, p. 13-26.

Kurtz, A.C., Kump, L.R., Arthur, M.A., Zachos, J.C., and Paytan, A., 2003, Early Cenozoic decoupling of the global carbon and sulfur cycles: Paleoceanography, v. 18.

Levin, L.A., 2003, Oxygen Minimum Zone Benthos: Adaptation and Community Response to Hypoxia: Oceanography and Marine Biology, v. 41, p. 1-45.

Li, X., Coles, B., Ramsey, M., and Thorton, I., 1995, Sequential extraction of soils for multielement analysis by ICP-AES: Chemical Geology, v. 124, p. 109-123.

Lourens, L.J., Sluijs, A., Kroon, D., Zachos, J.C., Thomas, E., Rohl, U., Bowles, J., and Raffi, I., 2005, Astronomical pacing of late Palaeocene to early Eocene global warming events: Nature, v. 435, p. 1083-1087.

Lyle, A.O., and Lyle, M.W., 2002, Determination of Biogenic Opal in Pelagic Marine Sediments: A Simple Method Revisited: College Station.

Malone, M., 2000, DATA REPORT: GEOCHEMISTRY AND MINERALOGY OF PERIPLATFORM CARBONATE SEDIMENTS: SITES 1006, 1008, AND 1009: College Station, TX.

Mehra, O.P., and Jackson, M.L., 2002, Iron Oxide Removal from Soils and Clays by a Dithionite-Citrate System Buffered with Sodium Biocarbonate: New York, Pergamn Press, 317-327 p.

Miller, K.G., Janecek, T.R., Katz, M.E., and Keil, D.J., 1987, Abyssal circulation and benthic foraminiferal changes near the Paleocene/Eocene boundary: Paleoceanography, v. 2, p. 741-761.

Mita, I., 2001, DATA REPORT: Early to late Eocene calcareous nannofossil assemblages of Sites 1051 and 1052, Blake Nose, northwestern Atlantic Ocean, Proceeds of the Ocean Drilling Program, Scientific Results, Volume 171 B, p. 1-28.

Moore, T.C., and Rabionowitz, P.D., 1984: Washington, D.C., U.S. Gonvernment Printing Office.

Muller, 1985, Nannofossil biostratigraphy, Leg 80.

Nicolo, M.J., Dickens, G.R., Hollis, C.J., and Zachos, J.C., 2007, Multiple early Eocene hyperthermals: Their sedimentary expression on the New Zealand continental margin and in the deep sea: Geology, v. 35, p. 699-702.

Östlund, H.G., 1987, GEOSECS Atlantic, Pacific, and Indian Ocean expeditions : volume 7, shorebased data and graphics: Washington, National Science Foundation, xxxvi, 200 p. p.

Party, S.S., 1997, Site 1001: College Station, TX, Ocean Drilling Program.

—, 2002, Site 1209, *in* Bralower, T.J., Premoli-Silva, I., and Malone, M., eds., Proceedings of the Ocean Drilling Program, Initial Reports, Volume 198: College Station, TX, Ocean Drilling Program.

—, 2004, 1263: College Station, TX, Ocean Drilling Program.

Pearson, P.N., van Dongen, B.E., Nicholas, C.J., Pancost, R.D., Schouten, S., Singano, J.M., and Wade, B.S., 2007, Stable warm tropical climate through the Eocene Epoch: Geology, v. 35, p. 211-214.

Poppe, L.J., Eliason, A.H., Fredericks, J.J., Rendigs, R.R., Blackwood, D., and Polloni, C.F., 2003, Grain-Size Analysis of Marine Sediments: Methodology adn Data Processing, U. S. Geological Survey.

Ravizza, G., Norris, R.N., Blusztajn, J., and Aubry, M.P., 2001, An osmium isotope excursion associated with the late Paleocene thermal maximum: Evidence of intensified chemical weathering: Paleoceanography, v. 16, p. 155-163.

Rea, D.K., 1994, The Paleoclimatic Record Provided by Eolian Deposition in the Deep Sea: the Geologic History of Wind: Reviews of Geophysics, v. 32, p. 159-195.

Rea, D.K., and Hovan, S.A., 1995, Grain size distribution and depositional processes of the mineral component of abyssal sediments; lessons from the North Pacific: Paleoceanography, v. 10, p. 251-258.

Rea, D.K., and Janecek, T.R., 1981, Mass accumulation rates of the non-authigenic inorganic crystalline (eolian) component of deep sea sediments from teh western Mid-Pacific Mountains, Initial Reports of the Deep Sea Drilling Project, Volume 62, p. 653-659.

Rea, D.K., Leinen, M., and Janecek, T.R., 1985, Geologic approach to the long-term history of atmospheric circulation: Science, v. 227, p. 721-725.

Reay, M.B., 1993, Geology of the middle part of the Clarence Valley: Institute of Geological & Nuclear Sciences Geological, v. Map 10, p. 1-144.

Rohl, U., Bralower, T.J., Norris, R.D., and Wefer, G., 2000, New chronology for the late Paleocene thermal maximum and its environmental implications: Geology, v. 28, p. 927-930.

Schmitz, B., Asaro, F., Molina, E., Monechi, S., von Salis, K., and Speijer, R.P., 1997, High-resolution iridium, d13C, d18O, foraminifera and nannofossil profiles across the latest Paleocene benthic extinction event at Zumaya, Spain: Palaeogeography Palaeoclimatology Palaeoecology, v. 133, p. 49-68.

Schmitz, B., Pujalte, V., and Nunez-Betelu, K., 2001, Climate and sea-level perturbations during the initial eocene thermal maximum: evidence from siliciclastic units in the Basque Basin (Ermua, Zumaia and Trabakua Pass), northern Spain: Palaeogeography Palaeoclimatology Palaeoecology, v. 165, p. 299-320.

Sluijs, A., Brinkhuis, H., Schouten, S., Bohaty, S.M., John, C.M., Zachos, J.C., Reichart, G.J., Damste, J.S.S., Crouch, E.M., and Dickens, G.R., 2007, Environmental precursors to rapid light carbon injection at the Palaeocene/Eocene boundary: Nature, v. 450, p. 1218-U5.

Sluijs, A., Schouten, S., Pagani, M., Woltering, M., Brinkhuis, H., Damste, J.S.S., Dickens, G.R., Huber, M., Reichart, G.J., Stein, R., Matthiessen, J., Lourens, L.J., Pedentchouk, N., Backman, J., and Moran, K., 2006, Subtropical arctic ocean temperatures during the Palaeocene/Eocene thermal maximum: Nature, v. 441, p. 610-613.

Speijer, R.P., and Morsi, M.A.-M., 2002, Ostracode turnover and sea-level changes associated with the Paleocene-Eocene thermal maximum: Geology, v. 30, p. 23-26.

SpieB, V., 1990, Cenozoic magnetostratigraphy of Leg 113 dril sites, Maud Rise, Weddell Sea, Antarctica, *in* Barker, P.F., and Kennett, J.P., eds., Proceeds

of the Ocean Drilling Program, Scientific Results, Volume 113: College Station, TX, Ocean Drilling Program, p. 261-315.

Stineman, R.W., 1980, A consistently well-behaved method of interpolation: Creative Computing.

Stoll, H.M., 2005, Limited range of interspecific vital effects in coccolith stable isotopic records during the Paleocene-Eocene thermal maximum: Paleoceanography, v. 20.

Stoll, H.M., Shimizu, N., Archer, D., and Ziveri, P., 2007, Coccolithophore productivity response to greenhouse event of the Paleocene-Eocene Thermal Maximum: Earth and Planetary Science Letters, v. 258, p. 192-206.

Strong, C.P., Hollis, C.J., and Wilson, G.J., 1995, Foraminiferal, Radiolarian, and Dinoflagellate Biostratigraphy of Late Cretaceous to Middle Eocene Pelagic Sediments (Muzzle Group), Mead Stream, Marlborough, New-Zealand: New Zealand Journal of Geology and Geophysics, v. 38, p. 171-209.

Svensen, H., Planke, S., Malthe-Sorenssen, A., Jamtveit, B., Myklebust, R., Eidem, T.R., and Rey, S.S., 2004, Release of methane from a volcanic basin as a mechanism for initial Eocene global warming: Nature, v. 429, p. 542-545.

Swart, P.K., and Eberli, G., 2005, The nature of the d13C of periplatform sediments: Implications for stratigraphy and the global carbon cycle: Sedimentary Geology, v. 175, p. 115-129.

Thomas, D.J., Bralower, T.J., and Jones, C.E., 2003, Neodymium isotopic reconstruction of late Paleocene - early Eocene thermohaline circulation: Earth and Planetary Science Letters, v. 209, p. 309-322.

Thomas, D.J., Zachos, J.C., Bralower, T.J., Thomas, E., and Bohaty, S., 2002, Warming the fuel for the fire: Evidence for the thermal dissociation of methane hydrate during the Paleocene-Eocene thermal maximum: Geology, v. 30, p. 1067-1070.

Thomas, E., 2003, Extinction and food at the seafloor: A high-resolution benthic foraminiferal record across the Initial Eocene Thermal Maximum, Southern Ocean Site 690, *in* Wing, S.L., Gingerich, P.D., Schmitz, B., and Thomas, E., eds., Causes and consequences of globally warm climates in the early Paleogene, Volume Special Paper 369, Geological Society of America, p. 319-332.

Thomas, E., and Zachos, J.C., 2000, Was the late Paleocene thermal maximum a unique event?: Gff, v. 122, p. 169-170.

Von de Borch, C.C., and Sclater, J.G., 1974: Washington, D. C., U. S. Government Printing Office.

Westerhold, T., Rohl, U., Laska, J., Raffi, I., Bowles, J., Lourens, L.J., and Zachos, J.C., 2007, On the duration of magnetochrons C24r and C25n and the timing of early Eocene global warming events: Implications from the Ocean Drilling Program Leg 208 Walvis Ridge depth transect: Paleoceanography, v. 22.

Wing, S.L., Harrington, G.J., Smith, F.A., Bloch, J.I., Boyer, D.M., and Freeman, K.H., 2005, Transient Floral Change and Rapid Global Warming at the Paleocene-Eocene Boundary: Science, v. 310, p. 993-996.

Zachos, J., Kroon, D., and Blum, P., 2004, Proceedings of the Ocean Drilling Program, Initial Reports, Volume 208: College Station, Texas, Ocean Drilling Program.

Zachos, J., Pagani, M., Sloan, L., Thomas, E., and Billups, K., 2001, Trends, rhythms, and aberrations in global climate 65 Ma to present: Science, v. 292, p. 686-693.

Zachos, J.C., Dickens, G.R., and Zeebe, R.E., 2008, An early Cenozoic perspective on greenhouse warming and carbon-cycle dynamics: Nature, v. 451, p. 279-283.

Zachos, J.C., Rohl, U., Schellenberg, S.A., Sluijs, A., Hodell, D.A., Kelly, D.C., Thomas, E., Nicolo, M., Raffi, I., Lourens, L.J., McCarren, H., and Kroon, D., 2005, Rapid acidification of the ocean during the Paleocene-Eocene thermal maximum: Science, v. 308, p. 1611-1615.

Zachos, J.C., Wara, M.W., Bohaty, S., Delaney, M.L., Petrizzo, M.R., Brill, A., Bralower, T.J., and Premoli-Silva, I., 2003, A transient rise in tropical sea surface temperature during the Paleocene-Eocene Thermal Maximum: Science, v. 302, p. 1551-1554.

Zeebe, R.E., and Zachos, J.C., 2007, Reversed deep-sea carbonate ion basin gradient during Paleocene-Eocene thermal maximum: Paleoceanography, v. 22.

APPENDIX 1.

DATA REPORT: Terrigenous Grain-Size Distributions at Sites 1263 and 1267: Testing the Applicability of Leg 208 Sediments for Eolian Analysis

Micah J. Nicolo[1], and Gerald R. Dickens[1]

[1]Department of Earth Science, Rice University, Houston, TX 77005, USA

published in:

Proceedings of the Ocean Drilling Program, Scientific Results, 208

[Dec. 7th, 2006]

ABSTRACT

The only Southern Hemisphere eolian grain-size record constructed to date for the early Paleogene comes from DSDP Site 215. Ten early Paleogene sediment samples from Site 215 were collected and processed to show that the existing eolian grain-size record at this site can be reproduced. Five samples each from Sites 1263 and 1267 were similarly examined to test the possibility of generating new Southern Hemisphere eolian grain-size records for the early Paleogene. Our results indicate that an eolian grain-size signal can be constructed at Walvis Ridge, although the record will be complicated by hemipelagic terrigenous inputs. Further, we assert that a record generated at a site located on the deep flanks of Walvis Ridge is particularly susceptible to hemipelagic influence.

INTRODUCTION

The median grain-size of eolian material extracted from deep-sea sediment can be used to constrain past zonal wind intensity (e.g. Janecek and Rea, 1983; Rea et al., 1985; Miller et al., 1987; Hovan and Rea, 1992; Rea, 1994). Sediment sequences from several locations in the Northern Hemisphere have been examined for changes in eolian grain-size over the Cenozoic, and specifically the early Paleogene. These records show a major fining in eolian material from the Paleocene to the Eocene, an observation interpreted as a relative decrease in the intensity of zonal winds and, more generally, atmospheric circulation (Rea and Janecek, 1983; Rea et al., 1985; Miller et al., 1987; Rea, 1994). To date, one eolian grain-size record has been generated using lower Paleogene sediment

deposited in the Southern Hemisphere. This record, from DSDP Site 215 adjacent to Ninetyeast Ridge in the central Indian Ocean also shows a significant drop in grain size across the Paleocene-Eocene transition (Hovan and Rea, 1992). However, more records from the Southern Hemisphere are clearly needed to confirm these results and further substantiate broad zonal interpretations.

One major hurdle facing studies of eolian material is site selection. Sediment sequences need to contain biogenic carbonate, which can be dated, and to be bereft of chert, which limits the chemical isolation of all siliciclastic material, including eolian grains. Appropriate sites also need to be located far away from continents so that the terrigenous fraction of sediment is not completely dominated by non-eolian (riverine/hemipelagic) material. Often, the principle concern is hemipelagic material (Rea, 1994). At locations beyond the continental shelf, reworked riverine material settles to water depths of supportable density (> ~2000 mbsl) and travels as a hemipelagic cloud hundreds of kilometers from the margin (Honjo, 1982; Rea, 1994).

Walvis Ridge is located in the South Atlantic Ocean and extends west from Africa to the mid-ocean ridge. The sites of interest to this study were all drilled on Walvis Ridge greater than 1200 km from Namibia. Deep Sea Drilling Project (DSDP) Site 527, cored in 1980 at ~4430 mbsl, recovered a thick Cenozoic sediment sequence on a deep flank of this ridge (Moore et al., 1984). Preliminary work at this site indicated that hemipelagic material heavily dominates the terrigenous component of the lower Paleogene section (Rea and Hovan, 1995), making it problematic for studies of eolian material.

Ocean Drilling Program (ODP) Leg 208 returned to Walvis Ridge, recovering good lower Paleogene sediment sequences at five proximal sites that span a depth transect of ~2 km (Zachos et al., 2004). Site 1267 was drilled close to Site 527, and presumably holds a Paleogene terrigenous record dominated by hemipelagic material. However, Site 1263 was drilled near the crest of the ridge at ~2700 mbsl, and could contain a terrigenous record with significant amounts of eolian material. The object of this work is to evaluate whether the newly acquired lower Paleogene sequence at Site 1263 is appropriate for eolian grain-size studies. Our results suggest that a high-age resolution eolian grain-size record could be generated at Site 1263, providing long-desired information regarding early Paleogene atmospheric circulation in the Southern Hemisphere.

SITES AND SAMPLES

Site 215

DSDP Site 215 is located at ~5300 mbsl on the western flank of Ninetyeast Ridge far from any continents in the central Indian Ocean (von der Borch et al., 1974). The existing early Paleogene eolian grain-size record for the Southern Hemisphere (Hovan and Rea, 1992) was generated using sediment samples recovered between 83 and 130 mbsf. This record (Figure A.1) shows a significant ~6 μm decrease in the median grain-size of eolian material near the Paleocene-Eocene boundary (~103.3 mbsf), from ~9.6 μm in upper Paleocene sediment (109.37 mbsf) to ~3.8 μm in lower Eocene sediment (84.83 mbsf).

The isolation and analysis of eolian material from marine sediment is a labor-intensive process involving many steps (Appendix 2); the subsequent

analysis of the extracted component requires reliable measurements. Our first goal, therefore, was to test whether we could reproduce the published eolian grain-size record at DSDP Site 215. Ten samples were collected between 85 and 107 mbsf, with most samples taken within 5 cm of those examined by Hovan and Rea (1992).

Leg 208

All Leg 208 Sites currently lie well off the continental shelf greater than 1200 km away from the African continent (and likely a greater distance in the early Paleogene due to a higher sea-level). Drilling at Sites 1263 and 1267 recovered lower Paleogene sediment sequences on Walvis Ridge but at much different water depths, both now and in the past. Site 1263 is presently at ~2700 mbsl whereas Site 1267 is presently at ~4350 mbsl. Near the Paleocene-Eocene boundary ca. 55 Ma, however, water depths were probably around ~1500 m for Site 1263 and ~3200 m for Site 1267 (Zachos et al., 2005).

The Paleocene-Eocene boundary has been identified at both Sites 1263 and 1267 (Zachos et al., 2005). Close to this time horizon, ages can be assigned to sediment depths fairly accurately using a model (Zachos et al., 2005) that ties changes in the carbon isotope composition of carbonate to those observed at ODP Site 690, which has been calibrated using cyclostratigraphy (Rohl et al., 2000). Thus, "time-coincident" sediment samples can be taken from Sites 1263 and 1267 around the Paleocene-Eocene boundary. Five such samples were collected from each site. "Time-coincidence" was emphasized so that potential differences in the

delivery of eolian and hemipelagic components to the two sites at similar times could be explored.

METHODS

Terrigenous sediment isolation

Bulk marine sediment comprises multiple components, so that the terrigenous component (eolian and hemipelagic material) needs to be isolated for study. Previous work (e.g., Mehra and Jackson, 1960; Rea and Janecek, 1981; Hovan and Rea, 1992; Lyle et al., 2002) has developed a method to chemically extract the non-terrigenous components. The general procedure involves removing carbonate with weak acetic acid, removing metalliferous oxides and hydroxides with a buffered sodium citrate-sodium hydrosulfite mixture, and removing biogenic silica with one of several sediment-dependent steps. In this study, we adopted a specific procedure for extracting the terrigenous component (outlined in Appendix 2).

Grain-size distributions

Once extracted, the terrigenous component was homogenized and the grain-size distribution of all 20 samples was examined using a Coulter Multisizer II housed in the Civil and Environmental Engineering Department at Rice University. This device measures the electronic resistance of individual particles and divides results into 256 channels over a size range applicable to the material being analyzed, in this case 1-30 μm. Previous work (Poppe et al., 2003) as well

as repeat analyses conducted for this study indicates that the precision of this instrument is within plus or minus 10%.

Nominally 0.1 g of isolated terrigenous material and 15 mL of 0.008 M sodium hexametaphosphate were placed into a clean, labeled sample vial. The solution was sonicated for 5 min, and mixed overnight in a hand-action shaker. After running clean electrolyte solution through the Coulter Multisizer II for 3 min to obtain a background count, ~2 mL of stirred solution was slowly added to clean electrolyte solution until a desired sample density was met. Following subtraction of background counts, grain-size measurements were collected by averaging three 3 min sample runs on the Coulter Multisizer II. This method typically allows counting of ~100,000 – 200,000 individual particles.

RESULTS

DSDP Site 215

The median grain-size of the extracted terrigenous component ranges from 6.6 – 3.6 μm for the 10 samples collected from Site 215 (Table A.1; Figure A.1). As highlighted by Hovan and Rea (1992), we find a general drop in median grain size from upper Paleocene sediment into lower Eocene sediment, although this change is not as great as that previously recorded. We note, however, that our samples are not true replicates and do not span the entire depth interval examined by Hovan and Rea (1992). For the 9 samples collected within 5 cm (and on average 3 cm) of those analyzed by Hovan and Rea (1992), we measured an average difference in grain size of about 0.4 μm (Figure A.1), which is approximately equal to the precision of the instrument for particles of this size.

ODP Site 1267

All five samples analyzed at Site 1267 show a relatively flat grain-size distribution over a broad size range (Figure A.2). The median grain sizes range from 7.6 to 10.1 μm, while the modal grain size varies from 6.5 to 11.5 μm (Table A.2). The overall shapes of the grain size patterns are similar to those observed at Site 527 by Rea and Hovan (1995).

ODP Site 1263

In contrast to samples from Site 1267, grain-size distributions for the five samples from Site 1263 show a distinct mode (Figure A.2). However, similar to the samples measured at Site 1267, Site 1263 samples record a broad grain-size distribution indicative of hemipelagic terrigenous material influence. The median grain sizes range from 5.5 to 6.9 μm, while the modal grain size varies from 5.6 to 6.9 μm (Table A.2).

DISCUSSION

Robust grain-size records

Previous work on terrigenous material in deep-sea sediment indicates that, given similar extraction procedures and analytical methods, measurements of grain size are reproducible (e.g., Rea, 1994). For closely-spaced lower Paleogene sediment samples at Site 215, the median grain-size that we determined for the extracted terrigenous component is similar to that reported by Hovan and Rea

(1992). We therefore conclude that our approach for isolating and examining the terrigenous component will render robust grain-size information.

Terrigenous component on Walvis Ridge: a mixture of hemipelagic and eolian material

The grain-size distributions of the terrigenous component extracted from upper Paleocene-lower Eocene sediment at Site 1267 are similar to those observed for the terrigenous component extracted from contemporaneous sediment at nearby Site 527 (Rea and Hovan, 1995). In both cases, the isolated component has a flat pattern characterized by low weight percents of material spread across a wide grain-size range (Figure A.2). This pattern suggests that hemipelagic material dominates the terrigenous component (Rea and Hovan, 1995; Boven and Rea, 1998).

Grain-size analyses of the terrigenous component in time-coincident samples at Site 1263 clearly vary from those at Site 1267 (Figure A.2). Isolated samples from Site 1263, the shallower location, contain a pronounced grain-size mode centered between 5 and 7 μm. Such a grain-size distribution is consistent with a large fraction of eolian material in the terrigenous component (Boven and Rea, 1998).

Even in open-ocean settings, the terrigenous component of deep-sea sediment may comprise a mixture of eolian and hemipelagic material (Rea, 1994; Rea and Hovan, 1995). Using extensive data sets of terrigenous grain-size distributions from Pacific Ocean sediments, Boven and Rea (1998) developed a two component-mixing model to determine the relative proportion of each

component. This approach is based on the observation that hemipelagic grain-size distributions are broad with peak weight percents typically low near 1%, while eolian grain-size distributions depict a dominant mode with greater peak weight percents near 5% (Boven and Rea, 1998). The model compares the peak weight percent of a sample's grain-size distribution to end-member eolian and hemipelagic distributions. According to this model, our results suggest that the terrigenous component of sediment deposited near the Paleocene/Eocene boundary contains ~6-11 % eolian material at the relatively deep Site 1267 but upwards of 20-40 % eolian material at the relatively shallow Site 1263. This indicates that the shallow site received a higher concentration of eolian material than did the deep sites. However, sites 1263 and 1267 have likely received a similar flux of eolian material through time because they are proximal to each other. This indicates that the deep flank of Walvis Ridge received a higher flux of hemipelagic sediment than the shallow crest. This finding conforms to general views of hemipelagic deposition, considering the paleodepths of Sites 1267 (~3200 mbsl at ~55 Ma) and 1263 (~1500 mbsl at ~55 Ma). Hemipelagic material should have settled and moved at >2000 m water depth, such that greater amounts of hemipelagic material would have accumulated at Site 1267 (and Site 527).

Site 1263 eolian grain-size record: mode vs. median

An eolian grain-size record can probably be gleaned from the early Paleogene sequence recovered at Site 1263 on Walvis Ridge. However, there is an issue regarding measurement because, even at this shallow location, the terrigenous component contains a mixture of hemipelagic and eolian material.

Large amounts of hemipelagic material broaden the grain-size distribution so that the median and modal grain-size of the terrigenous component differs significantly (Figure A.2). While previous studies of eolian grain-size have generally used the median for paleoenvironmental reconstructions, we suggest that the mode more accurately measures the grain-size of the eolian fraction in mixed hemipelagic-eolian systems (where an eolian signal is detectable). This is particularly evident in samples with lower eolian percents such as the Site 1263 sample illustrated in pane "A" of Figure A.2. Sample "A" shows the lowest Site 1263 eolian percent and the highest mode-median offset of 1.1 μm, while samples "B-E" have eolian percents ranging from 32-38 % and a mode-median difference of only 0.1-0.2 μm. Further, samples collected from Site 215 that have been shown to be of eolian origin (Hovan and Rea, 1992) record a mode-median average difference of 0.1 μm.

CONCLUSIONS

The terrigenous component of lower Paleogene marine sediment can be isolated and subsequently analyzed for precise grain-size measurements. It is probable that an early Paleogene Southern Hemisphere eolian grain-size record can be constructed at Site 1263 on the crest of Walvis Ridge. Interpretation of such a record needs to consider the mixed eolian-hemipelagic nature of the terrigenous component. Modal grain size may be a more important measurement than median grain size for eolian proxies at this site, as it appears to retain a grain-size distribution signal characteristic of eolian sediments. Sites at greater water depth and on the flank of Walvis Ridge contain a higher abundance of

hemipelagic material, which limits their utility for analyses of the eolian component. This probably reflects the general process of hemipelagic deposition, where material settles in waters of sufficiently high density (often > 2000 m water depth) to support and transport mineral grains.

ACKNOWLEDGMENTS

This research used samples and/or data provided by the Ocean Drilling Program (ODP). ODP is sponsored by the U.S. National Science Foundation (NSF) and participating countries under management of Joint Oceanographic Institutions (JOI), Inc. Funding for this research was provided by the U. S. Science Support Program of JOI. We also thank Dr. Mark Wiesner and Dr. Jonathan Brant of the Rice University Civil and Environmental Engineering Department for Coulter Multisizer use, and Dr. Leah Joseph for helpful procedural and analytical comments.

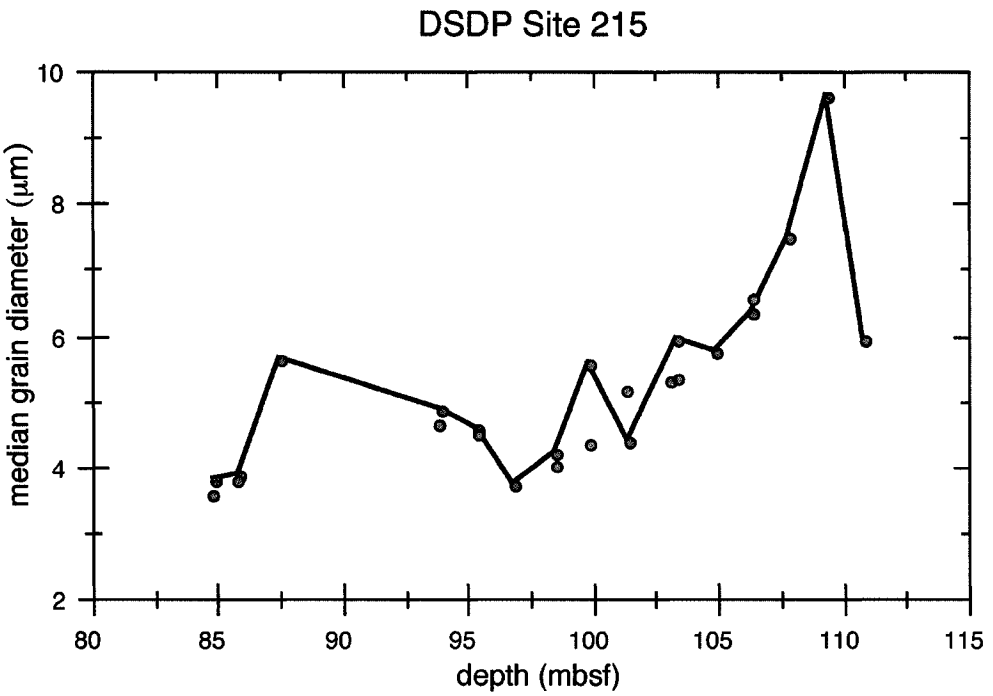

Figure A-1: Median grain-size of the early Paleogene terrigenous sediment component at DSDP Site 215. Blue circles represent data published by Hovan and Rea (1992); red circles depict results generated for this study.

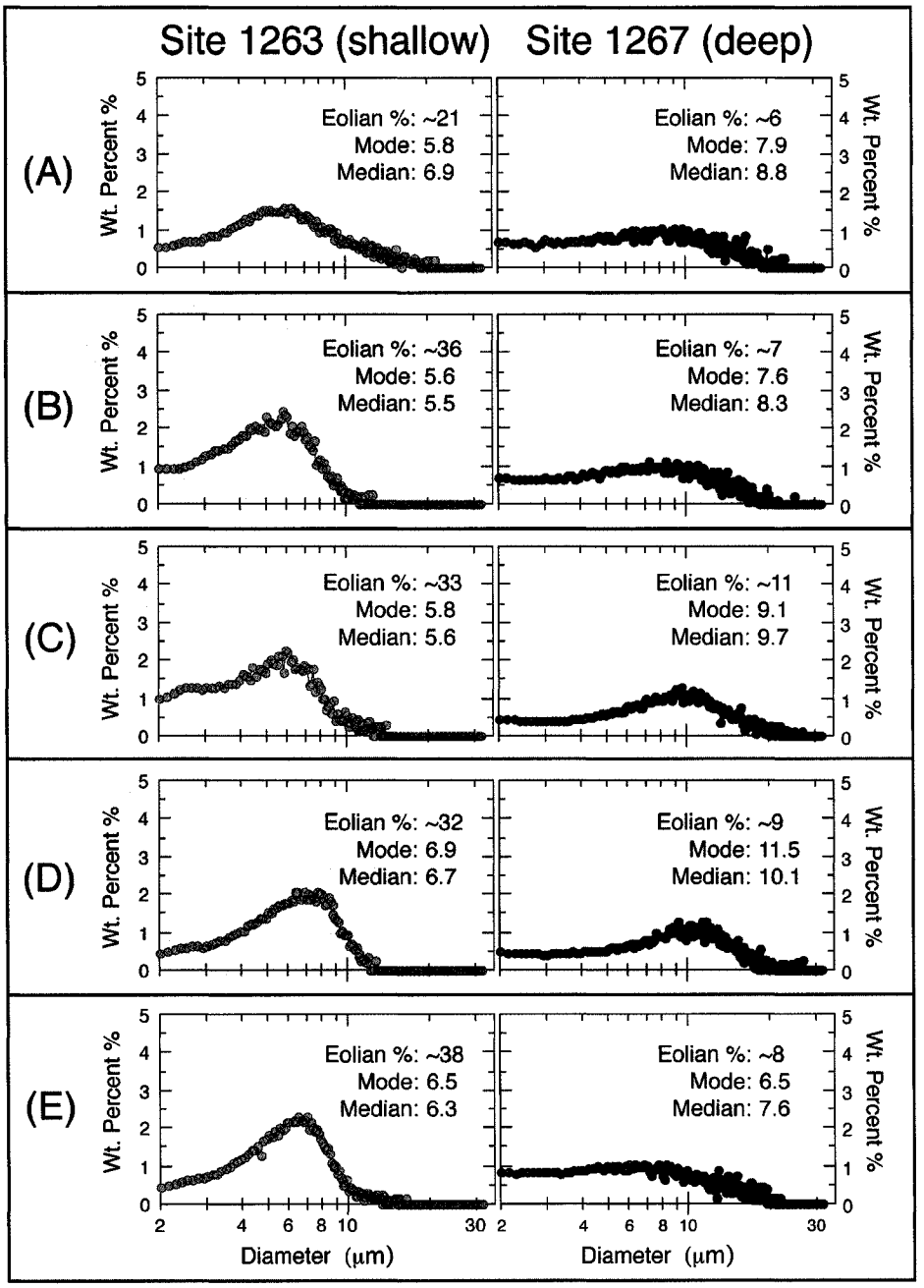

Figure A-2: Site 1263 and Site 1267 grain-size distributions. Five sets of time coincident (< ~16 kyrs difference) grain-size distributions are illustrated, such that each pane ("A" through "E") contains one distribution from the shallower Site 1263 and one distribution from the deeper Site 1267. All distributions are plotted on identical axes of grain diameter in mm and weight percent. All Site 1263 data is represented by blue circles, while all Site 1267 data is presented as red circles. Eolian percent (%) has been calculated after the two-component mixing model of Boven and Rea (1998).

Table A.1. Median grain-size of eolian material at DSDP Site 215.

Core, Type, Section, Interval (cm)		Mean Depth (mbsf)	Median Grain-Size (μm)
Top	Base		
10, R, 1, 128	10, R, 1, 130	84.79	3.6
10, R, 1, 131	10, R, 1, 134	84.83	3.8
10, R, 2, 75	10, R, 2, 78	85.77	3.8
10, R, 2, 80	10, R, 2, 83	85.82	3.9
10, R, 3, 94	10, R, 3, 97	87.46	5.6
11, R, 1, 83	11, R, 1, 85	93.84	4.7
11, R, 1, 85	11, R, 1, 88	93.87	4.9
11, R, 2, 81	11, R, 2, 84	95.33	4.5
11, R, 2, 85	11, R, 2, 88	95.37	4.6
11, R, 3, 85	11, R, 3, 88	96.87	3.7
11, R, 4, 92	11, R, 4, 95	98.44	4.0
11, R, 4, 95	11, R, 4, 98	98.47	4.2
11, R, 5, 80	11, R, 5, 82	99.81	4.4
11, R, 5, 82	11, R, 5, 85	99.84	5.6
11, R, 6, 82	11, R, 6, 85	101.34	5.2
11, R, 6, 85	11, R, 6, 88	101.37	4.4
12, R, 1, 50	12, R, 1, 57	103.04	5.3
12, R, 1, 83	12, R, 1, 85	103.34	5.4
12, R, 1, 85	12, R, 1, 88	103.37	6.0
12, R, 2, 85	12, R, 2, 88	104.87	5.8
12, R, 3, 83	12, R, 3, 86	106.35	6.6
12, R, 3, 85	12, R, 3, 88	106.37	6.3
12, R, 4, 83	12, R, 4, 86	107.85	7.5
12, R, 5, 85	12, R, 5, 88	109.37	9.6
12, R, 6, 85	12, R, 6, 88	110.87	6.0

grey rows = Hovan and Rea (1992) results

Table A.2. Leg 208 terrigenous grain-size median and mode, and percent eolian.

Figure 2 Grouping	Site	Hole	Sample Depth (mbsf)	Grain-Size (μm)		*Percent Eolian (%)
				Median	Mode	
A	1263	C	284.12	6.9	5.8	21
	1267	B	205.28	8.8	7.9	6
B	1263	C	284.41	5.5	5.6	36
	1267	B	205.53	8.3	7.6	7
C	1263	C	284.51	5.6	5.8	33
	1267	B	205.58	9.7	9.1	11
D	1263	C	285.01	6.7	6.9	32
	1267	B	205.73	10.1	11.5	9
E	1263	A	284.48	6.3	6.5	38
	1267	B	205.78	7.6	6.5	8

grey rows = Site 1263 results

* = calculated using the model of Boven and Rea (1998)

APPENDIX 2.

EXTRACTION FOR ISOLATING TERRIGENOUS MATERIAL

A series of papers have discussed the isolation of terrigenous material from deep-sea sediment (e.g., Rea and Janecek, 1981; Hovan and Rea, 1992; Lyle et al., 2002). In general, these works have used a similar overall procedure, which involves sequential extraction to remove carbonate, metalliferous oxides and hydroxides, and biogenic silica. Rarely, however, are the actual steps presented. Following are the detailed steps used in this study to extract terrigenous material. The steps were modified somewhat from notes kindly provided to us by Dr. Leah Joseph.

Carbonate removal

1) Place weighed masses of sample (~10 bulk g) into clean, labeled 500 mL Erlenmeyer flasks.
2) Slowly add ~125 mL of 4.5 N (25% by volume) acetic acid to each flask in 10 mL increments to avoid loss by bubbling.
3) Shake flasks with mechanical wrist-action shaker for 2 hrs.
4) Pour solutions from flasks into labeled 250 mL centrifuge bottles.
5) Centrifuge for 13 min at ~4500 rpm, and decant supernatant.
6) Add ~125 mL of 4.5 N (25% by volume) acetic acid to each 250 mL centrifuge bottle.
7) Sonicate for 5 min.

8) Pour sample solutions back into corresponding Erlenmeyer flasks, and re-shake with mechanical wrist-action shaker for 2 hrs.

9) Pour solutions from flasks into corresponding 250 mL centrifuge bottles.

10) Centrifuge for 13 min at ~4500 rpm, and decant supernatant.

Metalliferous oxyhydroxide removal

1) Fill a water bath with tap water to ~3/4 full, and heat on hot plate to ~85^{0}C.

2) Fill a 1000 mL beaker full and 1 600 ml beaker with mixture of half ultra pure DI water and half 0.3 M sodium citrate (50/50), and place on separate hot plate (sol. hot plate) at a slightly lower setting.

3) Add 40 mL of 0.3 M sodium citrate into each 250 mL centrifuge bottle.

4) Slowly add 5 mL of 1.0 M sodium bicarbonate to each 250 mL centrifuge bottle.

5) Place bottles in hot water bath and leave for 10-15 min. While waiting, fill 1 1000 mL beaker full and 1 600 mL beaker with 0.3 M sodium citrate, and place on sol. hot plate (only fill the sodium citrate beakers during 1st of 2 repeats, i.e. step 9).

6) Add ~1g of sodium dithionate (a.k.a. sodium hydrosulfite) to each 250 mL centrifuge bottle, stir continuously for 30 sec, and return to hot-water bath.

7) After 5-10 min, add 100 mL of 50/50 solution to each centrifuge bottle and stir thoroughly.

8) Centrifuge for 13 min at ~4500 rpm, and decant supernatant.

9) Repeat oxides/hydroxides extraction steps 2 – 8.

10) Add 100 mL of hot 0.3 M sodium citrate and stir thoroughly.

11) Centrifuge for 13 min at ~4500 rpm, and decant supernatant.

12) Repeat steps 3-11 so that each sample has received two extractions and a hot rinse twice. Samples should now be a grayish-green color. If they are still a reddish-orange color, another oxyhydroxide removal sequence may be necessary.

13) Centrifuge for 13 min at ~4500 rpm, and decant supernatant.

Opal removal

1) Wash each sample into a clean, labeled 600 mL beaker with ultra pure DI water.

2) Fill beakers with ultra pure DI water to 400 mL, and cover with watch glass.

3) Place beakers directly on hot plate and bring to ~85^{0}C.

4) Add 24 g of sodium hydroxide (NaOH) to each beaker (=1.5M NaOH), stir thoroughly, and replace watch glass.

5) Leave beakers on hot plate for 2 hrs at ~85^{0}C. Stir solution after one hr.

6) Remove beakers from hot plate and let cool for several min.

7) Pour sample/solution into corresponding 250 mL centrifuge bottle, centrifuge for 13 min at ~4500 rpm, and decant supernatant.

Note: The opal removal step was not conducted on sediment samples from Leg 208 sites because they lack radiolarians and diatoms (Zachos et al, 2004).

Final Rinse

1) Fill each 250 mL centrifuge bottle with ~40 mL of hot, ultra pure DI water and stir thoroughly.

2) Wash solution and remnant sample into corresponding clean, dry, labeled, and pre-weighed 50 mL centrifuge tube.

3) Centrifuge for 13 minutes at ~4500 rpm, and decant supernatant.

4) Repeat steps 1-3 four times.

5) Freeze the residue in the centrifuge tube for 12 hrs.

6) Freeze-dry the residue in the centrifuge tube for 48 hrs.

7) Tare the dried residue.

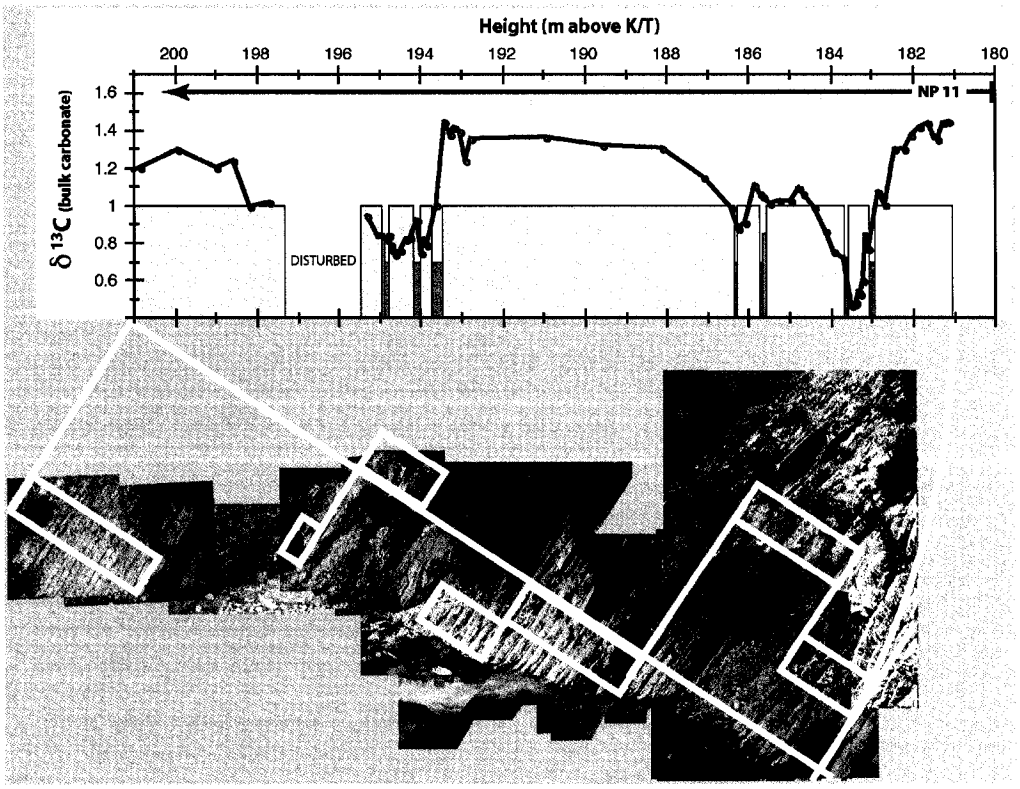

Figure A.3. Mead Stream H1-I2 interval. NP 11 refers to nannofossil zone 11. white boxes represent sampling scheme.

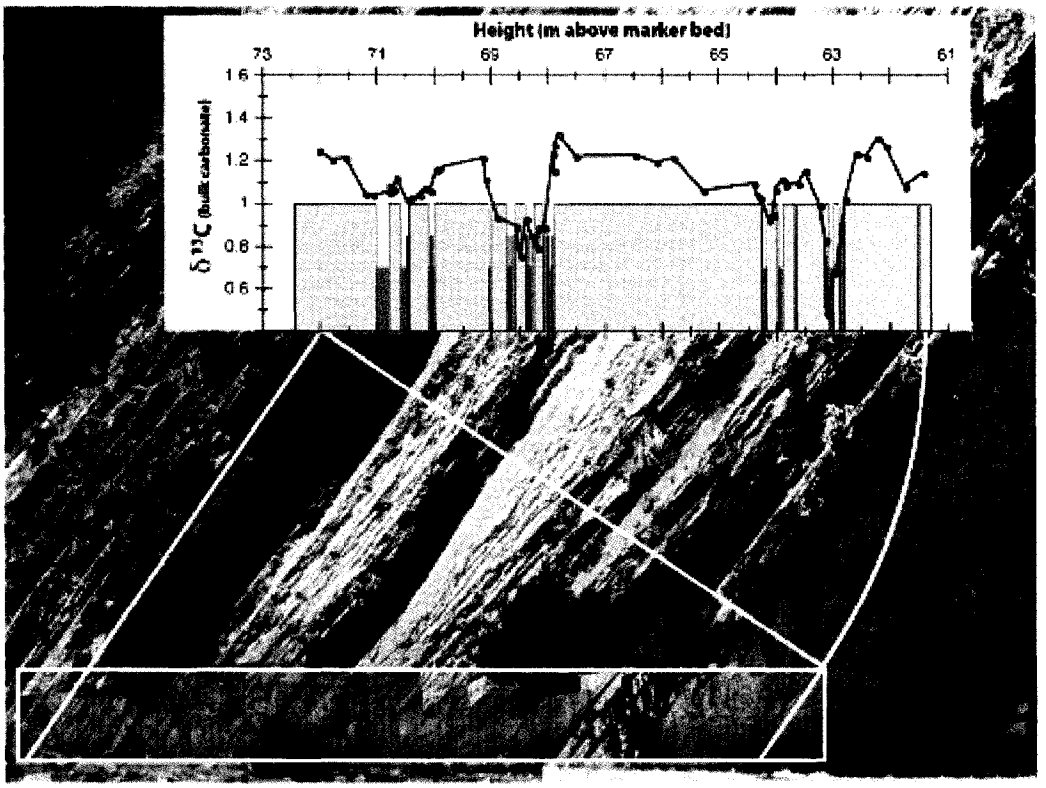

Figure A.4. Dee Stream H1-I2 interval. White box represents sampling zone.

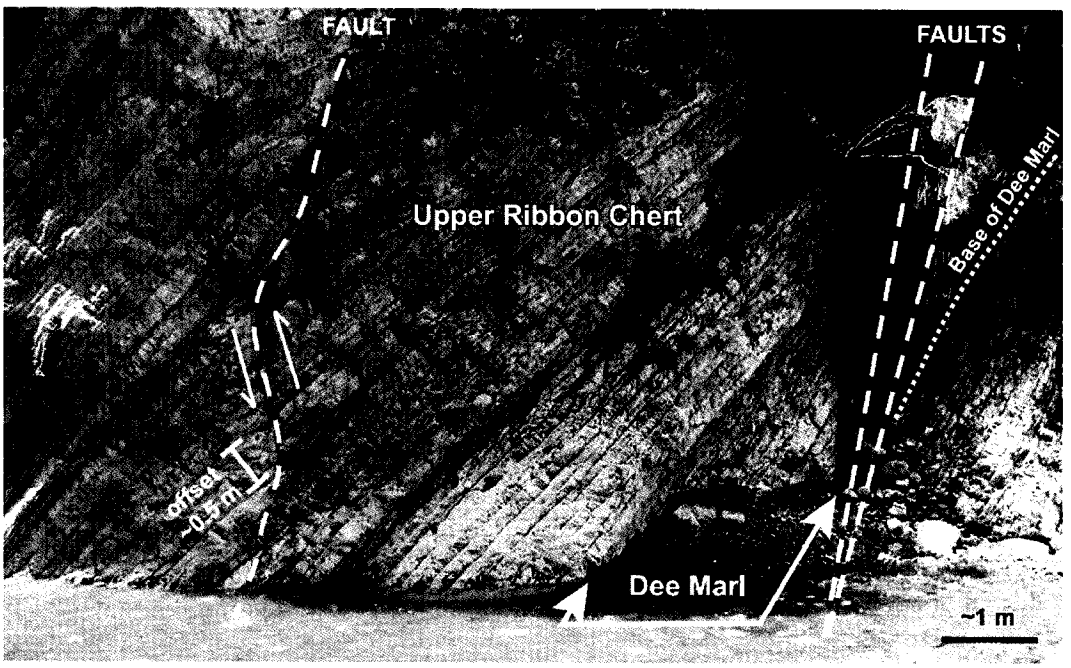

Figure A.5. Mead Stream PETM Dee Marl. After Hollis et al., (2005). True left of Mead Stream outcrop through the PETM section with small faults detailed.

Figure A.6. Entrance to Mead Stream, New Zealand.